chapter**NINETEEN**

Nuclear Magnetic Resonance Spectroscopy

Nuclear magnetic resonance (NMR) spectroscopy is based on the measurement of absorption of electromagnetic radiation in the radio-frequency region of roughly 4 to 900 MHz. In contrast to ultraviolet (UV), visible, and infrared (IR) absorption, nuclei of atoms rather than outer electrons are involved in the absorption process. Furthermore, to cause nuclei to develop the energy states required for absorption to occur, it is necessary to place the analyte in an intense magnetic field. In this chapter we describe the theory, instrumentation, and applications of NMR spectroscopy.

NMR spectroscopy is one of the most powerful tools available to chemists and biochemists for elucidating the structure of chemical species. The technique is also useful for the quantitative determination of absorbing species. NMR spectroscopy is one of the few instrumental methods applicable to solids, liquids, and gases.

Throughout this chapter, this logo indicates an opportunity for online self-study at **www.tinyurl.com/skoogpia7**, linking you to interactive tutorials, simulations, and exercises.

The theoretical basis for NMR spectroscopy[1] was proposed by W. Pauli in 1924. He suggested that certain atomic nuclei have the properties of spin and magnetic moment and that, as a consequence, exposure to a magnetic field would lead to splitting of their energy levels. During the next decade, these postulates were verified experimentally. It was not until 1946, however, that Felix Bloch at Stanford and Edward Purcell at Harvard, working independently, demonstrated that nuclei absorb electromagnetic radiation in a strong magnetic field as a result of the energy level splitting that is induced by the magnetic field. The two physicists shared the 1952 Nobel Prize in Physics for their work.

In the first few years following the discovery of NMR, chemists became aware that the molecular environment influences the absorption of radio-frequency (RF) radiation by a nucleus in a magnetic field and that this effect can be correlated with molecular structure. In 1953 the first high-resolution NMR spectrometer designed for chemical structural studies was marketed by Varian Associates. Since then, the growth of NMR spectroscopy has been explosive, and the technique has had profound effects on the development of organic and inorganic chemistry and biochemistry. It is unlikely that there has ever been as short a delay between a scientific discovery and its widespread acceptance and application.[2]

Two general types of NMR spectrometers are currently in use, *continuous-wave* (CW) and *pulsed*, or *Fourier transform* (FT-NMR), spectrometers. All early studies were carried out

[1]The following references are recommended for further study: J. Keeler, *Understanding NMR Spectroscopy*, 2nd ed., Chichester, UK: Wiley, 2010; J. B. Lambert, E. P. Mazzola, *Nuclear Magnetic Resonance Spectroscopy*, Upper Saddle River, NJ: Pearson/Prentice-Hall, 2004; R. M. Silverstein, F. X. Webster, D. Kiemle, and D. L. Bryce, *Spectrometric Identification of Organic Compounds*, 8th ed., New York: Wiley, 2015; M. H. Levitt, *Spin Dynamics: Basics of Nuclear Magnetic Resonance*, 2nd ed., Chichester, UK: Wiley, 2008; E. D. Becker, *High Resolution NMR*, 3rd ed., New York: Academic Press, 2000; H. Günther, *NMR Spectroscopy: Basic Principles, Concepts and Applications in Chemistry*, 3rd ed., Weinheim, Germany: Wiley-VCH, 2013.

[2]For interesting discussions of the history of NMR, see D. L Rabenstein, *Anal. Chem.*, **2001**, *73*, 214A, **DOI**: 10.1021/ac012435q; E. D. Becker, *Anal. Chem.*, **1993**, *65*, 295A, **DOI**: 10.1021/ac00054a716.

with CW instruments. In about 1970, however, FT-NMR spectrometers became available commercially, and now this type of instrument dominates the market. In both types of instruments, the sample is positioned in a powerful magnetic field that has a strength of several tesla.[3] CW spectrometers are similar in principle to optical absorption instruments in that an absorption signal is monitored as the frequency of the source is slowly scanned. In some instruments, the frequency of the source is held constant while the strength of the field is scanned. In pulsed instruments, the sample is irradiated with periodic pulses of RF energy that are directed through the sample at right angles to the magnetic field. These excitation pulses elicit a time-domain signal that decays in the interval between pulses. This signal is then converted to a frequency-domain signal by using a Fourier transformation to give a spectrum similar to that obtained by using a CW instrument.

Nearly all NMR instruments produced today are of the FT type, and the use of CW instruments is largely limited to special routine applications, such as the determination of the extent of hydrogenation in petroleum process streams and the determination of water in oils, food products, and agricultural materials. Despite this predominance of pulsed instruments in the marketplace, we find it convenient to base our initial development of NMR theory on CW experiments and move from there to a discussion of pulsed NMR measurements.

19A THEORY OF NMR

As we noted with optical spectroscopy, both classical mechanics and quantum mechanics are useful in explaining the NMR phenomenon. The two treatments yield identical relationships. Quantum mechanics, however, is more useful in relating absorption frequencies to energy states of nuclei, while at the same time, classical mechanics is more helpful in providing a physical picture of the absorption process and how it is measured.

In this section, we first present a quantum description of NMR applicable to both CW and pulsed NMR measurements. Then, we take a classical approach to NMR and show how it provides a useful picture of CW-NMR. Finally, we complete this section with a discussion of Fourier transform measurements based again on a classical picture.

[3]The SI symbol for magnetic fields is B; an older convention, however, which is still widely used, employed the symbol H instead. The derived unit for describing the field strength is the tesla (T), which is defined as $1\ T = 1\ kg\ s^{-2}\ A^{-1}$. Another unit that was popular in the past and still is frequently encountered is the gauss (G). The relationship between the two units is $10^4\ G = 1\ T$. Also, $1\ T = 1\ Vs/m^2$, where V = volts.

19A-1 Quantum Description of NMR

To account for the properties of certain nuclei, we must assume that they rotate about an axis and thus have the property of *spin*. Nuclei with spin have angular momentum p. Furthermore, the maximum observable component of this angular momentum is quantized and must be an integral or a half-integral multiple of $h/2\pi$, where h is Planck's constant. The maximum number of spin components or values for p for a particular nucleus is its spin quantum number I. The nucleus will then have $2I + 1$ discrete states. The component of angular momentum for these states in any chosen direction will have values of $I, I - 1, I - 2, \ldots, -I$. In the absence of an external field, the various states have identical energies.

The four nuclei that have been of greatest use to organic chemists and biochemists are ^1H, ^{13}C, ^{19}F, and ^{31}P, and they are the only four we will discuss. The spin quantum number for these nuclei is 1/2. Thus, each nucleus has two spin states corresponding to $I = +1/2$ and $I = -1/2$. Heavier nuclei have spin numbers that range from zero, which implies that they have no net spin component, to at least 9/2.

A spinning, charged nucleus creates a magnetic field analogous to the field produced when electricity flows through a coil of wire. The resulting magnetic moment μ is oriented along the axis of spin and is proportional to the angular momentum p. Thus

$$\mu = \gamma p \tag{19-1}$$

where the proportionality constant γ is the *magnetogyric*, or *gyromagnetic*, *ratio*, which has a different value for each type of nucleus. As we shall see, the magnetogyric ratio is also a factor in the proportionality constant in the relationship between the frequency of the absorbed energy and the magnetic field strength (see Equation 19-5). Magnetogyric ratios for the four elements we are considering are found in the second column of Table 19-1.

The relationship between nuclear spin and magnetic moment leads to a set of observable magnetic quantum states m given by

$$m = I, I - 1, I - 2, \ldots, -I \tag{19-2}$$

Thus, the nuclei that we will consider have two magnetic quantum numbers, $m = +1/2$ and $m = -1/2$. Note that the rules for determining nuclear quantum numbers are similar to those for electronic quantum numbers.

Energy Levels in a Magnetic Field

As shown in Figure 19-1, when a nucleus with a spin quantum number of 1/2 is brought into an external magnetic field B_0, its magnetic moment becomes oriented in one of two directions with respect to the field, depending on its magnetic quantum state. The potential energy E of a nucleus in these two orientations, or quantum states, is given by

$$E = -\frac{\gamma m h}{2\pi} B_0 \tag{19-3}$$

TABLE 19-1 Magnetic Properties of Important Nuclei with Spin Quantum Numbers of 1/2

Nucleus	Magnetogyric Ratio, Radian T^{-1} s^{-1}	Isotopic Abundance, %	Relative Sensitivity[a]	Absorption Frequency, MHz[b]
^{1}H	2.6752×10^{8}	99.98	1.00	200.00
^{13}C	6.7283×10^{7}	1.11	0.016	50.30
^{19}F	2.5181×10^{8}	100.00	0.83	188.25
^{31}P	1.0841×10^{8}	100.00	0.066	81.05

[a]At constant field for equal number of nuclei.

[b]At a field strength of 4.69 T.

The energy for the lower energy $m = +1/2$ state (see Figure 19-1) is given by

$$E_{+1/2} = -\frac{\gamma h}{4\pi} B_0$$

For the $m = -1/2$ state the energy is

$$E_{-1/2} = \frac{\gamma h}{4\pi} B_0$$

Thus, the difference in energy ΔE between the two states is given by

$$\Delta E = \frac{\gamma h}{4\pi} B_0 - \left(-\frac{\gamma h}{4\pi} B_0\right) = \frac{\gamma h}{2\pi} B_0 \qquad (19\text{-}4)$$

As in other types of spectroscopy, transitions between energy states can be brought about by absorption or emission of electromagnetic radiation of a frequency ν_0 that corresponds in energy to ΔE. Thus, by substituting the Planck relationship $\Delta E = h\nu_0$ into Equation 19-4, we obtain the frequency of the radiation required to bring about the transition

$$\nu_0 = \frac{\gamma B_0}{2\pi} \qquad (19\text{-}5)$$

As we suggested previously, the frequency of a magnetic transition is proportional to the applied field strength B_0 with a proportionality constant of $\gamma/2\pi$.

Example 19-1 reveals that RF radiation of approximately 200 MHz is required to bring about a change in alignment of the magnetic moment of the proton from a direction that parallels the field to one that opposes it.

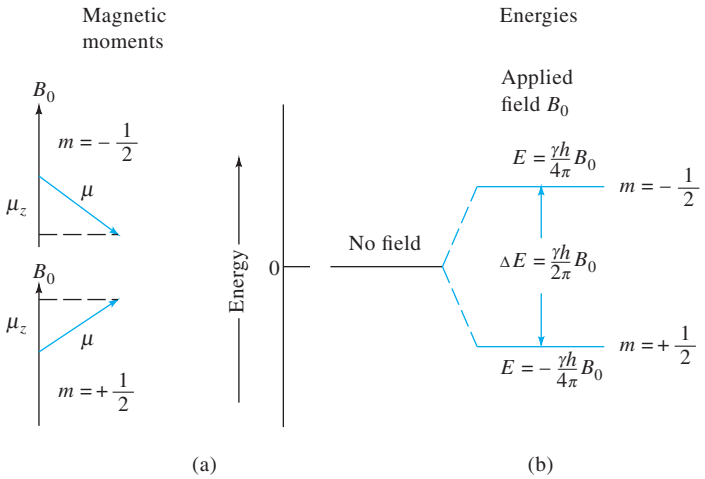

FIGURE 19-1 Magnetic moments and energy levels for a nucleus with a spin quantum number of 1/2.

EXAMPLE 19-1

Some proton NMR instruments are equipped with a magnet that provides a field strength of 4.69 T. At what frequency would the hydrogen nucleus absorb in such a field?

Solution

Substituting the magnetogyric ratio for the proton (Table 19-1) into Equation 19-5, we find

$$\nu_0 = \frac{(2.68 \times 10^8\ \mathrm{T^{-1}\,s^{-1}})(4.69\ \mathrm{T})}{2\pi}$$
$$= 2.00 \times 10^8\ \mathrm{s^{-1}} = 200\ \mathrm{MHz}$$

Distribution of Nuclei between Magnetic Quantum States

In the absence of a magnetic field, the energies of the magnetic quantum states of a nucleus are identical. Consequently, a large collection of protons contains an identical number of nuclei with magnetic quantum numbers $m = +1/2$ and $m = -1/2$. When placed in a magnetic field, however, the nuclei tend to orient themselves so that the lower energy state ($m = +1/2$) predominates. It is instructive to calculate the extent of this predominance in a typical NMR experiment. For this purpose, the Boltzmann equation (Equation 8-1) can be written in the form

$$\frac{N_j}{N_0} = \exp\left(\frac{-\Delta E}{kT}\right) \tag{19-6}$$

where N_j is the number of protons in the higher energy state ($m = -1/2$), N_0 is the number in the lower state ($m = +1/2$), k is Boltzmann's constant (1.38×10^{-23} J K^{-1}), T is the absolute temperature, and ΔE is defined by Equation 19-4.

Substituting Equation 19-4 into 19-6 gives

$$\frac{N_j}{N_0} = \exp\left(\frac{-\gamma h B_0}{2\pi kT}\right) \tag{19-7}$$

Example 19-2 illustrates that the success of the NMR measurement depends on a remarkably small, ~33 ppm, excess of lower-energy protons. If the numbers of nuclei in the two states were identical, however, we would observe no net absorption because the number of nuclei excited by the radiation would exactly equal the number producing *induced* emission.

EXAMPLE 19-2

Calculate the relative number of protons in the higher and lower magnetic states when a sample is placed in a 4.69 T field at 20°C.

Solution

Substituting numerical values into Equation 19-7 gives

$$\frac{N_j}{N_0} = \exp\left(\frac{-(2.68 \times 10^8\ \mathrm{T^{-1}\,s^{-1}})(6.63 \times 10^{-34}\ \mathrm{J \cdot s})(4.69\ \mathrm{T})}{2\pi(1.38 \times 10^{-23}\ \mathrm{J\,K^{-1}})(293\ \mathrm{K})}\right)$$
$$= e^{-3.28 \times 10^{-5}} = 0.999967$$

or

$$\frac{N_0}{N_j} = 1.000033$$

Thus, for exactly 10^6 protons in higher energy states there will be

$$N_0 = 10^6/0.999967 = 1{,}000{,}033$$

in the lower energy state. This figure corresponds to a 33-ppm excess.

If we expand the right side of Equation 19-7 as a Maclaurin series and truncate the series after the second term, we obtain the important result that

$$\frac{N_j}{N_0} = 1 - \frac{\nu h B_0}{2\pi kT} \tag{19-8}$$

Equation 19-8 demonstrates that the relative number of excess low-energy nuclei is linearly related to the magnetic field strength. Thus, the intensity of an NMR signal increases linearly as the field strength increases. This dependence of signal sensitivity on magnetic field strength has led manufacturers to produce magnets with field strengths as large as 23.5 T (1 GHz proton resonance).

19A-2 Classical Description of NMR

To understand the absorption process, and in particular the measurement of absorption, a classical picture of the behavior of a charged particle in a magnetic field is helpful.

Precession of Nuclei in a Field

Let us first consider the behavior of a nonrotating magnetic body, such as a compass needle, in an external magnetic field. If momentarily displaced from alignment with the field, the needle will swing in a plane about its pivot as a consequence of the force exerted by the field on its two ends; in the absence of friction, the ends of the needle will fluctuate back and forth indefinitely about the axis of the field. A quite different motion occurs, however, if the magnet is spinning rapidly around its north-south axis. Because of the gyroscopic effect, the force applied by the field to the axis of rotation causes movement not in the plane of the force but perpendicular to this plane; the axis of the rotating particle, therefore, moves in a circular path. That is, the rotational axis of the rotating particle precesses around the vector representing the

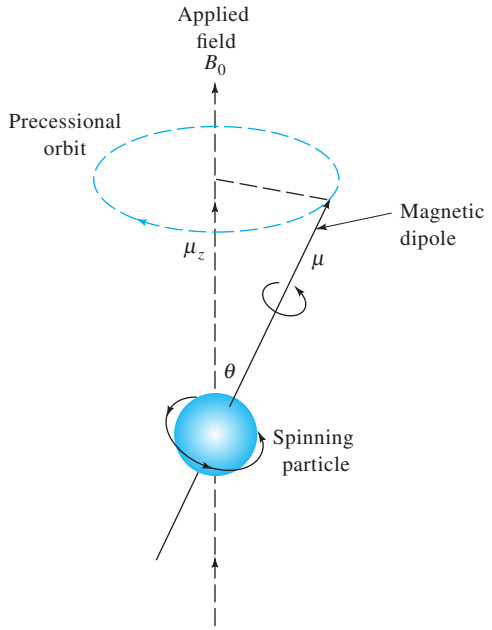

FIGURE 19-2 Precession of a rotating particle in a magnetic field.

applied magnetic field. This motion, illustrated in Figure 19-2, is similar to the motion of a gyroscope when it is displaced from the vertical by application of a lateral force. The angular velocity of this motion ω_0, in radians per second, is given by

$$\omega_0 = \gamma B_0 \tag{19-9}$$

The angular velocity can be converted to the frequency of precession ν_0, known as the *Larmor frequency*, by dividing by 2π. Thus,

$$\nu_0 = \frac{\gamma B_0}{2\pi} \tag{19-10}$$

A comparison of Equation 19-10 with Equation 19-5 reveals that the Larmor frequency is identical to the frequency of absorbed radiation derived from quantum mechanical considerations.

Absorption in CW Experiments

The potential energy E of the precessing charged particle shown in Figure 19-2 is given by

$$E = -\mu_z B_0 = -\mu B_0 \cos\theta \tag{19-11}$$

where θ is the angle between the magnetic field vector and the spin axis of the particle, μ is the magnetic moment of the particle, and μ_z is the component of μ in the direction of the magnetic field. When RF energy is absorbed by a nucleus, its angle of precession θ must change. Hence, we imagine for a nucleus having a spin quantum number of 1/2 that absorption involves a flipping of the magnetic moment oriented in the field direction to the opposite direction. The process is pictured in Figure 19-3. For the magnetic dipole to flip, there must be a magnetic force at right angles to the fixed field that moves in a circular path in phase with the precessing dipole. The magnetic moment of *circularly polarized radiation* of a suitable frequency has these necessary properties; that is, the magnetic vector of such radiation has a circular component, as represented by the dashed circle in Figure 19-3.[4] If the rotational frequency of the magnetic vector of the radiation is the same as the precessional frequency of a nucleus, absorption and flipping can occur. As discussed in the next paragraph, circularly polarized radiation of suitable frequency can be produced by an RF oscillator coil.

The radiation produced by the coil of an RF oscillator, which serves as the source in NMR instruments, is plane polarized. Plane-polarized radiation, however, consists of d and l circularly polarized radiation. As shown in Figure 19-4b, the vector of the d component rotates clockwise as the radiation approaches the observer; the vector of the l component rotates in the opposite sense. Addition of the two vectors leads to a vector sum that vibrates in a single plane (Figure 19-4a).

Thus, electromagnetic radiation from an oscillator coil oriented at 90° to the direction of the fixed magnetic field introduces circularly polarized radiation into the sample volume in the proper plane for absorption by sample nuclei. Only the magnetic component of the excitation radiation that rotates in the precessional direction is absorbed.

Relaxation Processes in NMR

When a nucleus is exposed to radiation of a suitable frequency, absorption occurs because of the slight excess of lower-energy-state nuclei present in the strong magnetic field. This excess is small, as indicated by the result of Example 19-2, so there is always danger that the absorption process will equalize the number of nuclei in the two states and cause the absorption signal to decrease and to approach zero. When this occurs, the spin system is said to be *saturated*. To avoid saturation, the rate of relaxation of excited nuclei to their lower energy state must be as great or greater than the rate at which they absorb the RF energy. One apparent relaxation path is the emission of radiation of a frequency corresponding to the energy difference between the states as occurs in fluorescence. Radiation theory, however, shows that the probability of spontaneous reemission of photons varies as the cube of the frequency and that at radio frequencies this process does not occur to a significant extent. In NMR studies, then, nonradiative relaxation processes are of prime importance.

To reduce saturation and produce a readily detectable absorption signal, relaxation should occur as rapidly as possible; that is, the lifetime of the excited state should be small. A second factor—the inverse relationship between the lifetime of an excited state and the width of its absorption line—negates

Tutorial: Learn more about **NMR theory** at www.tinyurl.com/skoogpia7

[4]It is important to note here that in contrast to optical spectroscopy, where it is the electric field of electromagnetic radiation that interacts with absorbing species, in NMR spectroscopy it is the *magnetic field* of the radiation that excites absorbing species.

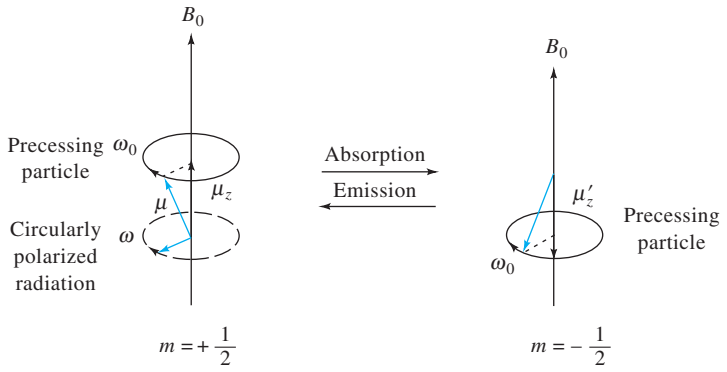

FIGURE 19-3 Model for the absorption of radiation by a precessing particle.

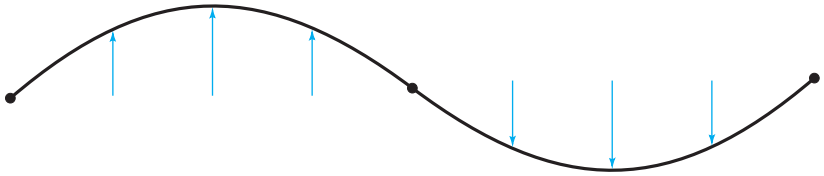

(a) Plane-polarized beam

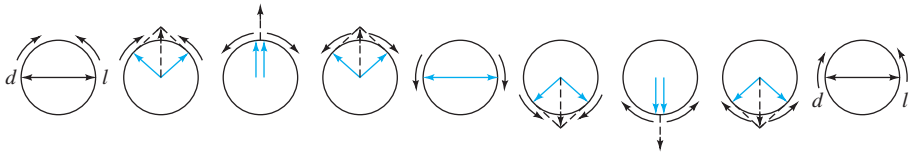

(b) *d*, *l* circularly polarized beams

FIGURE 19-4 Equivalency of a plane-polarized beam to two (*d*, *l*) circularly polarized beams of radiation.

the advantage of very short lifetimes. Thus, when relaxation rates are high, or the lifetimes low, line broadening prevents high-resolution measurements. These two opposing factors cause the optimal half-life for an excited species to range from about 0.1 to 10 s.

Two types of relaxation processes are important in NMR spectroscopy: (1) *spin-lattice*, or *longitudinal*, *relaxation* and (2) *spin-spin*, or *transverse*, *relaxation*.

Spin-Lattice Relaxation. The absorbing nuclei in an NMR experiment are part of the larger collection that constitute the sample. The entire collection is termed the *lattice*, regardless of whether the sample is a solid, a liquid, or a gas. In the latter two states, particularly, the various nuclei comprising the lattice are in violent vibrational and rotational motion, which creates a complex field about each magnetic nucleus. As a result, the lattice field contains a continuum of magnetic components, at least some of which must correspond in frequency and phase with the precessional frequency of the magnetic nucleus of interest. These vibrationally and rotationally developed components interact with and convert nuclei from a higher to a lower spin state. The absorbed energy then simply increases the amplitude of the thermal vibrations or rotations. This change produces a minuscule temperature rise in the sample.

Spin-lattice relaxation is a *first-order exponential decay* characterized by a relaxation time T_1, which is a measure of the average lifetime of the nuclei in the higher-energy state. The relaxation time not only depends on the magnetogyric ratio of the absorbing nuclei, but is also strongly influenced by the mobility of the lattice. In crystalline solids and viscous liquids, where mobilities are low, T_1 is large. As the mobility increases (at higher temperatures, for example), the vibrational and rotational frequencies increase, enhancing the probability of a magnetic fluctuation of the proper magnitude for a relaxation transition. As a consequence, T_1 becomes shorter. At very high mobilities, on the other hand, the fluctuation frequencies are further increased and spread over such a broad range that the probability of a suitable frequency for a spin-lattice transition again decreases. The result is a minimum in the relationship between T_1 and lattice mobility.

Spin-Spin Relaxation. Several other effects tend to diminish relaxation times and thereby broaden NMR lines. These effects are normally lumped together and described by a transverse, or spin-spin, relaxation time T_2. Values for T_2 are generally so small for crystalline solids or viscous liquids (as low as 10^{-4} s) as to preclude the use of samples of these kinds for high-resolution spectra unless special techniques are used. These techniques are described briefly in a later section dealing with ^{13}C NMR studies of solids.

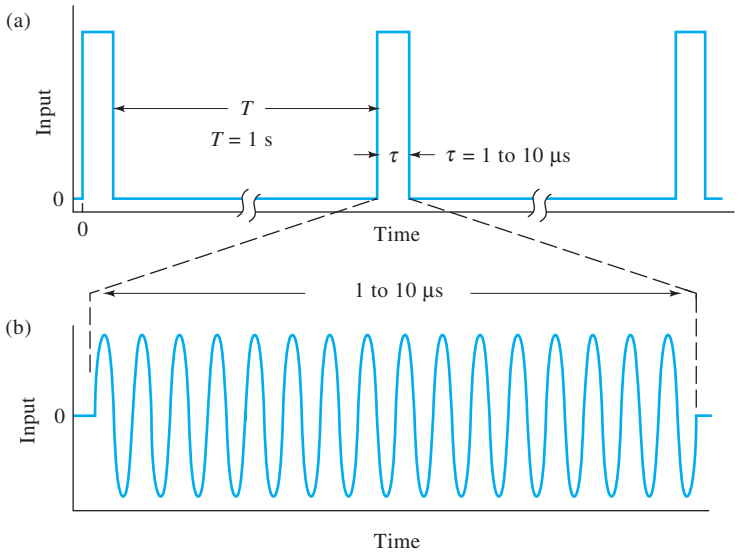

FIGURE 19-5 Typical input signal for pulsed NMR: (a) pulse sequence; (b) expanded view of RF pulse, typically at a frequency of several hundred MHz. The time axis is not drawn to scale.

When two neighboring nuclei of the same kind have identical precession rates, but are in different magnetic quantum states, the magnetic fields of each can interact to cause an interchange of states. That is, a nucleus in the lower spin state is excited, and the excited nucleus relaxes to the lower energy state. No net change in the relative spin-state population, and thus no decrease in saturation, results, but the average lifetime of a particular excited nucleus is shortened. Line broadening is the result.

Two other causes of line broadening should be noted. Both arise if B_0 in Equation 19-10 differs slightly from nucleus to nucleus. Under these circumstances, a band of frequencies, rather than a single frequency, is absorbed. One cause for such a variation in the static field is the presence in the sample of other magnetic nuclei whose spins create local fields that may enhance or diminish the external field acting on the nucleus of interest. In a mobile lattice, these local fields tend to cancel because the nuclei causing them are in rapid and random motion. In a solid or a viscous liquid, however, the local fields may persist long enough to produce a range of field strengths and thus a range of absorption frequencies. Variations in the static field also result from small inhomogeneities in the source field itself. This effect can be largely offset by rapidly spinning the entire sample in the magnetic field.

19A-3 Fourier Transform NMR

In pulsed NMR measurements,[5] nuclei in a strong magnetic field are subjected periodically to very brief pulses of intense RF radiation as shown in Figure 19-5. The waveform in part (a) of the figure illustrates the pulse train, pulse width, and time interval between pulses. The expanded view of one of the pulses shows that each pulse is actually a packet of RF radiation. The waveforms are intended to be illustrative and are not drawn to scale. The packet of radiation consists of many more cycles than are depicted. The length of the pulses τ is usually less than 10 μs, and the frequency of the radiation is on the order of 10^2 to 10^3 MHz. The interval between pulses T is typically one to several seconds. The pulse excites a transient signal, called the *free-induction decay* (FID), which occurs as the nuclei relax during time T. The FID signal can be detected with a radio receiver coil perpendicular to the static magnetic field. Often, a single coil is used to both irradiate the sample with RF pulses and detect the decay signal. The FID signal is digitized and stored in a computer for data processing. Ordinarily, the time-domain decay signals from numerous successive pulses are added to improve the signal-to-noise ratio as described in Section 5C-2. The resulting summed data are then converted to a frequency-domain signal by a Fourier transformation, and finally, digital filtering may be applied to the data to further increase the signal-to-noise ratio. The resulting frequency-domain output is similar to the spectrum produced by a scanning CW experiment.

To describe the events that occur in a pulsed NMR experiment, it is helpful to use a set of Cartesian coordinates with the magnetic field pointing along the z-axis as shown in Figure 19-6a. The narrow arrows are the magnetic moment vectors of a few of the nuclei in the lower energy ($m = +1/2$) state. The orientations of these vectors around the z-axis are random, and they are rotating at the Larmor frequency ν_0. These excess nuclei impart a stationary net magnetic moment M aligned along the z-axis as shown by the blue arrow.

[5]For more extensive discussions see H. Friebolin, *Basic One- and Two-Dimensional NMR Spectroscopy*, 5th ed., Weinheim, Germany: Wiley-VCH, 2011; J. Keeler, *Understanding NMR Spectroscopy*, 2nd ed., Chichester, UK: Wiley, 2010; J. B. Lambert, E. P. Mazzola, *Nuclear Magnetic Resonance Spectroscopy*, Upper Saddle River, NJ: Pearson/Prentice-Hall, 2004; S. Berger and S. Braun, *200 and More NMR Experiments*, New York: Wiley-VCH, 2004.

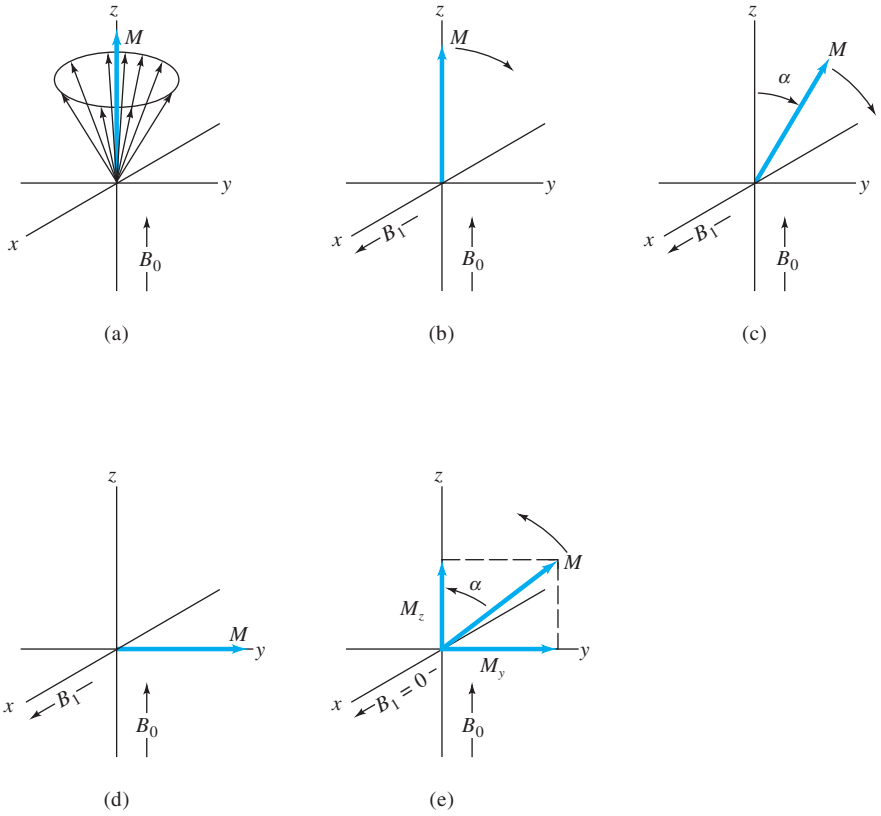

FIGURE 19-6 Behavior of magnetic moments of nuclei in a rotating field of reference, 90° pulse experiment: (a) magnetic vectors of excess lower-energy nuclei just before pulse; (b), (c), (d) rotation of the sample magnetization vector *M* during lifetime of the pulse; (e) relaxation after termination of the pulse.

It is helpful in the discussion that follows to imagine that the coordinates in Figure 19-6 are rotating around the *z*-axis at exactly the Larmor frequency. With such a rotating frame of reference, the individual magnetic moment vectors in Figure 19-6a become fixed in space at the orientation shown in the figure. Unless otherwise noted, the remaining parts of this figure are discussed in terms of this *rotating frame of reference* rather than a static, or *laboratory, frame of reference*.

Pulsed Excitation

Figure 19-6b shows the position of the net magnetic moment at the instant the pulse of RF radiation, traveling along the *x*-axis, strikes the sample. The magnetic field of the incident electromagnetic radiation is given the symbol B_1. In the rotating frame, B_1 and the sample magnetization vector *M* are both static, one along the *x*-axis and the other at right angles to it. Basic physics tells us that, with each pulse, *M* experiences a torque that tips it off the *z*-axis. As shown in Figure 19-6c and d, this torque rotates the sample magnetic moment *M* around the *x*-axis in the *yz* plane.[6] The extent of rotation depends on the length of the pulse τ as given by the equation

$$\alpha = \gamma B_1 \tau \tag{19-12}$$

where α is the angle of rotation in radians. For many Fourier transform experiments, a pulse length is chosen so that α is 90°, or $\pi/2$ radians, as shown in Figure 19-6d. Typically, the time required to achieve this angle is 1 to 10 μs. Once the pulse is terminated, nuclei begin to relax and return to their equilibrium position as shown in Figure 19-6e. As discussed in the previous section, relaxation takes place by two independent mechanisms: spin-lattice and spin-spin interactions. After several seconds, as a result of these interactions, the nuclei return to their original state as depicted in Figure 19-6a.

When a nucleus returns to its equilibrium state after being tipped by a pulse of RF radiation as shown in Figure 19-6e, the magnetic moment M_y along the *y*-axis decreases and the magnetic moment M_z along the *z*-axis increases. Figure 19-7 provides a more detailed picture of the mechanisms of the two relaxation processes as viewed now in the stationary frame of reference. In spin-lattice relaxation, the magnetization along the *z*-axis increases until it returns to its original value as shown in Figure 19-6a. In spin-spin relaxation, nuclei exchange spin energy with one another so that some now precess faster than the Larmor frequency and others proceed more slowly.

[6] An insight into why NMR is a "resonance" technique can be gained from Figure 19-6. Resonance is a condition in which energy is transferred in such a way that a small periodic perturbation produces a large change in some parameter of the system being perturbed. NMR is a resonance technique because the small periodic perturbation B_1 produces a large change in the orientation of the sample magnetization vector *M* (Figure 19-6d). In most experiments, B_1 is two or more orders of magnitude smaller than B_0.

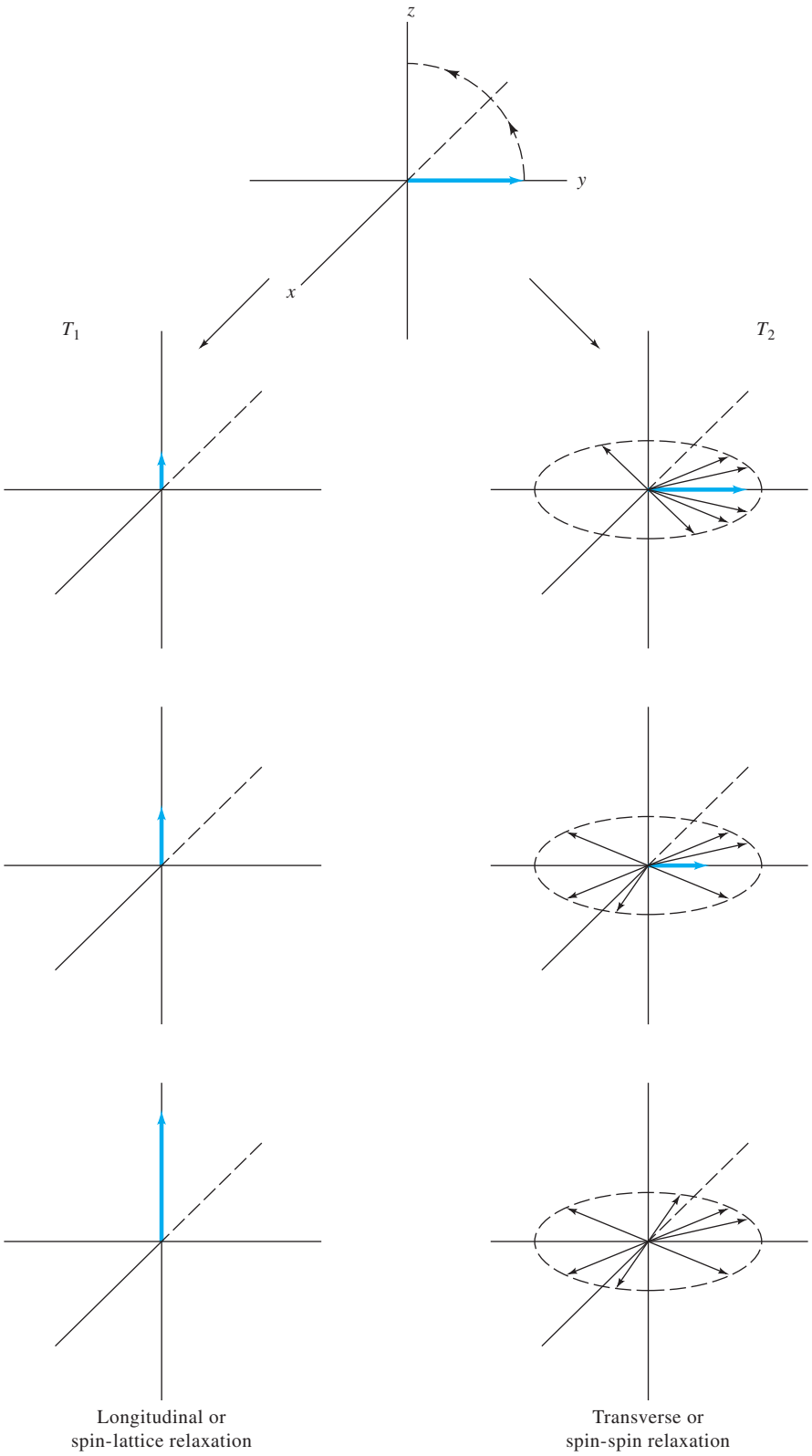

FIGURE 19-7 Two nuclear relaxation processes. Longitudinal (spin-lattice) relaxation takes place in the *xy* plane; transverse (spin-spin) relaxation in the *xy* plane. (Courtesy of Professor Stanford L. Smith, University of Kentucky, Lexington, KY.)

The result is that the spins begin to fan out in the *xy* plane as shown on the right-hand side of Figure 19-7. Ultimately, this leads to a decrease to zero of the magnetic moment along the *y*-axis. No residual magnetic component can remain in the *xy* plane by the time relaxation is complete along the *z*-axis, which means that $T_2 \leq T_1$.

Free-Induction Decay

Let us turn again to Figure 19-6d and consider the situation when the signal B_1 goes to zero at the end of the pulse. Now, however, it is useful to picture what is happening in the static frame of reference rather than the rotating frame. If the coordinates are fixed, the magnetic moment M must now rotate clockwise around the *z*-axis at the Larmor frequency. This motion gives rise to an RF signal that can be detected by a coil along the *x*-axis. As mentioned earlier, it can be detected with the same coil used to produce the original pulse. As relaxation proceeds, this signal decreases exponentially and approaches zero as the magnetic vector approaches the *z*-axis. This time-domain signal is the FID, which is eventually converted to a frequency-domain signal by the Fourier transformation.

Figure 19-8 illustrates the FID that is observed for ^{13}C nuclei when they are excited by an RF pulse having a frequency that is *exactly* the same as the Larmor frequency of the nuclei. The signal is produced by the four ^{13}C nuclei in dioxane, which behave identically in the magnetic field. The FID in Figure 19-8a is an exponential curve that approaches zero after a few tenths of a second. The apparent noise superimposed on the decay pattern is an experimental artifact caused by spinning sidebands and for the purposes of our discussion can be disregarded. Figure 19-8b is the Fourier transform of

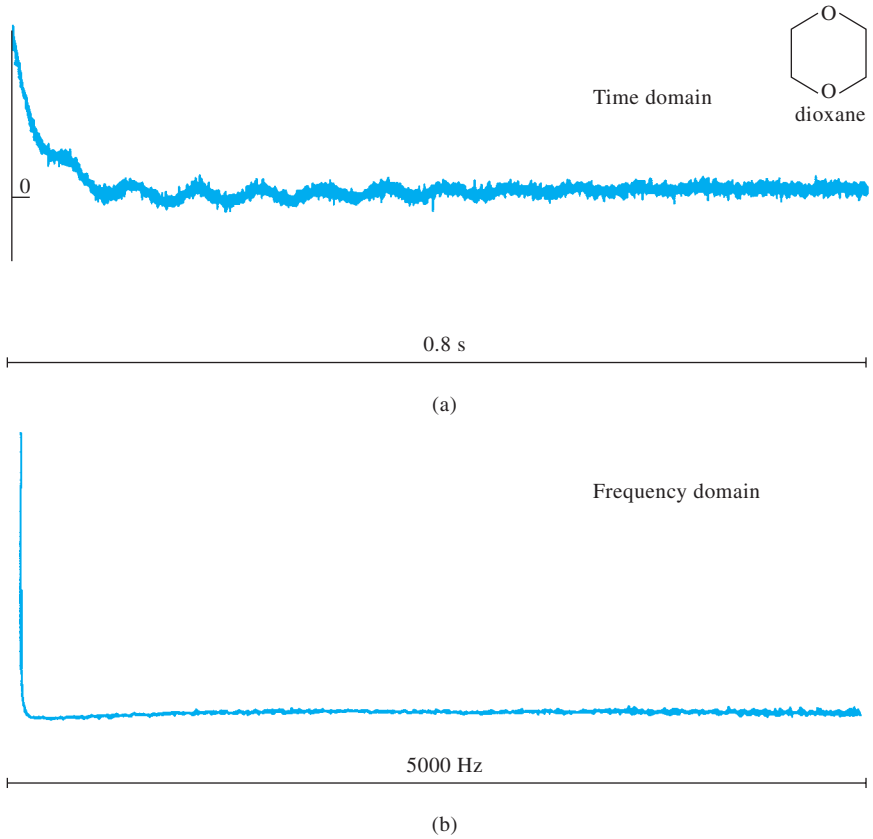

FIGURE 19-8 (a) ^{13}C FID signal for dioxane when pulse frequency is identical to Larmor frequency; (b) Fourier transform of (a). (From R. J. Abraham, J. Fisher, and P. Loftus, *Introduction to NMR Spectroscopy*, p. 89, New York: Wiley, 1988. Reprinted by permission of John Wiley & Sons, Inc.)

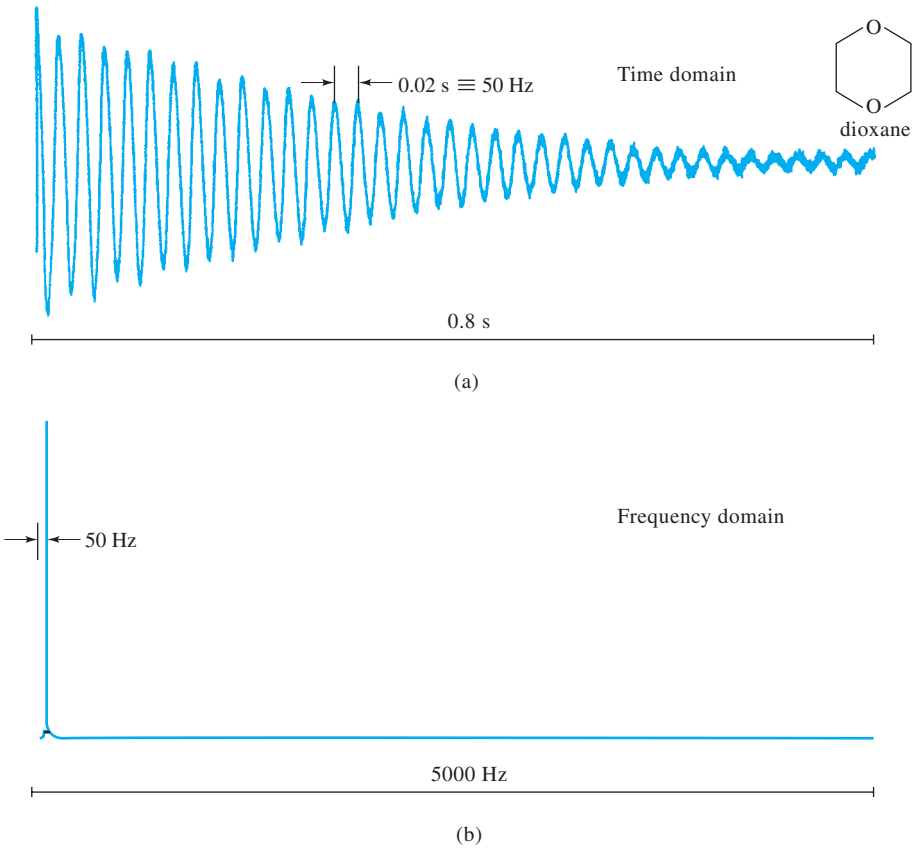

FIGURE 19-9 (a) ^{13}C FID signal for dioxane when pulse frequency differs from Larmor frequency by 50 Hz; (b) Fourier transform of (a). (From R. J. Abraham, J. Fisher, and P. Loftus, *Introduction to NMR Spectroscopy*, p. 90, New York: Wiley, 1988. Reprinted by permission of John Wiley & Sons, Inc.)

the curve in Figure 19-8a, which shows on the left the single ^{13}C absorption peak for dioxane. When the irradiation frequency ν differs from the Larmor frequency $\omega_0/2\pi$ by a small amount, as it usually will, the exponential decay is modulated by a sine wave of frequency $|\nu - (\omega_0/2\pi)|$. This effect is shown in Figure 19-9, in which the difference in the two frequencies is 50 Hz.

When magnetically different nuclei are present, the FID develops a distinct beat pattern such as that in Figure 19-10a, which is the spectrum for the ^{13}C nuclei in cyclohexene. This compound contains three pairs of magnetically different carbon atoms: the pair of olefinic carbons, the pair of aliphatic carbons adjacent to the olefinic pair, and the pair directly opposite the olefinic group. The lines in Figure 19-10b that differ by 62 Hz arise from the two pairs of aliphatic carbon atoms. The pair of olefinic carbons is responsible for the single resonance on the left. With compounds having several absorption lines, the FID becomes very complex. In every case, however, the time-domain decay signal contains all of the information required to produce an absorption spectrum in the frequency domain using Fourier transformation.

19A-4 Types of NMR Spectra

There are several types of NMR spectra, depending on the kind of instrument used, the type of nucleus involved, the physical state of the sample, the environment of the analyte nucleus, and the purpose of the data collection. Most NMR spectra can, however, be categorized as either *wide line* or *high resolution*.

Wide-Line Spectra

Wide-line spectra are those in which the bandwidth of the source of the lines is large enough that the fine structure due to the chemical environment is obscured. Figure 19-11 is a wide-line spectrum for a mixture of several isotopes. A single resonance is associated with each species. Wide-line spectra are useful for the quantitative determination of isotopes and for studies of the physical environment of the absorbing species. Wide-line spectra are usually obtained at relatively low magnetic field strength.

High-Resolution Spectra

Most NMR spectra are *high resolution* and are collected by instruments capable of differentiating between very small

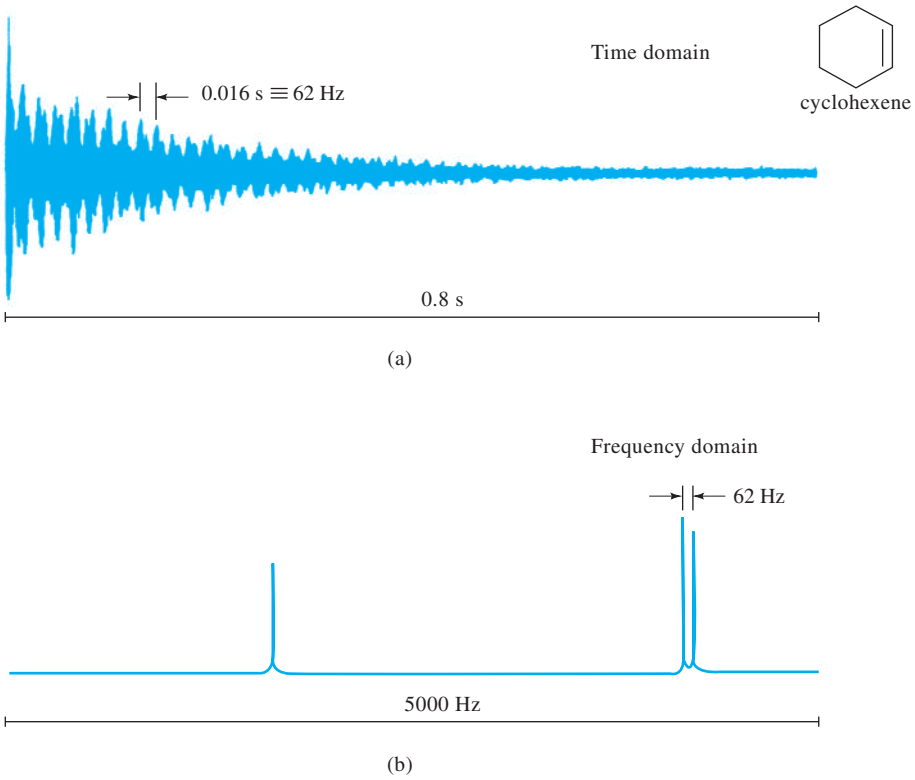

FIGURE 19-10 (a) ^{13}C FID signal for cyclohexene; (b) Fourier transform of (a). (From R. J. Abraham, J. Fisher, and P. Loftus, *Introduction to NMR Spectroscopy*, p. 91, New York: Wiley, 1988. Reprinted by permission of John Wiley & Sons, Inc.)

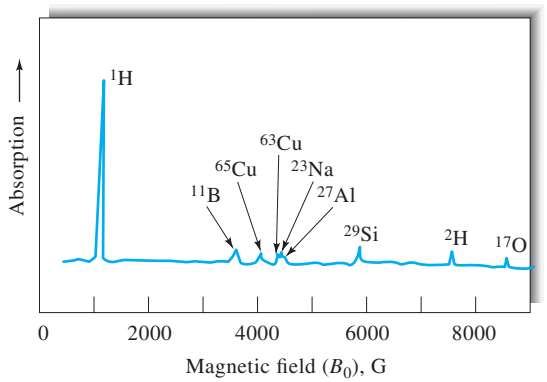

FIGURE 19-11 A low-resolution NMR spectrum of water in a glass container. Frequency = 5 MHz.

frequency differences of 0.01 ppm or less. For a given isotope such spectra usually exhibit several resonances that result from differences in their chemical environment. Figure 19-12 illustrates two spectra of different resolution for the protons in ethanol. In the upper spectrum, three peaks arise from absorption by the CH_3, CH_2, and OH protons. As shown in the higher-resolution spectrum of Figure 19-12b, two of the three peaks can be resolved into additional resonances. The discussions that follow deal exclusively with high-resolution spectra.

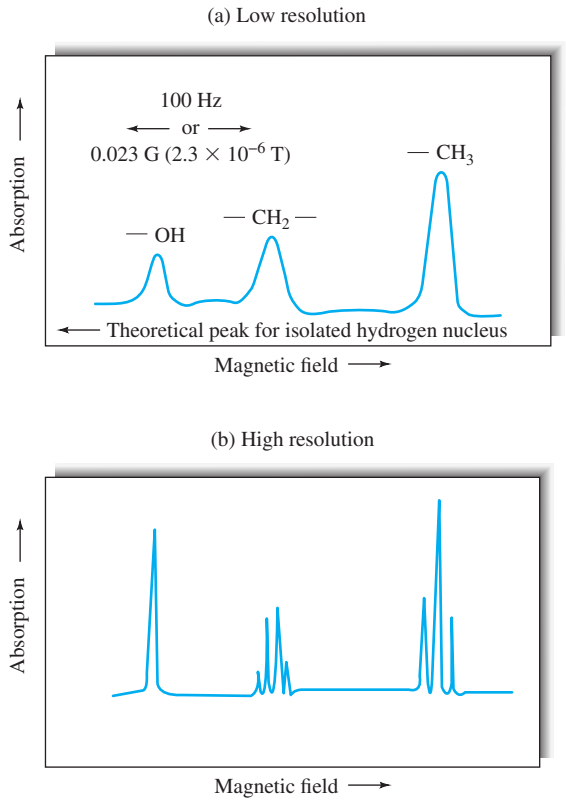

FIGURE 19-12 NMR spectra of ethanol at a frequency of 60 MHz. Resolution: (a) ~$1/10^6$; (b) ~$1/10^7$.

19B ENVIRONMENTAL EFFECTS ON NMR SPECTRA

The frequency of RF radiation that is absorbed by a given nucleus is strongly affected by its chemical environment—that is, by nearby electrons and nuclei. As a result, even simple molecules provide a wealth of spectral information that can be used to elucidate their chemical structure. The discussion that follows emphasizes proton spectra because ^{1}H is the isotope that has been studied most widely. Most of the concepts of this discussion also apply to the spectra of other isotopes as well.

19B-1 Types of Environmental Effects

The spectra for ethyl alcohol, shown in Figure 19-12, illustrate two types of environmental effects. The spectrum in Figure 19-12a, obtained with a lower-resolution instrument, shows three proton peaks with areas in the ratio 1:2:3 (left to right). On the basis of this ratio, it is logical to attribute the peaks to the hydroxyl, the methylene, and the methyl protons, respectively. This conclusion is confirmed by replacing the hydrogen atom of the hydroxyl group with deuterium in which case the first peak disappears from this part of the spectrum. We note in Figure 19-12a that the small differences that occur in the resonance frequency of the proton depend on the group to which the hydrogen atom is attached. This effect is called the *chemical shift*.

The higher-resolution spectrum of ethanol, shown in Figure 19-12b, reveals that two of the three proton resonances are split into additional peaks. This secondary environmental effect, which is superimposed on the chemical shift, has a different cause and is termed *spin-spin splitting*.

Both the chemical shift and spin-spin splitting are important in structural analysis. Experimentally, the two are easily distinguished, because the peak separations resulting from a chemical shift are directly proportional to the field strength or to the oscillator frequency. Thus, if the spectrum in Figure 19-12a is acquired at 100 MHz rather than at 60 MHz, the horizontal distance between any set of resonances is increased by 100/60 as illustrated in Figure 19-13. In contrast, the distance between the fine-structure peaks within a group, caused by spin-spin coupling, is not altered by this frequency change.

Origin of the Chemical Shift

The chemical shift is caused by small magnetic fields generated by electrons as they circulate around nuclei. These fields usually oppose the applied field. As a consequence, the nuclei are exposed to an effective field that is usually somewhat smaller than the external field. The magnitude of the field developed internally is directly proportional to the applied external field, so that we may write

$$B_0 = B_{\text{appl}} - \sigma B_{\text{appl}} = B_{\text{appl}}(1 - \sigma) \qquad (19\text{-}13)$$

where B_{appl} is the magnitude of the applied field and B_0 *is the magnitude of the resultant field, which determines the resonance behavior of the nucleus*. The quantity σ is the *shielding constant*, which is determined by the electron density and its spatial distribution around the nucleus. The electron density depends on the

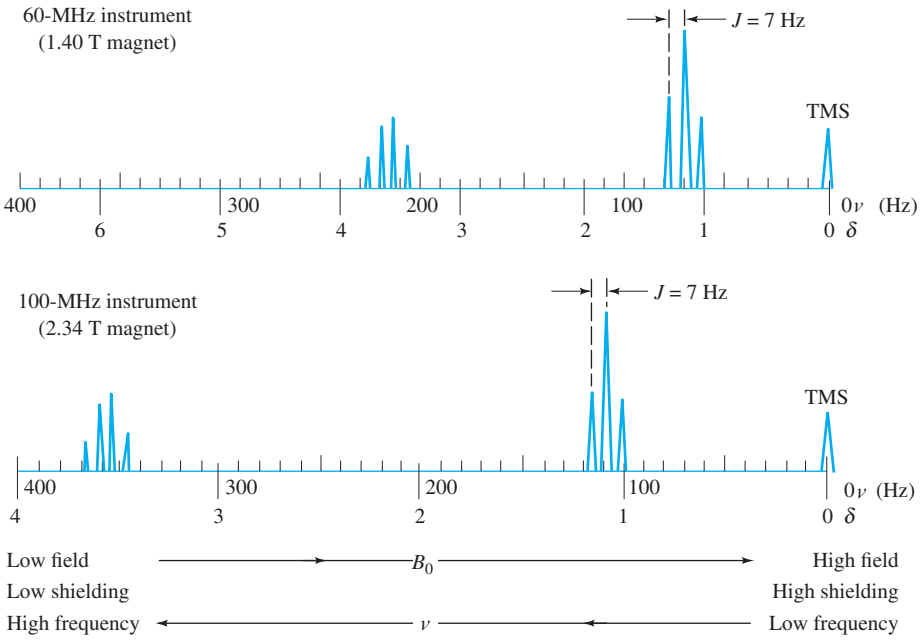

FIGURE 19-13 Abscissa scales for NMR spectra.

structure of the compound containing the nucleus. Substituting Equation 19-5 into Equation 19-13 gives the resonance condition in terms of frequency. That is,

$$\nu_0 = \frac{\gamma}{2\pi} B_0(1 - \sigma) = k(1 - \sigma) \tag{19-14}$$

where $k = \gamma B_0/2\pi$.

The shielding constant for protons in a methyl group is larger than the corresponding constant for methylene protons, and it is even smaller for the proton in an —OH group. For an isolated hydrogen nucleus, the shielding constant is zero. Thus, to bring any of the protons in ethanol into resonance at a given excitation oscillator frequency ν, it is necessary to apply a field B_{appl} that is greater than B_0 (Equation 19-13), the resonance value for the isolated proton. Alternatively, if the applied field is held constant, the oscillator frequency must be increased to bring about the resonance condition. Because σ differs for protons in various functional groups, the required applied field differs from group to group. This effect is shown in the ethanol spectrum of Figure 19-12a, in which the hydroxyl proton appears at the lowest applied field, the methylene protons next, and finally the methyl protons. Notice that all of these resonances occur at an applied field greater than the theoretical one for the isolated hydrogen nucleus, which lies far to the left of the spectra of Figure 19-12a. Note also that if the strength of the applied magnetic field is held constant at a level necessary to excite the methyl proton, the frequency must be increased to bring the methylene protons into resonance.

Origin of Spin-Spin Splitting

The splitting of chemical-shift resonances occurs as the magnetic moment of a nucleus interacts with the magnetic moments of immediately adjacent nuclei. The magnetic field created by a spinning nucleus affects the distribution of electrons in its bonds to other nuclei. This change in electron distribution then produces changes in the magnetic fields of adjacent nuclei and causes splitting of energy levels and hence multiple transitions. This magnetic coupling of nuclei that is transmitted by bonding electrons is often referred to as a *polarization interaction*. Thus, the fine structure of the methylene peak shown in Figure 19-12b can be attributed to the effect of the spins of the adjacent methyl protons. Conversely, the splitting of the methyl peak into three smaller peaks is caused by the adjacent methylene protons. These effects are independent of the applied field and are superimposed on the effects of the chemical shift. Spin-spin splitting is discussed in greater detail in Section 19B-3.

Abscissa Scales for NMR Spectra

The determination of the absolute magnetic field strength with the accuracy required for high-resolution NMR measurements is difficult or impossible. On the other hand, as will be shown in Section 19C, it is entirely feasible to determine the magnitude of a *change* in field strength to within a tenth of a milligauss or better. Thus, it is expedient to report the position of resonances relative to the resonance for an internal standard substance that can be measured during the experiment. The use of an internal standard is also advantageous in that chemical shifts can be reported in terms that are independent of the oscillator frequency.

The internal standard used depends on the nucleus being studied and the solvent system. The compound most generally used for proton studies is tetramethylsilane (TMS), $(CH_3)_4Si$. All of the protons in this compound are identical; and for reasons to be considered later, the shielding constant for TMS is larger than for most other protons. Thus, the compound provides a single sharp line at a high applied field that is nearly always isolated from the resonances of interest in a spectrum. In addition, TMS is inert, readily soluble in most organic liquids, and easily removed from samples by distillation (boiling point = 27°C). Unfortunately, TMS is not water soluble; in aqueous media, the sodium salt of 2,2-dimethyl-2-silapentane-5-sulfonic acid (DSS), $(CH_3)_3SiCH_2CH_2CH_2SO_3Na$, is often used in its place. The methyl protons of this compound produce a line at virtually the same place in the spectrum as that of TMS. The methylene protons of DSS give a series of small resonances that may interfere, however. For this reason, most DSS on the market has the methylene groups deuterated, which eliminates these undesirable absorptions.

To express the chemical shift for a sample nucleus relative to TMS in quantitative terms when measurements are made at a constant field strength B_0, we apply Equation 19-14 to the sample and the TMS resonances to obtain

$$\nu_s = k(1 - \sigma_s) \tag{19-15}$$

$$\nu_r = k(1 - \sigma_r) \tag{19-16}$$

where the subscripts r and s refer to the TMS reference and the analyte sample, respectively. Subtracting the first equation from the second gives

$$\nu_r - \nu_s = k(\sigma_s - \sigma_r) \tag{19-17}$$

Dividing this equation by Equation 19-15 to eliminate k gives

$$\frac{\nu_r - \nu_s}{\nu_r} = \frac{\sigma_r - \sigma_s}{1 - \sigma_r}$$

Generally, σ_r is much less than 1, so that this equation simplifies to

$$\frac{\nu_r - \nu_s}{\nu_r} = \sigma_r - \sigma_s \tag{19-18}$$

We then define the *chemical-shift parameter* δ as

$$\delta = (\sigma_r - \sigma_s) \times 10^6 \tag{19-19}$$

The quantity δ is dimensionless and expresses the relative shift in parts per million. A distinct advantage of this approach is that for a given resonance, δ is the same regardless of whether a 200- or a 800-MHz instrument is used. Most proton resonances lie in the δ range of 1 to 13. For other nuclei, the range of chemical shifts is greater because of the associated 2*p* electrons.

For example, the chemical shift for ^{13}C in various functional groups typically lies in the range 0 to 220 ppm but may be as large as 400 ppm or more. For ^{19}F, the range of chemical shifts may be as large as 800 ppm, whereas for ^{31}P it is 300 ppm or more.

Generally, NMR spectra are plotted with the abscissa linear in δ, and historically the data were plotted with the field increasing from left to right (see Figure 19-13). Thus, if TMS is used as the reference, its resonance appears on the far right-hand side of the plot, because σ for TMS is quite large. As shown, the zero value for the δ scale corresponds to the TMS peak, and the value of δ increases from right to left. Refer again to Figure 19-13 and note that the various peaks appear at the same δ value despite the two spectra having been obtained with instruments having markedly different fixed fields.

Spin-spin splitting is generally reported in units of hertz. It can be seen in Figure 19-13 that the spin-spin splitting in frequency units (J) is the same for the 60-MHz and the 100-MHz instruments. Note, however, that the chemical shift *in frequency units* is enhanced with the higher-frequency instrument.

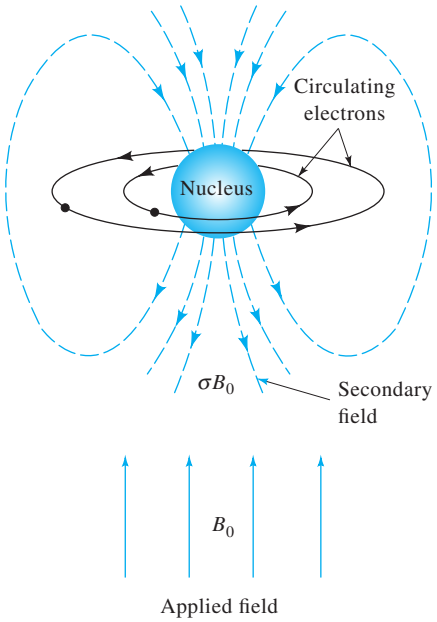

FIGURE 19-14 Diamagnetic shielding of a nucleus.

19B-2 Theory of the Chemical Shift

As noted earlier, chemical shifts arise from the secondary magnetic fields produced by the circulation of electrons in the molecule. These so-called local *diamagnetic currents*[7] are induced by the fixed magnetic field and result in secondary fields that may either decrease or enhance the field to which a given proton responds. The effects are complex, and we consider only the major aspects of the phenomenon here. More complete treatments can be found in several reference works.[8]

Under the influence of the magnetic field, electrons bonding the proton tend to precess around the nucleus in a plane perpendicular to the magnetic field (see Figure 19-14). A consequence of this motion is the development of a secondary field, which opposes the primary field, analogous to what happens when electrons pass through a wire loop. The nucleus then experiences a resultant field that is smaller, so the nucleus is said to be *shielded* from the full effect of the primary field. As a consequence, the external field must be increased to cause nuclear resonance.

The shielding experienced by a given nucleus is directly related to the electron density surrounding it. Thus, in the absence of the other influences, shielding would be expected to decrease with increasing electronegativity of adjacent groups. This effect is illustrated by the δ values for the protons in the methyl halides, CH_3X, which lie in the order I (2.16), Br (2.68), Cl (3.05), and F (4.26). In this example, the least electronegative halogen, iodine, is also the least effective at withdrawing electrons from the methyl protons. Thus, the electrons of iodine provide the smallest shielding effect. The position of the proton peaks in TMS is also explained by this model, because silicon is relatively electropositive.

Effect of Magnetic Anisotropy

An examination of the spectra of compounds containing double or triple bonds reveals that local diamagnetic effects are not sufficient to explain the position of certain proton resonances. Consider, for example, the irregular change in δ values for protons in the following hydrocarbons, arranged in order of increasing acidity, or increased electronegativity, of the groups to which the protons are bonded: $CH_3{-}CH_3$ ($\delta = 0.9$), $CH_2{=}CH_2$ ($\delta = 5.8$), and $HC{\equiv}CH$ ($\delta = 2.9$). Furthermore, the aldehydic proton RCHO ($\delta \approx 10$) and the protons in benzene ($\delta \approx 7.3$) appear considerably farther downfield than is expected on the basis of the electronegativity of the attached groups.

The effects of multiple bonds on the chemical shift can be explained by taking into account the anisotropic magnetic properties of these compounds. For example, the magnetic susceptibilities[9] of crystalline aromatic compounds have been found to differ appreciably from one another, depending on the orientation

[7]The intensity of magnetization induced in a diamagnetic substance is smaller than that produced in a vacuum with the same field. Diamagnetism is the result of motion induced in bonding electrons by the applied field; this motion, termed a *diamagnetic current*, creates a secondary field that opposes the applied field. Paramagnetism and the resulting *paramagnetic currents* operate in just the opposite sense.

[8]See, for example, J. B. Lambert, E. P. Mazzola, *Nuclear Magnetic Resonance Spectroscopy*, Upper Saddle River, NJ: Pearson/Prentice-Hall, 2004; E. D. Becker, *High Resolution NMR*, 3rd ed., New York: Academic Press, 2000.

[9]The magnetic susceptibility of a substance can be thought of as the extent to which it is susceptible to induced magnetization by an external field.

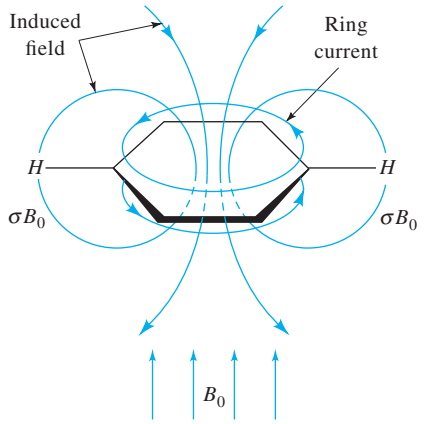

FIGURE 19-15 Deshielding of aromatic protons brought about by ring current.

of the ring with respect to the applied field. This anisotropy can be understood from the model shown in Figure 19-15. In this model, the plane of the ring is perpendicular to the magnetic field. In this position, the field can induce a flow of the π electrons around the ring to create a so-called ring current. A ring current is similar to a current in a wire loop; that is, a secondary field is induced that acts in opposition to the applied field. This induced field, however, exerts a magnetic effect on the protons attached to the ring in the direction of the field as shown in Figure 19-15. Thus, the aromatic protons require a lower external field to bring them into resonance. This effect is either absent or self-canceling in other orientations of the ring.

An analogous model operates for ethylenic or carbonyl double bonds. In such cases, we may imagine π electrons circulating in a plane along the bond axis when the molecule is oriented with the field, as presented in Figure 19-16a. Again, the secondary field produced acts on the proton to reinforce the applied field. Thus, deshielding shifts the peak to larger values

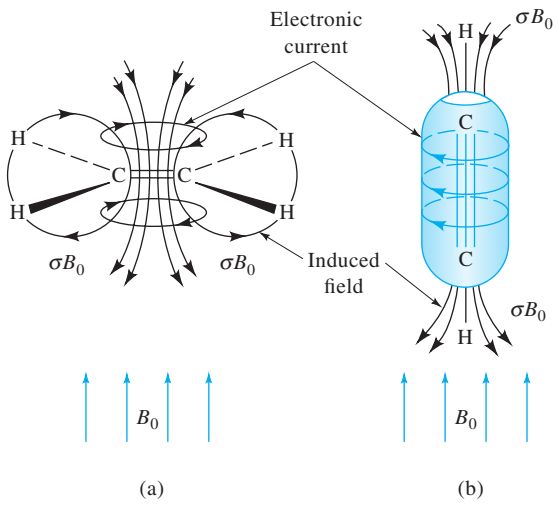

FIGURE 19-16 Deshielding of ethylene and shielding of acetylene brought about by electronic currents.

of δ. With an aldehyde, this effect combines with the deshielding brought about by the electronegative nature of the carbonyl group, and a very large value of δ results.

In an acetylenic bond, the symmetric distribution of π electrons about the bond axis permits electrons to circulate around the bond. In contrast, such circulation is prohibited by the nodal plane in the electron distribution of a double bond. From Figure 19-16b, we see that in this orientation the protons are shielded. This effect is apparently large enough to offset the deshielding resulting from the acidity of the protons and from the electronic currents at perpendicular orientations of the bond.

Correlation of Chemical Shift with Structure

The chemical shift is used to identify functional groups and to aid in determining structural arrangements of groups. These applications are based on empirical correlations between structure and shift. A number of correlation charts and tables[10] have been published, two of which are shown in Figure 19-17 and Table 19-2. Keep in mind that the exact values for δ may depend on the nature of the solvent as well as on the concentration of solute. These effects are particularly pronounced for protons involved in hydrogen bonding. An excellent example of this effect is the proton of the alcoholic functional group.

19B-3 Spin-Spin Splitting

As can be seen in Figures 19-12 and 19-13, the absorption bands for the methyl and methylene protons in ethanol consist of several narrow resonances that can be routinely separated with a high-resolution instrument. Careful examination shows that the spacing for the three components of the methyl band is identical to that for the four peaks of the methylene band. This spacing in hertz is called the *coupling constant* for the interaction and is given the symbol *J*. Moreover, the areas of the lines in a multiplet approximate an integer ratio to one another. Thus, for the methyl triplet, the ratio of areas is 1:2:1; for the quartet of methylene peaks, it is 1:3:3:1.

Origin

The splittings shown in Figure 19-13 can be attributed to the effect that the spins of one set of nuclei exert on the resonance behavior of another. In other words, there is a small interaction or coupling between the two adjacent groups of protons. The results of detailed theoretical calculations are consistent with the concept that coupling takes place via interactions between the nuclei and the bonding electrons rather than through free space. For our purposes only a brief discussion of the mechanism is necessary.

Let us first consider the effect of the methylene protons in ethanol on the resonance of the methyl protons. Recall that the ratio of protons in the two possible spin states is very nearly unity, even in a strong magnetic field. We then imagine that the two methylene protons in the molecule can have four possible

[10]R. M. Silverstein, F. X. Webster, D. Kiemle, and D. L. Bryce, *Spectrometric Identification of Organic Compounds*, 8th ed., Chap. 3, New York: Wiley, 2015; B. Lambert, E. P. Mazzola, *Nuclear Magnetic Resonance Spectroscopy*, Chap. 3, Upper Saddle River, NJ: Pearson/Prentice-Hall, 2004.

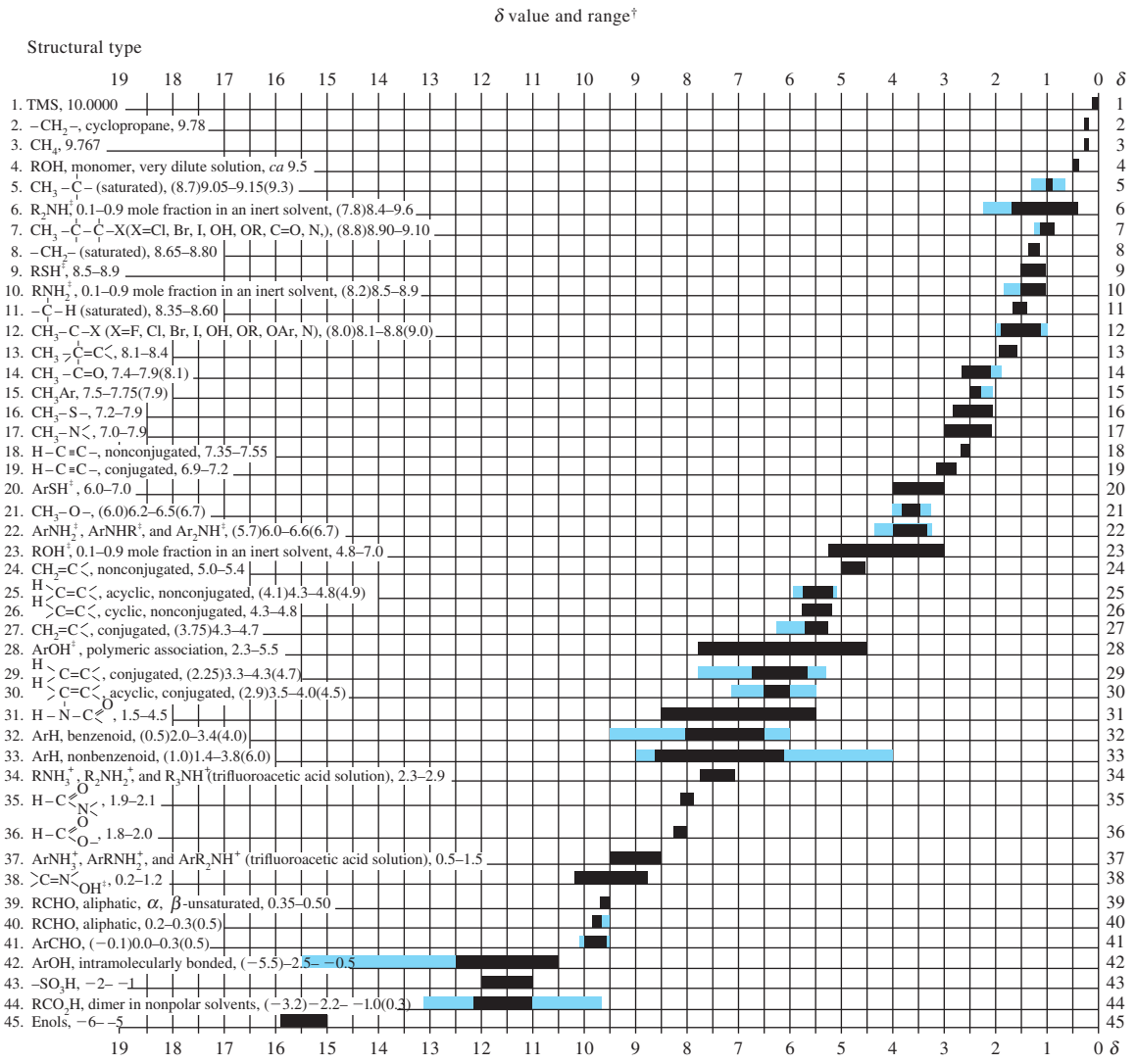

†Normally, absorptions for the functional groups indicated will be found within the range shown. Occasionally, a functional group will absorb outside this range. Approximate limits for this are indicated by absorption values in parentheses and by blue shading in the figure.
‡The absorption positions of these groups are concentration-dependent and are shifted to higher δ values in more dilute solutions.

FIGURE 19-17 Absorption positions of protons in various structural environments. (Table taken from J. R. Dyer, *Applications of Absorption Spectroscopy by Organic Compounds*, p. 85, Englewood Cliffs, NJ: Prentice-Hall, 1965. With permission.)

combinations of spin states and that in an entire sample the number of each of these combinations will be approximately equal. If we represent the spin orientation of each nucleus with a small arrow, the four states are as follows:

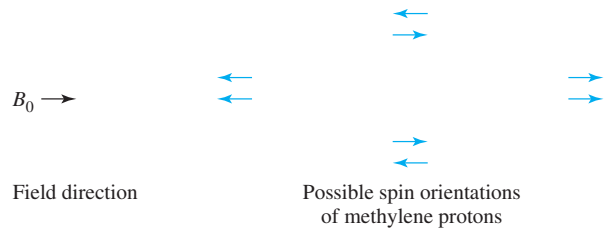

In the first combination on the left, spins of the two methylene protons are paired and aligned against the field, whereas in the second combination on the right, the paired spins are reversed. In the two combinations shown in the center, the spins are opposed to one another. The magnetic effect transmitted to the methyl protons on the adjacent carbon atom is determined by the instantaneous spin combinations in the methylene group. If the spins are paired and opposed to the external field, the effective applied field on the methyl protons is slightly decreased. Thus, a somewhat higher field is needed to bring them into resonance, and an upfield shift results. Spins paired and aligned with the field result in a downfield shift. Neither of

TABLE 19-2 Approximate Chemical Shifts for Certain Methyl, Methylene, and Methine Protons

Structure	δ, ppm		
	M = CH_3	M = CH_2	M = CH
Aliphatic α substituents			
M—Cl	3.0	3.5	4.0
M—Br	2.7	3.4	4.1
M—NO_2	4.3	4.4	4.6
M—OH (or OR)	3.2	3.4	3.6
M—O—C_6H_5	3.8	4.0	4.6
M—OC(=O)R	3.6	4.1	5.0
M—C=C	1.6	1.9	—
M—C≡C	1.7	2.2	2.8
M—C(=O)H	2.2	2.4	—
M—C(=O)R	2.1	2.4	2.6
M—C(=O)C_6H_5	2.4	2.7	3.4
M—C(=O)OR	2.2	2.2	2.5
M—C_6H_5	2.2	2.6	2.8
Aliphatic β substituents			
M—C—Cl	1.5	1.8	2.0
M—C—Br	1.8	1.8	1.9
M—C—NO_2	1.6	2.1	2.5
M—C—OH (or OR)	1.2	1.5	1.8
M—C—OC(=O)R	1.3	1.6	1.8
M—C—C(=O)H	1.1	1.7	—
M—C—C(=O)R	1.1	1.6	2.0
M—C—C(=O)OR	1.1	1.7	1.9
M—C—C_6H_5	1.1	1.6	1.8

the combinations of opposed spin has an effect on the resonance of the methyl protons. Thus, splitting into a triplet results (see Figure 19-12b). The area under the middle peak of the triplet is twice that of either of the other two, because two spin combinations are involved.

Let us now consider the effect of the three methyl protons on the methylene peak (middle peak in Figure 19-12a). Possible spin combinations for the methyl protons are as follows:

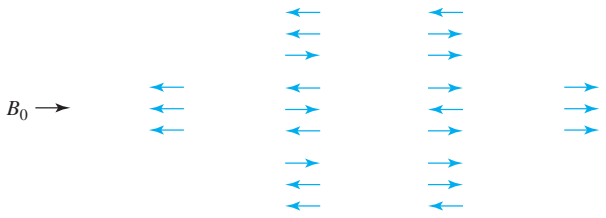

In this instance, we have eight possible spin combinations; however, among these are two groups containing three combinations that have equivalent magnetic effects. The methylene peak is thus split into a quartet having areas in the ratio 1:3:3:1 (Figure 19-12b). These two examples of the adjacent methyl and methylene groups in ethanol suggest the general rule that the number of peaks in a split band in a first-order spectrum is equal to the number n of magnetically equivalent protons[11] on adjacent atoms plus one. The number of such peaks is referred to as the *multiplicity*.

The interpretation of spin-spin splitting patterns is relatively straightforward for *first-order* spectra. First-order spectra are

[11]Magnetically equivalent protons are those that have identical chemical shifts and identical coupling constants.

TABLE 19-3 Relative Intensities of First-Order Multiplets ($I = 1/2$)

Number of Equivalent Protons, n	Multiplicity, $(n + 1)$	Relative Peak Areas
0	1	1
1	2	1 1
2	3	1 2 1
3	4	1 3 3 1
4	5	1 4 6 4 1
5	6	1 5 10 10 5 1
6	7	1 6 15 20 15 6 1
7	8	1 7 21 35 35 21 7 1

those in which the chemical shift between interacting groups of nuclei is large with respect to their coupling constant J. Rigorous first-order behavior requires that J/δ be smaller than 0.05. Frequently, however, analysis of spectra by first-order techniques can be accomplished down to a value of $\Delta\nu/J$ of somewhat greater than 0.1. The ethanol spectrum shown in Figure 19-13 is an example of a pure first-order spectrum, with J for the methyl and methylene peaks being 7 Hz and the separation between the centers of the two multiplets being about 140 Hz.

Interpretation of second-order NMR spectra is relatively complex and will not be considered here. Note, however, that because δ increases with increases in the magnetic field but J does not, spectra obtained with an instrument having a high magnetic field are much more readily interpreted than those produced by a spectrometer with a weaker magnet.

Rules Governing the Interpretation of First-Order Spectra

The following rules govern the appearance of first-order spectra:

1. Equivalent nuclei do not interact with one another to give multiple absorption peaks. The three protons in the methyl groups in ethanol give rise to splitting of only the adjacent methylene protons and not to splitting among themselves.
2. Coupling constants decrease significantly with separation of groups, and coupling is seldom observed at distances greater than four bond lengths.
3. The multiplicity of a band is determined by the number n of magnetically equivalent protons on the neighboring atoms and is given by the quantity $n + 1$. Thus, the multiplicity for the methylene band in ethanol is determined by the number of protons in the adjacent methyl groups and is equal to $3 + 1 = 4$.
4. If the protons on atom B are affected by protons on atoms A and C that are nonequivalent, the multiplicity of B is equal to $(n_A + 1)(n_C + 1)$, where n_A and n_C are the number of equivalent protons on A and C, respectively.
5. The approximate relative areas of a multiplet are symmetric around the midpoint of the band and are proportional to the coefficients of the terms in the expansion $(x + 1)^n$. The application of this rule is demonstrated in Table 19-3 and in the examples that follow.
6. The coupling constant is independent of the applied field; thus, multiplets are readily distinguished from closely spaced chemical-shift peaks by obtaining spectra at two different field strengths.

EXAMPLE 19-3

For each of the following compounds, calculate the number of multiplets for each band and their relative areas: (a) $Cl(CH_2)_3Cl$; (b) $CH_3CHBrCH_3$; (c) $CH_3CH_2OCH_3$.

Solution

(a) The multiplicity associated with the four equivalent protons on the two ends of the molecule is determined by the number of protons on the central carbon; thus, the multiplicity is $2 + 1 = 3$ and the areas have the ratio 1:2:1. The multiplicity of the central methylene protons is determined by the four equivalent protons at the ends and is $4 + 1 = 5$. Expansion of $(x + 1)^4$ gives the coefficients (Table 19-3), which are proportional to the areas of the peaks 1:4:6:4:1.

(b) The band for the six methyl protons is made up of $1 + 1 = 2$ peaks having relative areas of 1:1; the proton on the central carbon atom has a multiplicity of $6 + 1 = 7$. These peaks have areas (Table 19-3) in the ratio of 1:6:15:20:15:6:1.

(c) The right methyl protons are separated from the others by more than three bonds so that only a single peak is observed. The protons of the central methylene group have a multiplicity of $3 + 1 = 4$ and a ratio of 1:3:3:1. The left methyl protons have a multiplicity of $2 + 1 = 3$ and an area ratio of 1:2:1.

The preceding examples are relatively straightforward because all of the protons influencing the multiplicity of any single band are magnetically equivalent. A more complex splitting pattern results when a set of protons is influenced by two or more nonequivalent protons. As an example, consider the spectrum of 1-iodopropane, $CH_3CH_2CH_2I$. If we label the three carbon atoms (a), (b), and (c) from left to right, the chemical-shift bands are found at $\delta_{(a)} = 1.02$, $\delta_{(b)} = 1.86$, and $\delta_{(c)} = 3.17$. The band at $\delta_{(a)} = 1.02$ will be split by the two methylene protons on (b) into $2 + 1 = 3$ lines having relative areas of 1:2:1. A similar splitting of the band $\delta_{(c)} = 3.17$ will also be observed. The experimental coupling constants for the two shifts are $J_{(ab)} = 7.3$ and $J_{(bc)} = 6.8$. The band for the methylene protons (b) is influenced by two groups of protons that are not magnetically equivalent, as is evident from the difference between $J_{(ab)}$ and $J_{(bc)}$. Thus, invoking rule 4, the number of peaks is $(3 + 1)(2 + 1) = 12$. In cases such as this, derivation of a splitting pattern, as shown in Figure 19-18, is helpful. In this example, the effect of the (a) proton is first shown and leads to four peaks of relative areas 1:3:3:1 spaced at 7.3 Hz. Each of these is then split into three new peaks spaced at 6.8 Hz, having relative areas of 1:2:1. The same final pattern is produced if the original band is first split into a triplet. At a very high resolution, the spectrum for 1-iodopropane exhibits a series of lines that approximates the series shown at the bottom of Figure 19-18. If the resolution is sufficiently low that the instrument does not detect the difference between $J_{(ab)}$ and $J_{(bc)}$, only six peaks are observed with relative areas of 1:5:10:10:5:1.

Modern spectrometers contain software that can calculate spectra fairly accurately for systems with three or four spins. Usually, a trial-and-error approach is first used to estimate chemical shifts and coupling constants to produce a simulated spectrum to match the experimental spectrum. Then, chemical shifts are varied until the widths and locations of the multiplets approximately agree. Finally, coupling constants or their sums and differences are varied until a suitable agreement between observed and simulated spectra is obtained.

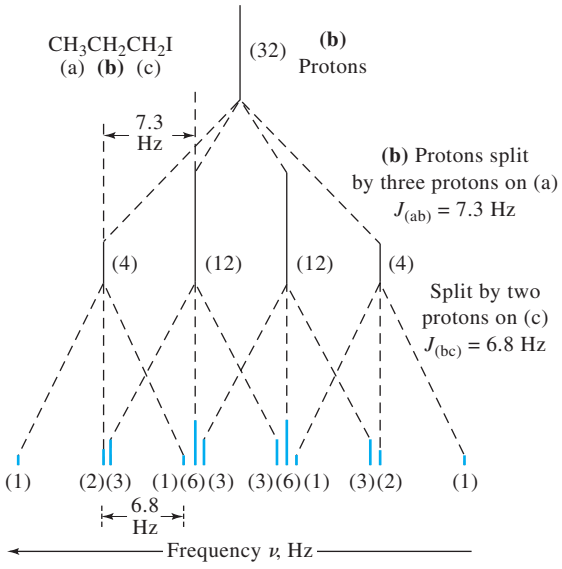

FIGURE 19-18 Splitting pattern for methylene (b) protons in $CH_3CH_2CH_2I$. Figures in parentheses are relative areas under peaks.

Second-Order Spectra

Coupling constants are usually smaller than 20 Hz, although chemical shifts may be as high as several thousand Hz. Therefore, the splitting behavior described by the rules in the previous section is common. However, when J/δ becomes greater than about 0.1 to 0.15, these rules no longer apply. Generally, as δ approaches J, the lines on the inner side of two multiplets tend to be enhanced at the expense of the lines on the outer side, and the symmetry of each multiplet is thus destroyed, as noted earlier. In addition, more, and sometimes many more, lines appear, so that the spacing between lines no longer correlates with the magnitude of the coupling constants. Analysis of a spectrum under these circumstances is difficult.

Effect of Chemical Exchange on Spectra

We now turn again to the NMR spectrum of ethanol (Figure 19-12) and consider why the OH proton resonance appears as a singlet rather than a triplet. The methylene protons and the OH proton are separated by only three bonds, so coupling should increase the multiplicity of both OH and the methylene bands. As shown in Figure 19-19, we actually observe the expected multiplicity in the NMR spectrum of a highly purified sample of the alcohol. Examine the triplet OH peaks and the eight methylene peaks in this spectrum. If we add a trace of acid or base to the pure sample, the spectrum reverts to the form shown in Figure 19-12.

The exchange of OH protons among alcohol molecules is known to be catalyzed by both acids and bases, as well as by the impurities that commonly occur in ethanol. It is thus plausible to associate the decoupling observed in the presence of these catalysts to an exchange process. If exchange is rapid, each

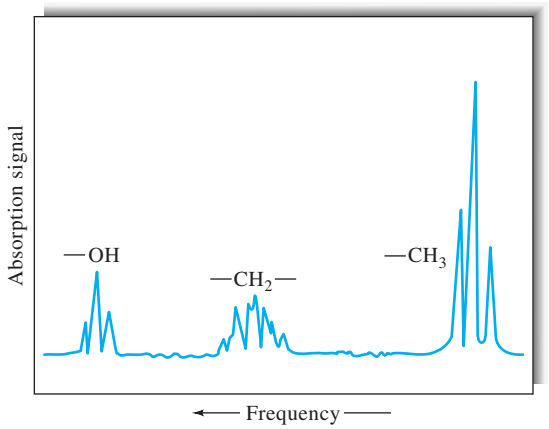

FIGURE 19-19 Spectrum of highly purified ethanol showing additional splitting of OH and CH_2 peaks (compare with Figure 19-12).

OH group will have several protons associated with it during any brief period; within this interval, all of the OH protons will experience the effects of the three spin arrangements of the methylene protons. Thus, the magnetic effects on the alcoholic proton are averaged, and a single sharp resonance is observed. Spin decoupling always occurs when the exchange frequency is greater than the separation frequency between the interacting components.

Chemical exchange can affect not only spin-spin coupling but also chemical shifts. Purified alcohol-water mixtures have two well-defined and easily separated OH proton peaks. When acid or base is added to the mixture, however, the two peaks coalesce to form a single sharp line. In this instance, the catalyst enhances the rate of proton exchange between the alcohol and the water and thus averages the shielding effect. A single sharp line is obtained when the exchange rate is significantly greater than the separation frequency between the alcohol and water lines. On the other hand, if the exchange frequency is about the same as this frequency difference, shielding is only partially averaged and a broad line results. The correlation of line breadth with exchange rates has provided a direct means for investigating the kinetics of such processes and represents an important application of the NMR experiment. Such studies are often accomplished by acquiring spectra at several different temperatures and determining the temperature at which multiplets coalesce to a simple band. Armed with this information, the activation energy and other kinetic parameters for the exchange process may be computed, and the mechanisms of the exchange process may be investigated.[12]

19B-4 Double Resonance Techniques

Double resonance experiments include a group of techniques in which a sample is simultaneously irradiated with two or more signals of different radio frequencies. Among the techniques that use this approach are *spin decoupling*, the *nuclear Overhauser effect*, *spin tickling*, and *internuclear double resonance*. These procedures aid in the interpretation of complex NMR spectra.[13] Only the first of these techniques, spin decoupling, is described here. The nuclear Overhauser effect is discussed briefly in Section 19E-1.

Figure 19-20 illustrates the spectral simplification that accompanies decoupling of similar nuclei, which is referred to as

[12]R. S. Drago, *Physical Methods for Chemists*, 2nd ed., Chap. 8, p. 290, Philadelphia: Saunders, 1992.

[13]For a more detailed discussion of double resonance methods, see H. Friebolin, *Basic One- and Two-Dimensional NMR Spectroscopy*, 5th ed., Chap. 5, Weinheim, Germany: Wiley-VCH, 2011; J. B. Lambert and E. P. Mazzola, *Nuclear Magnetic Resonance Spectroscopy*, Upper Saddle River, NJ: Pearson/Prentice-Hall, 2004; M. H. Levitt, *Spin Dynamics: Basics of Nuclear Magnetic Resonance*, New York: Wiley, 2001; E. D. Becker, *High Resolution NMR*, 3rd ed., New York: Academic Press, 2000.

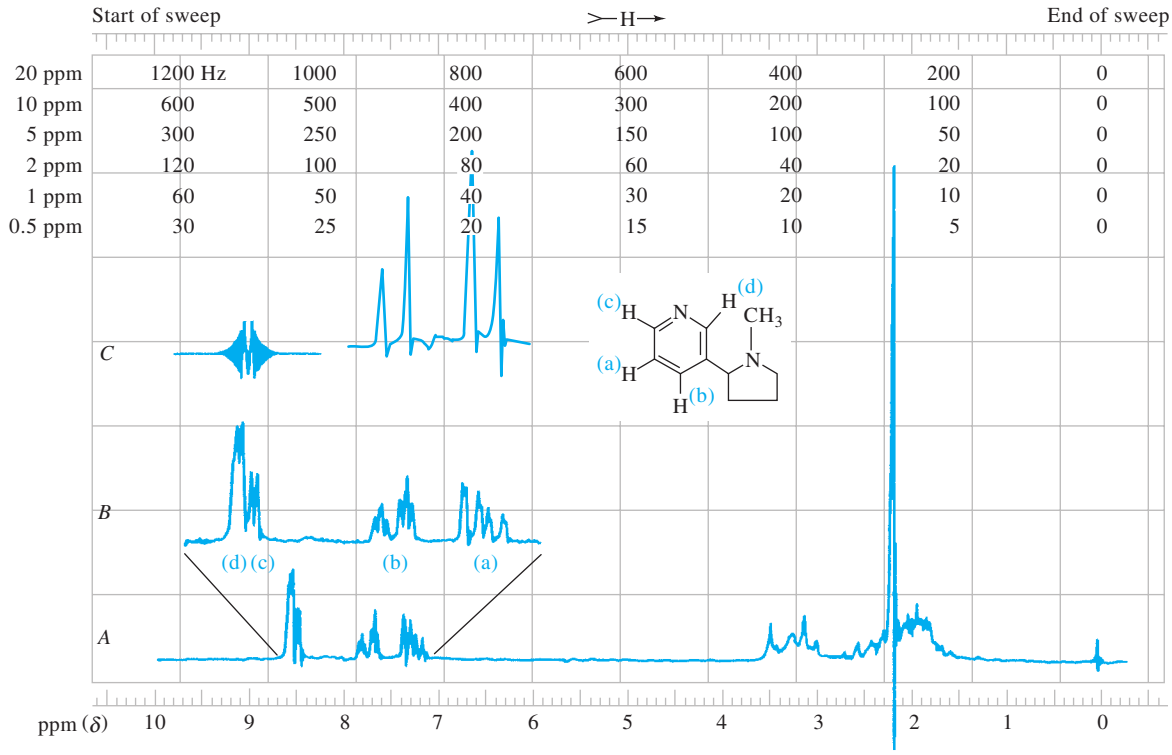

FIGURE 19-20 Effect of spin decoupling on the NMR spectrum of nicotine dissolved in $CDCl_3$. Spectrum *A*, the entire spectrum. Spectrum *B*, expanded spectrum for the four protons on the pyridine ring. Spectrum *C*, spectrum for protons (a) and (b) when decoupled from (d) and (c) by irradiation with a second beam that has a frequency corresponding to about 8.6 ppm. (Courtesy of Agilent Technologies, Santa Clara, CA.)

homonuclear spin decoupling. Spectrum *B* shows the absorption associated with the four protons on the pyridine ring of nicotine. Spectrum *C* was obtained by examining the same portion of the spectrum and simultaneously irradiating the sample with a second RF signal having a frequency of about 8.6 ppm, which corresponds to a chemical shift, centered on the absorption peaks of protons (c) and (d). The strength of the second signal is sufficient to cause saturation of the signal for these protons. The result is a decoupling of the interaction between the (c) and (d) protons and protons (a) and (b). Here, the complex absorption spectrum for (a) and (b) collapses to two doublet peaks that arise from coupling between these protons. Similarly, the spectrum for (c) and (d) is simplified by decoupling with a signal of frequency corresponding to the proton resonances (a) or (b).

Heteronuclear decoupling, which is decoupling of the interaction between dissimilar nuclei, is easily accomplished with modern NMR instrumentation. The most important example is encountered in ^{13}C NMR, where the technique is used to simplify spectra by decoupling protons (Section 19E-1).

19C NMR SPECTROMETERS

Instrument manufacturers market two general types of NMR spectrometers: *wide-line spectrometers* and *high-resolution spectrometers*. Wide-line instruments have magnets with strengths of a few tenths of a tesla and are considerably simpler and less expensive than are high-resolution instruments. High-resolution instruments are equipped with magnets with strengths that range from 1.4 to 23.5 T, which correspond to proton frequencies of 60 to 1000 MHz (1 GHz). Before about 1970, high-resolution NMR spectrometers were all of the CW type that used permanent magnets or electromagnets to supply the magnetic field. This type of instrument has been largely replaced by Fourier transform spectrometers equipped with superconducting magnets to provide the magnetic field. Computers are an integral part of modern NMR instruments; they digitize and store the signal, perform Fourier transformation of the FID to provide the frequency-domain signal, and deliver many other data-treatment and instrument-control functions. A major reason why Fourier transform instruments have become so popular is that they permit efficient signal averaging and thus yield greatly enhanced sensitivity (see Sections 5C-2 and 16B-1). Because of this greater sensitivity, routine applications of NMR to naturally occurring carbon-13, to protons in microgram quantities, and to other nuclei, such as fluorine, phosphorus, and silicon, have become widespread.

High-resolution NMR spectrometers are quite expensive, costing several hundred thousand dollars and more. Because almost all commercial NMR spectrometers today operate in the pulsed, or FT, mode, we confine our discussion here to FT-NMR instruments.

Tutorial: Learn more about **NMR instrumentation** at www.tinyurl.com/skoogpia7

19C-1 Components of Fourier Transform Spectrometers

Figure 19-21 is a simplified block diagram showing the instrument components of a typical FT-NMR spectrometer. The central component of the instrument is a highly stable magnet in which the sample is placed. The sample is surrounded by a transmitter-receiver coil.

RF radiation is produced by a crystal-controlled frequency synthesizer having an output carrier frequency of ν_c. This signal passes into a pulse switch and power amplifier, which creates an intense and reproducible pulse of RF current in the transmitter coil. The resulting RF radiation impinges on the sample, contained inside the coil. The length, amplitude, shape, and phase of the pulse are selected by the operator; entered into the console; and controlled by the computer. In Figure 19-21, a 5-μs pulse is shown. The resulting FID signal is picked up by the same coil, which now serves as a receiver. The signal is then amplified and transmitted to a phase-sensitive detector. The detector circuitry produces the difference between the nuclear signals ν_n and the crystal oscillator output ν_c, which leads to the low-frequency, time-domain signal shown on the right of the figure. This signal is digitized and collected in the memory of the computer for analysis by a Fourier transform program and other data-analysis software. The output from this program is plotted on a display device, giving a frequency-domain spectrum.

19C-2 Magnets

The heart of all NMR instruments is the magnet. The sensitivity and resolution of spectrometers are both critically dependent on the strength and quality of their magnets (see Example 19-2 and Figure 19-13). Because both sensitivity and resolution increase with increasing field strength, it is advantageous to operate at the highest possible field strength. In addition, the field must be highly homogeneous and reproducible. These requirements ensure that the magnet is by far the most expensive component of an NMR spectrometer.

Spectrometer magnets of three types have been used in NMR spectrometers: permanent magnets, conventional electromagnets, and superconducting solenoids. At present, conventional electromagnets are seldom incorporated into NMR instruments. Permanent magnets with field strengths of 0.7, 1.4, and 2.1 T have been used in commercial CW instruments; corresponding oscillator frequencies for proton studies are 30, 60, and 90 MHz. Permanent magnets are highly temperature sensitive and require extensive thermostatting and shielding as a consequence. Because of field-drift problems,

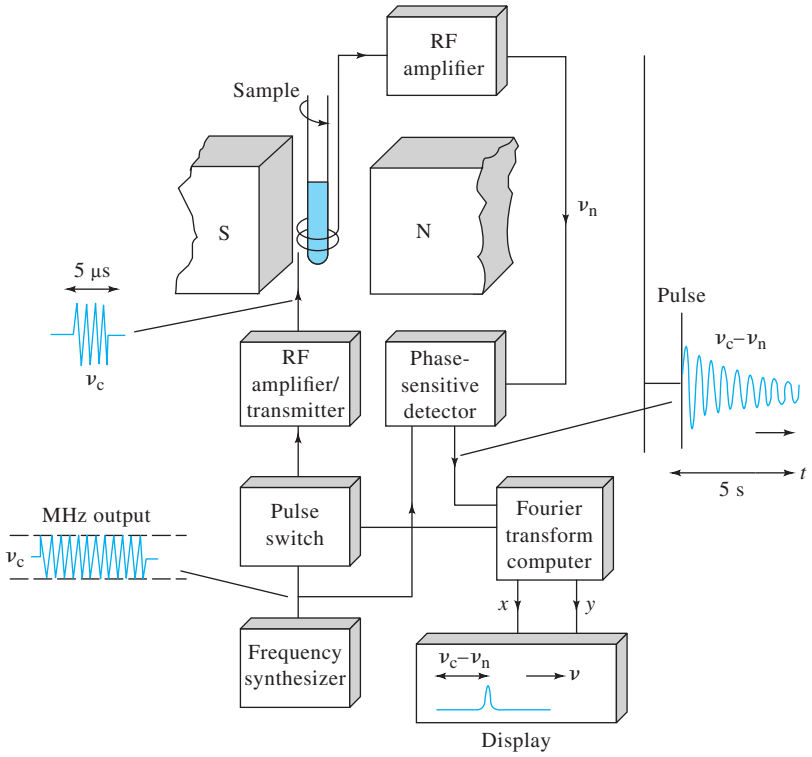

FIGURE 19-21 Block diagram of an FT-NMR spectrometer. (Adapted from J. W. Akitt, *NMR and Chemistry*, 2nd ed., p. 14, London: Chapman & Hall, 1983. With permission.)

permanent magnets are not ideal for extended periods of data accumulation, such as are often used in Fourier transform experiments.

Superconducting magnets are used in most modern high-resolution instruments. These magnets attain fields as large as 23.5 T, corresponding to a proton frequency of 1 GHz. To superconduct, the solenoid, wound from superconducting niobium-tin or niobium-titanium wire, is bathed in liquid helium at a temperature of 4 K. The helium Dewar flask is held in an outer liquid-nitrogen Dewar. Most superconducting magnet systems must be filled with liquid nitrogen about once a week and with liquid helium every few months. The advantages of superconducting solenoids, in addition to their high field strengths, are their high stability, low operating cost, and simplicity and small size compared with an electromagnet.

The performance specifications for a spectrometer magnet are stringent. The field produced must be homogeneous to a few parts per billion within the sample area and must be stable to a similar degree for the length of time required to acquire the sample data. Unfortunately, the inherent stability of most magnets is considerably lower than this figure, with variations as large as one part in 10^7 being observed over a period of 1 hour. Several measures are used in modern NMR instruments to compensate for both drift and field inhomogeneity.

Locking the Magnetic Field

To offset the effect of field fluctuations, a *field-frequency lock system* is used in commercial NMR instruments. In these systems, a reference nucleus is continuously irradiated and monitored at a frequency corresponding to its resonance maximum at the rated field strength of the magnet. Changes in the intensity of the reference signal control a feedback circuit, whose output is fed into coils in the magnetic gap in such a way as to correct for the drift. Recall that for a given type of nucleus, the ratio between the field strength and resonance frequencies is a constant *regardless of the nucleus* (Equation 19-5). Thus, the drift correction for the reference signal is applicable to the signals for all nuclei in the sample area. In modern spectrometers, the reference signal is provided by the deuterium in the solvent, and a second transmitter coil tuned to the frequency for deuterium monitors the reference. Most modern superconducting magnets are sufficiently stable that spectra can be obtained in an unlocked mode for a period of 1 to 20 min.

Shimming

Shim coils are pairs of wire loops through which carefully controlled currents are passed, producing small magnetic fields that compensate for inhomogeneities in the primary magnetic field. In contemporary instruments, the shim controls are under computer control with several algorithms available for optimizing field homogeneity. Ordinarily, shimming must be carried out

each time a new sample is introduced into the spectrometer. Shim coils are not shown in the simplified diagram shown in Figure 19-21.

Sample Spinning

The effects of field inhomogeneities are also counteracted by spinning the sample along its longitudinal axis. Spinning is accomplished by means of a small plastic turbine that slips over the sample tube. A stream of air drives the turbine at a rate of 20 to 50 revolutions per second. If this frequency is much greater than the frequency spread caused by magnetic inhomogeneities, the nuclei experience an averaged environment that causes apparent frequency dispersions to collapse toward zero. A minor disadvantage of spinning is that the magnetic field is modulated at the spinning frequency, which may lead to *sidebands*, or *spinning sidebands*, on each side of absorption bands.

19C-3 The Sample Probe

A key component of an NMR spectrometer is the sample probe, which serves multiple functions. It holds the sample in a fixed position in the magnetic field, contains an air turbine to spin the sample, and houses the coil or coils that permit excitation and detection of the NMR signal. In addition, the probe ordinarily contains two other transmitter coils, one for locking and the other for decoupling experiments that are discussed in Section 19E-1. Finally, most probes have variable temperature capability. The usual NMR sample cell consists of a 5-mm (outside diameter) glass tube containing 500–650 μL of liquid. Microtubes for smaller sample volumes and larger tubes for special needs are also available.

Transmitter-Receiver Coils

The adjustable probes in modern NMR spectrometers contain transmitter and receiver coils. The receiver coils are arranged according to the experiment purpose. For observing protons, the probe usually has an inner coil for ^{1}H detection and an outer coil, called the X-nucleus coil, for detecting nuclei such as ^{13}C or ^{15}N. The inner coil is generally the closest to the sample to maximize sensitivity. For experiments to detect nuclei other than protons, the X-nucleus coil is placed on the inside and the ^{1}H coil on the outside. Usually, proton spectra have such good signal-to-noise ratios that probe tuning is not extremely critical. When the X-nucleus coil is the primary observation coil, however, tuning can be very important.

The Pulse Generator. RF generators and frequency synthesizers produce a signal of essentially a single frequency. To generate Fourier transform spectra, however, the sample must be irradiated with a range of frequencies sufficiently great to excite nuclei with different resonance frequencies. Fortunately, a sufficiently short pulse of radiation, such as that shown in Figure 19-5, provides a relatively broad band of frequencies centered on the frequency of the oscillator. The frequency range of this band is about $1/(4\tau)$ Hz, where τ is the length in seconds of each pulse. Thus, a 1-μs pulse from a 100-MHz oscillator produces a frequency range of 100 MHz ± 125 kHz. This production of a band of frequencies from a narrow pulse can be understood by reference to Figure 6-6, where a rectangular waveform is synthesized from a series of sine or cosine waves differing from one another by small frequency increments. Conversely, Fourier analysis of a square waveform reveals that it consists of a broad range of frequency components. The narrower the square wave, the broader the range of component frequencies. Thus, a narrow pulse generated by rapidly switching an RF oscillator consists of a band of frequencies capable of exciting all nuclei whose resonances occur in the vicinity of the frequency of the oscillator.

As shown in Figure 19-21, the typical pulse generator consists of three parts: a frequency synthesizer, a gate to switch the pulse on and off at appropriate times, and a power amplifier to amplify the pulse to about 50 to 100 W.

The Receiver System. Voltages generated by the current in the detector coil are in the nanovolt-to-microvolt range and thus must be amplified to a range of about 0 to 10 V before the signal can be further processed and digitized. The first stage of amplification generally takes place in a preamplifier, which is mounted in the probe so that it is as close to the receiver coil as possible to minimize the effects of noise from other parts of the instrument. Further amplification then is carried out in an external RF amplifier as shown in Figure 19-21.

19C-4 The Detector and Data-Processing System

In the detector system shown in Figure 19-21, the high-frequency radio signal is first converted to an audio-frequency signal, which is much easier to digitize. The signal from the RF amplifier can be thought of as being made up of two components: a *carrier signal*, which has the frequency of the oscillator producing it, and a superimposed NMR signal from the analyte. The analyte signal differs in frequency from that of the carrier by a few parts per million. For example, the chemical shifts in a proton spectrum typically encompass a range of 10 ppm. Thus, the proton NMR data generated by a 500-MHz spectrometer would lie in the frequency range of 500,000,000 to 500,005,000 Hz. To digitize such high-frequency signals and extract the small differences attributed to the sample in the digital domain is not practical; therefore, the carrier frequency ν_c is subtracted electronically from the analyte signal frequency ν_n in the analog domain. In our example, this process yields a difference signal $(\nu_n - \nu_c)$ that lies in the audio-frequency range of 0 to 5000 Hz. This process is identical to the separation of audio signals from an RF carrier signal in home radios.

Sampling the Audio Signal

The sinusoidal audio signal obtained after subtracting the carrier frequency is then digitized by sampling the signal

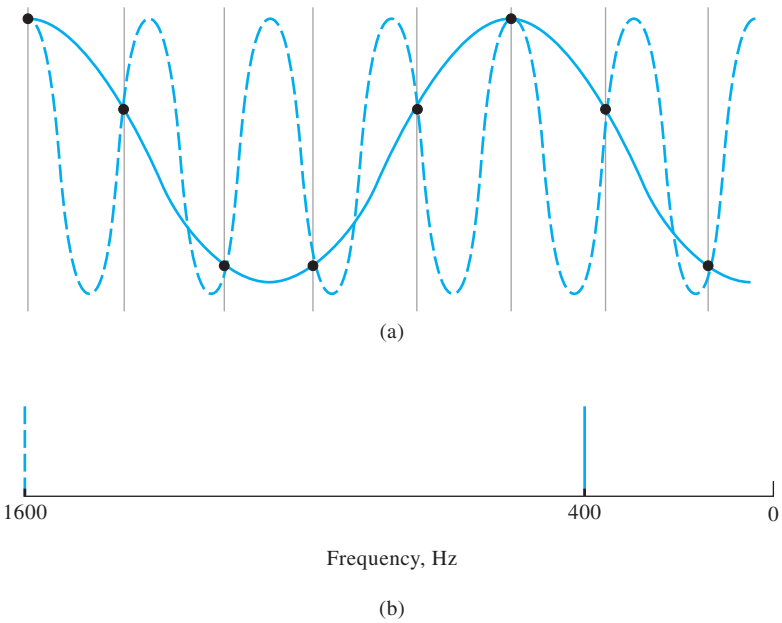

FIGURE 19-22 Folding of a spectral line brought about by sampling at a frequency that is less than the Nyquist frequency of 3200 Hz and that is sampled at a frequency of 2000 samples per second as shown by dots; solid line is a cosine wave having a frequency of 400 Hz. (b) Frequency-domain spectrum of dashed signal in (a) showing the folded line at 400 Hz. (Adapted from D. Shaw, *Fourier Transform NMR Spectroscopy*, 2nd ed., p. 159, New York: Elsevier, 1987. With permission, Elsevier Science Publishers.)

voltage, periodically converting it to a digital form with an analog-to-digital converter. To accurately represent a sine or a cosine wave digitally, it is necessary, according to the *Nyquist sampling theorem* (see Section 5C-2), to sample the signal at least twice during each cycle. If sampling is done at a frequency that is less than twice the signal frequency, *folding*, or *aliasing*, of the signal occurs. The effect of folding is illustrated in Figure 19-22a, which shows, as the dashed curve, a 1600-Hz cosine signal that is being sampled at a rate of 2000 data per second. The solid dots represent the times at which the computer sampled and digitized the data. This sampling rate is less than the Nyquist frequency, which is 2×1600 Hz $= 3200$ Hz. The effect of this inadequate sampling rate is demonstrated by the solid curve in Figure 19-22a, which is a 400-Hz cosine wave. Thus, as shown in Figure 19-22b, the line at 1600 Hz is absent and a folded line appears at 400 Hz in the frequency-domain spectrum.

In modern NMR spectrometers, quadrature phase-sensitive detectors make possible the determination of positive and negative differences between the carrier frequency and NMR frequencies. Because these detectors are able to sense the sign of the frequency difference, folding is avoided.

Signal Integration

The areas of proton NMR signals are almost always directly proportional to the number of protons involved. Hence, modern NMR spectrometers provide not only the NMR signal itself, but for ^{1}H spectra, the integral of the signal. For ^{13}C spectra, the signals are in general *not* proportional to the number of nuclei present. Usually, the integral data appear as step functions superimposed on the NMR spectrum as illustrated in Figure 19-23. Generally, the area data are reproducible to a few percent relative.

19C-5 Sample Handling

Until recently, high-resolution NMR studies have been restricted to samples that could be converted to a nonviscous liquid state. Most often, a 2% to 15% solution of the sample is used, although pure liquid samples can also be examined if their viscosities are sufficiently low.

Solvents must have no resonances of their own in the spectral region of interest. Usually, NMR solvents are deuterated to provide the field-frequency lock signal (see Section 19C-2). The most commonly used solvent for organic compounds is

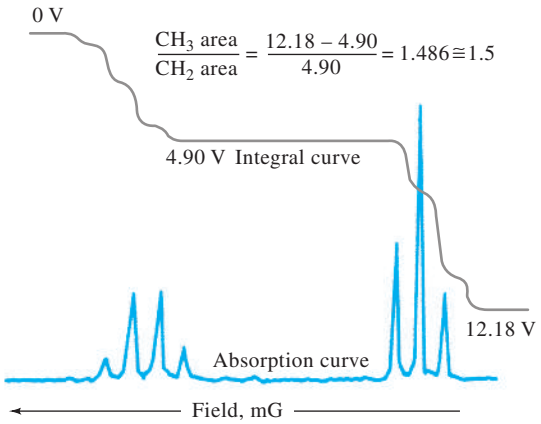

FIGURE 19-23 Absorption and integral curve for a dilute ethylbenzene solution (aliphatic region). (Courtesy of Agilent Technologies, Santa Clara, CA.)

deuterated chloroform ($CDCl_3$). Polar compounds are often not sufficiently soluble in $CDCl_3$ to obtain good spectra. For these types of compounds, CD_3OD, acetone-d_6, and DMSO-d_6 are often used. For highly polar and ionic compounds, D_2O can be used along with a water-suppression method to remove the intense HOD solvent signal.

High-quality NMR tubes are necessary with modern high-field spectrometers. If tubes have been previously used, they must be carefully cleaned and thoroughly dried prior to use. Sample-tube cleaners are available commercially for this purpose. Cleaning solutions, such as chromic acid–sulfuric acid, should never be used because paramagnetic chromium ions can adsorb to the walls and broaden proton NMR spectra.

It is now possible to routinely collect high-resolution spectra for solid samples. Techniques have been developed and are being applied in increasing numbers to obtain ^{13}C spectra of polymers, fossil fuels, and other high-molecular-mass substances. A brief discussion of the modifications necessary to produce useful NMR spectra of solids is in Section 19E.

19D APPLICATIONS OF PROTON NMR

The most important chemical applications of proton NMR spectroscopy have been to the identification and structural elucidation of organic, metal-organic, and biochemical molecules. In addition, however, the method is often useful for quantitative determination of absorbing species.

19D-1 Identification of Compounds

An NMR spectrum, like an IR spectrum, seldom suffices by itself for the identification of an organic compound. However, in conjunction with mass, IR, and UV spectra, as well as elemental analysis, NMR is a powerful and indispensable tool for the characterization of pure compounds. The examples that follow give some idea of the kinds of information that can be extracted from NMR spectra.

EXAMPLE 19-4

The proton NMR spectrum shown in Figure 19-24 is for an organic compound having the empirical formula $C_5H_{10}O_2$. Identify the compound.

Solution

The spectrum suggests the presence of four types of protons. From the peak integrals and the empirical formula, we deduce that these four types are populated by 3, 2, 2, and 3 protons, respectively. The single peak at $\delta = 3.6$ must be due to an isolated methyl group. Inspection of Figure 19-17 and Table 19-3 suggests that the peak may result from the functional group

The empirical formula and the 2:2:3 distribution of the remaining protons indicate the presence of an *n*-propyl group as well. The structure

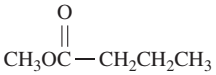

is consistent with all of these observations. In addition, the positions and the splitting patterns of the three remaining peaks are entirely compatible with this hypothesis. The triplet at $\delta = 0.9$ is typical of a methyl group adjacent to a methylene. From Table 19-3, the two protons of the methylene adjacent to the carboxylate peak should yield the observed triplet peak at about $\delta = 2.2$. The other methylene group would be expected to produce a pattern of $3 \times 4 = 12$ peaks at about $\delta = 1.7$. Only six are observed, presumably because the resolution of the instrument is insufficient to produce the fine structure of the band.

EXAMPLE 19-5

The proton NMR spectra shown in Figure 19-25 are for colorless, isomeric liquids containing only carbon and hydrogen. Identify the two compounds.

Solution

The single peak at about $\delta = 7.2$ in the upper figure suggests an aromatic structure; the relative area of this peak corresponds to five protons. This information suggests that we may have a monosubstituted derivative of benzene. The seven peaks for the single proton appearing at $\delta = 2.9$ and the six-proton doublet at $\delta = 1.2$ can only be explained by the structure

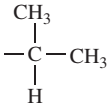

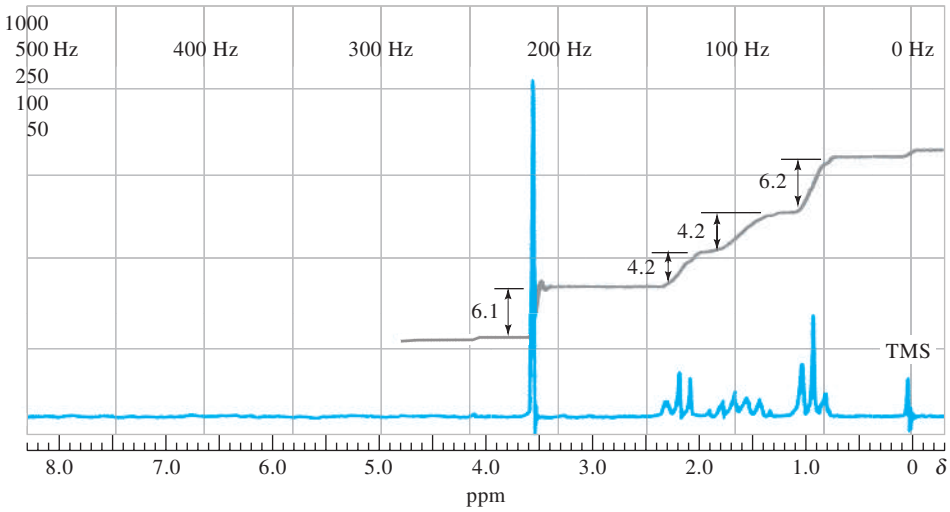

FIGURE 19-24 NMR spectrum and peak integral curve for the organic compound $C_5H_{10}O_2$ in CCl_4. (From R. M. Silverstein, G. C. Bassler, and T. C. Morrill, *Spectrometric Identification of Organic Compounds*, 3rd ed., p. 296, New York: Wiley, 1974. With permission.)

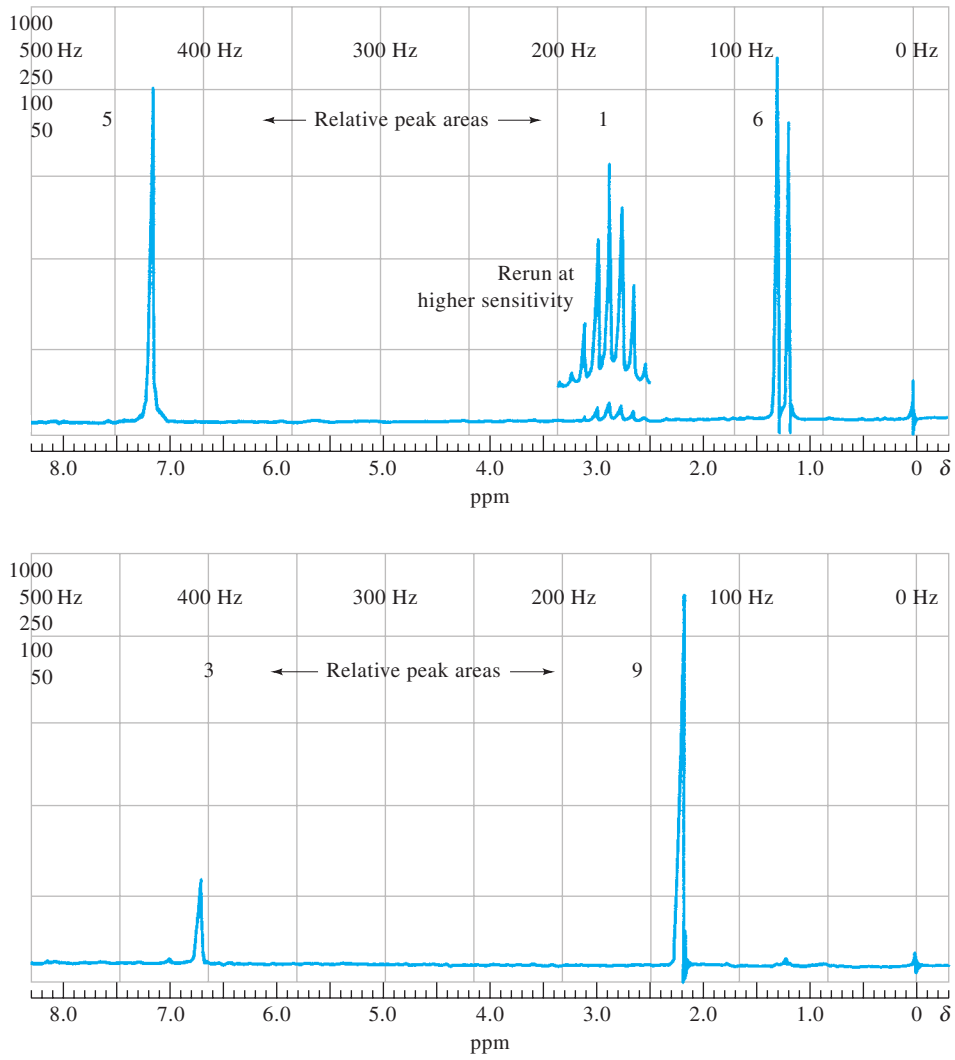

FIGURE 19-25 NMR spectra for two organic isomers in $CDCl_3$. (Courtesy of Agilent Technologies, Santa Clara, CA.)

Thus, we conclude that this compound is cumene.

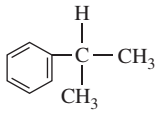

The isomeric compound has an aromatic peak at $\delta = 6.8$. Its relative area suggests a trisubstituted benzene, which can only mean that the compound is $C_6H_3(CH_3)_3$. The relative peak areas confirm this deduction.

EXAMPLE 19-6

The proton spectrum shown in Figure 19-26 is for an organic compound having a molecular mass of 72 and containing carbon, hydrogen, and oxygen only. Identify the compound.

The triplet peak at $\delta \approx 9.8$ appears to be that of an aliphatic aldehyde, RCHO (see Figure 19-17). If this hypothesis is valid, R has a molecular mass of 43, which corresponds to a C_3H_7 fragment. The triplet at $\delta \approx 9.8$ means that there is a methylene group adjacent to the carbonyl. Thus, the compound appears to be *n*-butyraldehyde, $CH_3CH_2CH_2CHO$.

The triplet peak at $\delta = 0.97$ appears to be that of the terminal methyl. We expect the protons on the adjacent methylene to show a complicated splitting pattern of $4 \times 3 = 12$ peaks, and the grouping of peaks around $\delta = 1.7$ is compatible with this prediction.

Finally, the peak for the protons on the methylene group adjacent to the carbonyl should appear as a sextet downfield from the other methylene proton resonances. The group at $\delta = 2.4$ is consistent with our prediction.

19D-2 Application of NMR to Quantitative Analysis

A unique aspect of proton NMR spectra is the direct proportionality between peak areas and the number of nuclei responsible for the peak. As a result, a quantitative determination of a specific compound does not require pure samples for calibration. Thus, if an identifiable resonance for one of the constituents of a sample does not overlap resonances of the other constituents, the area of this peak can be used to establish the concentration of the species directly, provided only that the signal area per proton is known. This latter quantity can be obtained conveniently from a known concentration of an internal standard. For example, if the solvent present in a known amount were benzene, cyclohexane, or water, the areas of the single-proton peak for these compounds could be used to give the desired information. Of course, the resonance of the internal standard should not overlap with any of the sample resonances. Organic silicon derivatives are uniquely attractive for calibration purposes because of the high upfield location of their proton resonances.

Methods for the analysis of many multicomponent mixtures have been reported. For example, aspirin, phenacetin, and caffeine have been determined in commercial analgesic preparations. Benzene, heptane, ethylene, glycol, and water have been determined in a wide range of mixtures.

Simulation: Learn more about **NMR spectral interpretation** at www.tinyurl.com/skoogpia7

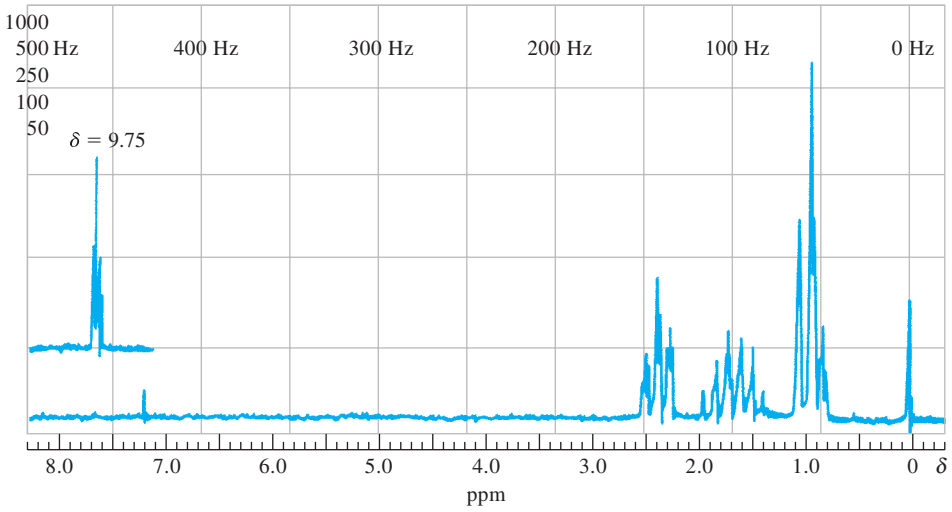

FIGURE 19-26 NMR spectrum of a pure organic compound containing C, H, and O only.

One of the useful applications of NMR has been in the determination of functional groups, such as hydroxyl groups in alcohols and phenols, aldehydes, carboxylic acids, olefins, acetylenic hydrogens, amines, and amides.[14] Relative errors in the range of 1% to 5% are reported.

NMR spectroscopy has also been used for elemental analysis. For example, it is possible to make accurate quantitative determinations of total hydrogen in organic mixtures. Likewise, the resonance of fluorine-19 can be used for the quantitative analysis of that element in organic compounds—an analysis that is difficult to carry out by classical methods. For quantitative work, a low-resolution or wide-line spectrometer may be used.

Despite the preceding examples, the widespread use of NMR spectroscopy for quantitative work has been inhibited by the cost of the instruments. In addition, the probability of overlapping resonances becomes greater as the complexity of the sample increases. Also, NMR is often neither as sensitive nor as convenient as competing techniques.

19E CARBON-13 NMR

Carbon-13 NMR was first studied in 1957, but its widespread use did not begin until the early 1970s. The reason for this delay was the time required for the development of instruments sensitive enough to detect the weak NMR signals from the ^{13}C nucleus. These weak signals result from the low natural abundance of the isotope (1.1%) and the small magnetogyric ratio, which is about 0.25 that of the proton. These factors combine to make ^{13}C NMR about 6000 times less sensitive than proton NMR.

The most important developments in NMR signal enhancement that have led directly to the explosive growth of ^{13}C magnetic resonance spectroscopy include higher-field-strength magnets and Fourier transform instruments. Without these developments, ^{13}C NMR would be restricted to the study of highly soluble low-molecular-mass solids, neat liquids, and isotopically enriched compounds.[15]

Carbon-13 NMR has several advantages over proton NMR in terms of its power to elucidate organic and biochemical structures. First, ^{13}C NMR provides information about the backbone of molecules rather than about the periphery. In addition, the chemical-shift range for ^{13}C for most organic compounds is about 200 ppm, compared with 10 to 15 ppm for the proton. As a result, there is less spectral overlap in ^{13}C spectra than in proton spectra. For example, it is often possible to observe individual resonances for each carbon atom in compounds ranging in molecular mass from 200 to 400. In addition, *homonuclear* spin-spin coupling between carbon atoms is not observed because in natural-abundance samples the probability of two ^{13}C atoms occurring adjacent to each other is small. Furthermore, *heteronuclear* spin coupling between ^{13}C and ^{12}C does not occur because the spin quantum number of ^{12}C is zero. However, heteronuclear coupling between carbon and hydrogen does occur. A number of excellent methods can be used to decouple the interaction between ^{13}C atoms and protons. With decoupling, the spectrum for a particular type of carbon generally exhibits only a single line.

19E-1 Proton Decoupling

Three primary types of proton decoupling experiments are used in ^{13}C NMR, *broadband decoupling*; *off-resonance decoupling*; and *pulsed*, or *gated*, *decoupling*.

Broadband Decoupling

Broadband decoupling is a type of heteronuclear decoupling in which spin-spin splitting of ^{13}C lines by ^{1}H nuclei is avoided by irradiating the sample with a broadband RF signal that encompasses the entire proton spectral region, whereas the ^{13}C spectrum is obtained in the usual way. Ordinarily, the proton signal is produced by a second coil located in the sample probe. The effect of broadband decoupling is demonstrated in Figure 19-27.

Off-Resonance Decoupling

Although broadband decoupling considerably simplifies most ^{13}C spectra, it also removes spin-spin splitting information that may be of importance in structural assignments. In the past, this limitation was sometimes rectified by substituting off-resonance decoupling.

In this technique, the decoupling frequency is set at 1000 to 2000 Hz above the proton spectral region, which leads to a partially decoupled spectrum in which all but the largest spin-spin shifts are absent. Under this circumstance, primary carbon nuclei (bearing three protons) yield a quartet, secondary carbons give triplets, tertiary carbon nuclei appear as doublets, and quaternary carbons exhibit a single line. Figure 19-28 demonstrates the utility of this technique for identifying the source of the resonances in a ^{13}C spectrum.

Pulsed Decoupling

Modern NMR spectrometers provide decoupling information through the application of complex pulsing schemes, which yield higher signal-to-noise ratios more rapidly than off-resonance decoupling. These techniques are described in specialized manuscripts, but beyond the scope of this chapter.[16]

[14]See R. H. Cox and D. E. Leyden in *Treatise on Analytical Chemistry*, 2nd ed., P. J. Elving, M. M. Bursey, and I. M. Kolthoff, eds., Part I, Vol. 10, pp. 127–36, New York: Wiley, 1983.

[15]For additional information, see D. L. Pavia, G. M. Lampman, G. S. Kritz, and J. R. Vyvyan, *Introduction to Spectroscopy*, 5th ed., Chap. 6, Stamford, CT: Cengage, 2015; K. Pihlaja and E. Kleinpeter, *Carbon-13 NMR Chemical Shifts in Structural and Stereochemical Analysis*, New York: Wiley-VCH, 1994; N. Beckmann, *Carbon-13 NMR Spectroscopy of Biological Systems*, New York: Academic Press, 1995; E. Breitmaier and W. Voelters, *Carbon-13 NMR Spectroscopy*, 3rd ed., New York: VCH, 1987.

[16]See H. Friebolin, *Basic One- and Two-Dimensional NMR Spectroscopy*, 5th ed., Weinheim, Germany: Wiley-VCH, 2010; J. K. M. Sanders and B. K. Hunter, *Modern NMR Spectroscopy: A Guide for Chemists*, 2nd ed., New York: Oxford, 1993.

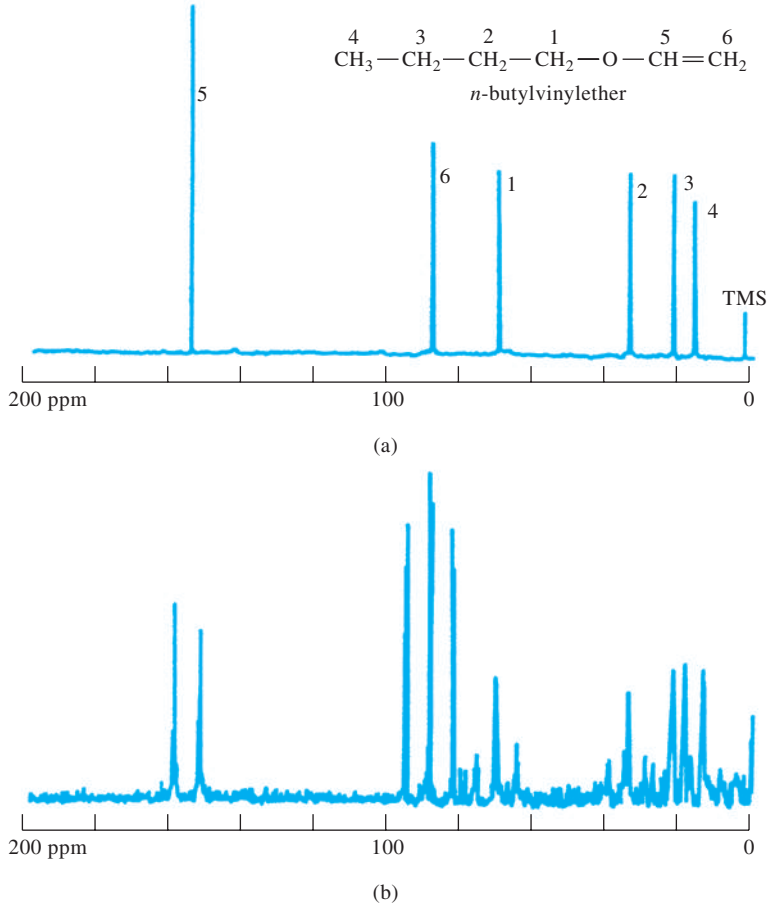

FIGURE 19-27 Carbon-13 NMR spectra for *n*-butylvinylether obtained at 25.2 MHz: (a) proton decoupled spectrum and (b) spectrum showing effect of coupling between ^{13}C atom and attached protons. (From R. J. Abraham and P. Loftus, *Proton and Carbon-13 NMR Spectroscopy*, p. 103, Philadelphia: Heyden, 1978. With permission.)

Nuclear Overhauser Effect

Under conditions of broadband decoupling, it is found that the areas of ^{13}C peaks are enhanced by a factor that is significantly greater than would be expected from the collapse of the multiple structures into single lines. This phenomenon is a manifestation of the *nuclear Overhauser effect* (NOE), which is a general effect encountered in decoupling experiments. The enhancement arises from direct magnetic coupling between a decoupled proton and a neighboring ^{13}C nucleus that results in an increase in the population of the lower energy state of the ^{13}C nucleus over that predicted from the Boltzmann relation. The ^{13}C signal is enhanced by as much as a factor of 3 as a result. Although the NOE does increase the sensitivity of ^{13}C measurements, it has the disadvantage that the proportionality between peak areas and number of nuclei may be lost. The theory of the NOE, which is based on dipole-dipole interactions, is discussed in specialized manuscripts.[17]

19E-2 Application of ^{13}C NMR to Structure Determination

As with proton NMR, the most important and widespread applications of ^{13}C NMR are for the determination of structures of organic and biochemical species. Such determinations

[17]See D. Neuhaus and M. P. Williamson, *The Nuclear Overhauser Effect in Structural and Conformational Analysis*, 2nd ed., New York: Wiley-VCH, 2000; D. Shaw, *Fourier Transform NMR Spectroscopy*, 2nd ed., p. 233, New York: Elsevier, 1984.

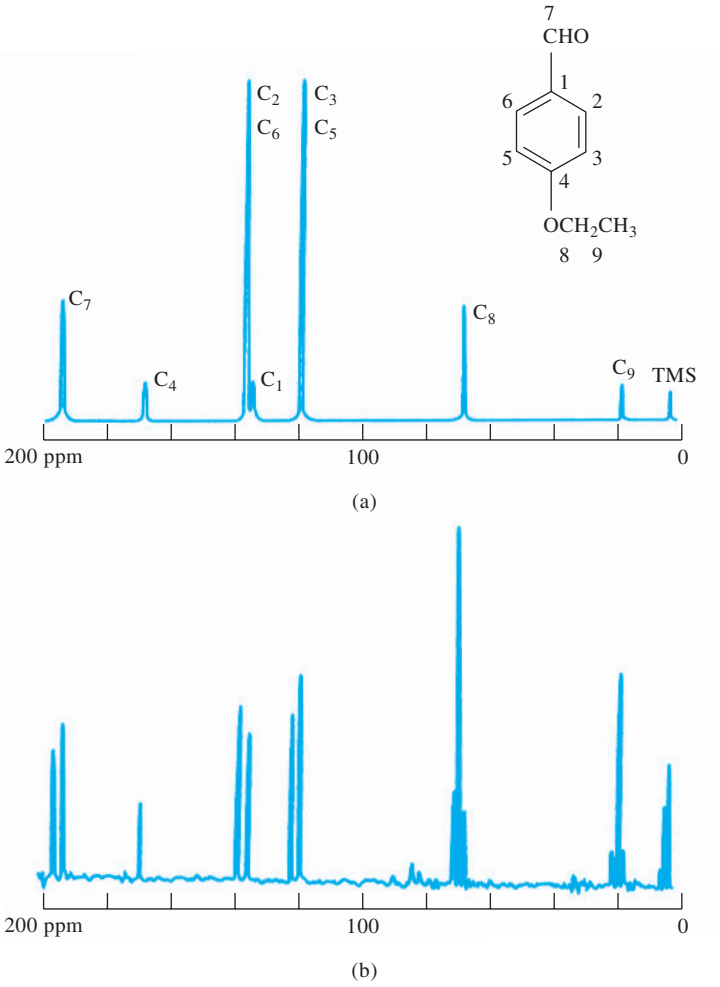

FIGURE 19-28 Comparison of (a) broadband and (b) off-resonance decoupling in ^{13}C spectra of *p*-ethoxybenzaldehyde. (From R. J. Abraham, J. Fisher, and P. Loftus, *Introduction to NMR Spectroscopy*, p. 106, New York: Wiley, 1988. With permission.)

are based largely on chemical shifts, with spin-spin data playing a lesser role than in proton NMR. Figure 19-29 shows some of the chemical shifts that are observed for ^{13}C in various chemical environments. As with proton spectra, these shifts are relative to TMS, with δ values ranging from 0 to 200 ppm. In general, environmental effects are analogous to those for the proton, which were described in Section 19B-2. In contrast to proton spectra, however, the effect of substituents on ^{13}C shifts is not limited to the nearest atom. For example, substitution of chlorine on the C_1 carbon in *n*-pentane results in a chemical shift for that carbon of 31 ppm. When chlorine substitution is on the C_2 carbon, the shift for the C_1 carbon is 10 ppm; similarly, substitutions on the C_3, C_4, and C_5 carbons result in shifts of -5.3, -0.5, and -0.1 ppm, respectively.

Application of ^{13}C NMR to Solid Samples

As was noted earlier, NMR spectra for solids[18] have in the past not been very useful for structural studies because of line broadening, which eliminates or obscures the characteristic sharp individual peaks of NMR. Much of this broadening is attributable to two causes: static dipolar interactions between ^{13}C and ^{1}H and from anisotropy in ^{13}C-shielding tensors. In isotropic liquids, these effects are averaged to zero because of the rapid and

[18]See D. C. Apperley, R. K. Harris, P. Hodgkinson, *Solid State NMR: Basic Principles & Practice*, New York: Momentum Press, 2012; M. J. Duer, *Solid-State NMR Spectroscopy*, Oxford: Blackwell Science, 2002; C. Dybowski and S. Bai, *Anal. Chem.*, **2008**, *80*, 4295, **DOI**: 10.1021/ac800573y; S. Bai, W. Wang, and C. Dybowski, *Anal. Chem.*, **2010**, *82*, 4917, **DOI**: 10.1021/ac100761m.

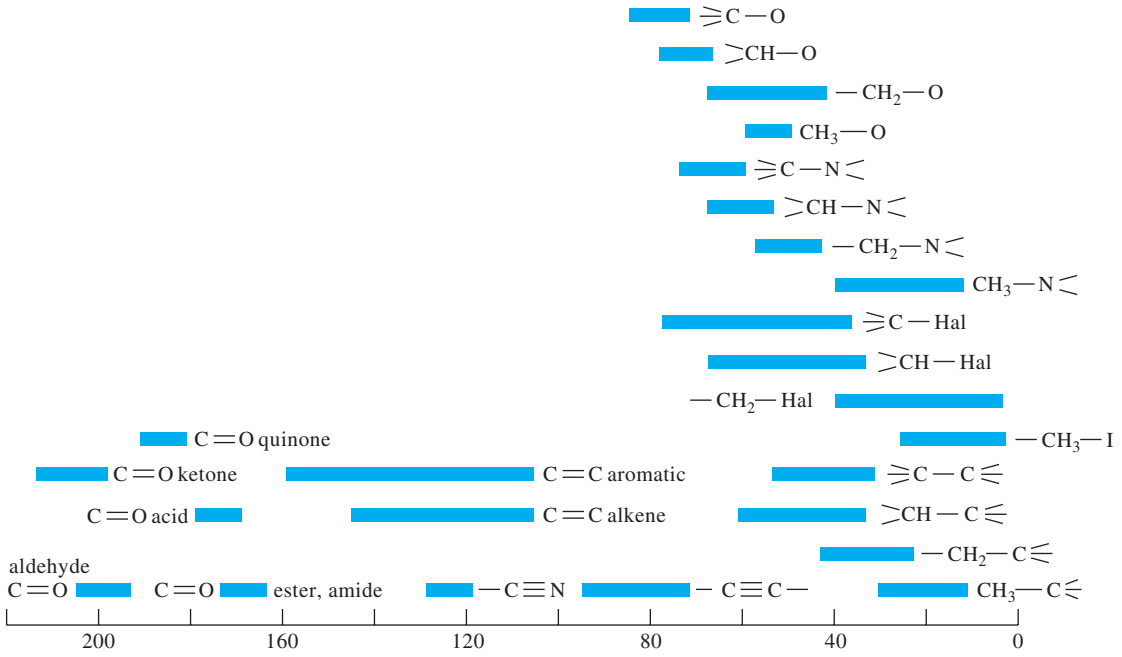

FIGURE 19-29 Chemical shifts for ^{13}C. (From D. E. Leyden and R. H. Cox, *Analytical Applications of NMR*, p. 196, New York: Wiley, 1977. With permission.)

random motion of molecules. In solids, heteronuclear dipolar interactions between magnetic nuclei, such as ^{13}C and protons, result in characteristic dipolar line splittings, which depend on the angle between C—H bonds and the external field. In an amorphous solid, there is a large number of fixed orientations of these bonds and therefore a large number of splittings can occur. The broad absorption bands in this instance are made up of the numerous lines arising from these individual dipolar interactions. It is possible to remove dipolar splitting from a ^{13}C spectrum by irradiating the sample at proton frequencies while the spectrum is being obtained. This procedure, called *dipolar decoupling*, is similar to spin decoupling, which was described earlier for liquids, except that a much higher power level is required.

A second type of line broadening for solids is caused by chemical-shift anisotropy, which was discussed in Section 19B-2. The broadening produced here results from changes in the chemical shift with the orientation of the molecule or part of the molecule with respect to an external magnetic field. From NMR theory, it is known that the chemical shift $\Delta\delta$ brought about by magnetic anisotropy is given by the equation

$$\Delta\delta = \Delta\chi(3\cos^2\theta - 1)/R^3 \qquad (19\text{-}20)$$

where θ is the angle between the double bond and the applied field, $\Delta\chi$ is the difference in magnetic susceptibilities between the parallel and perpendicular orientation of the double bond, and R is the distance between the anisotropic functional group and the nucleus. When θ is exactly 54.7°, $\Delta\delta$, as defined by Equation 19-20, is zero. Experimentally, line broadening due to chemical-shift anisotropy is eliminated by *magic angle spinning*, which involves rotating solid samples rapidly at a frequency greater than 2 kHz in a special sample holder that is maintained at an angle of 54.7° with respect to the applied field. In effect, the solid then acts like a liquid being rotated in the field.

One further limitation in ^{13}C FT-NMR of solids is the long spin-lattice relaxation time for excited ^{13}C nuclei. The rate at which the sample can be pulsed depends on the relaxation rate. That is, after each excitation pulse, enough time must elapse for the nuclei to return to the equilibrium ground state. Unfortunately, spin-lattice relaxation times for ^{13}C nuclei in solids are often several minutes, which means that several hours or even days of signal averaging would be required to give a good spectrum.

The problem caused by slow spin-lattice relaxation times is overcome by *cross polarization*, a complicated pulsed technique that causes the Larmor frequencies of proton nuclei and ^{13}C nuclei to become identical—that is, $\gamma_C B_{1C} = \gamma_H B_{1H}$. Under these conditions, the magnetic fields of the precessing proton nuclei interact with the fields of the ^{13}C nuclei, causing the latter to relax.

Instruments are available commercially that incorporate dipolar decoupling, magic angle spinning, and cross polarization, thus making possible the acquisition of high-resolution ^{13}C spectra from solids. Figure 19-30, which shows spectra for crystalline adamantane collected under various conditions, illustrates the power of these instruments.

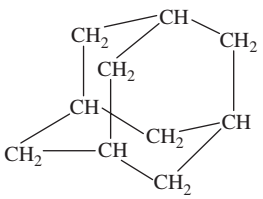

adamantane

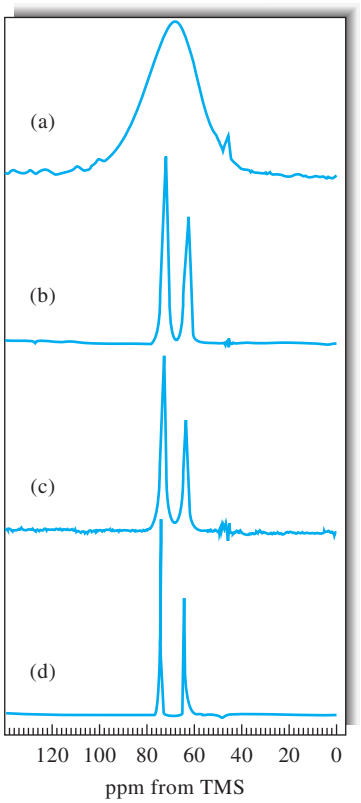

FIGURE 19-30 Carbon-13 spectra of crystalline adamantane: (a) nonspinning and with no proton decoupling; (b) nonspinning but with dipolar decoupling and cross polarization; (c) with magic angle spinning but without dipolar decoupling or cross polarization; and (d) with spinning, decoupling, and cross polarization. (From F. A. Bovey, *Nuclear Magnetic Resonance Spectroscopy*, 2nd ed., p. 415, New York: Academic Press, 1988. With permission.)

19F APPLICATION OF NMR TO OTHER NUCLEI

More than 200 isotopes have magnetic moments and thus, in principle, can be studied by NMR. Among the most widely studied nuclei are ^{31}P, ^{15}N, ^{19}F, ^{2}D, ^{11}B, ^{23}Na, ^{14}N, ^{29}Si, ^{55}Mn, ^{109}Ag, ^{199}Hg, ^{113}Cd, and ^{207}Pb. The first three of these are particularly important in the fields of organic chemistry, biochemistry, and biology.

19F-1 Phosphorus-31

Phosphorus-31, with spin number 1/2, exhibits sharp NMR peaks with chemical shifts extending over a range of 700 ppm. The resonance frequency of ^{31}P at 4.7 T is 81.0 MHz. Numerous investigations, particularly in the biochemical field, have been based on ^{31}P resonance. An example is shown in Figure 19-31. The species under study is adenosine triphosphate (ATP), a triply charged anion that plays a vital role in carbohydrate metabolism and in energy storage and release in the body.

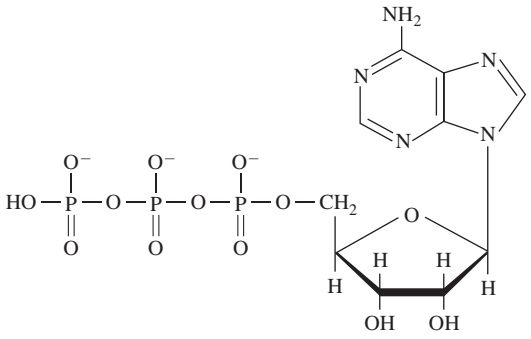

adenosine-5′-triphosphate (ATP)

The bottom spectrum, which is for ATP in an aqueous environment, is made up of three sets of peaks corresponding to the three phosphorus atoms. The triplet undoubtedly arises from the central phosphorus, which is coupled to the other two phosphorus atoms. The doublet at about 14 ppm shows some poorly defined indications of proton coupling and thus probably arises from the phosphorus that is adjacent to the methylene group.

Magnesium ions are known to play a part in the metabolic role of ATP, and the upper six spectra in Figure 19-31 suggest that complex formation between the anionic phosphorus and the cation takes place to cause the phosphorus chemical shifts to move downfield as the magnesium ion concentration is increased.

19F-2 Fluorine-19

Fluorine-19 has a spin quantum number of 1/2 and a magnetogyric ratio close to that of ^{1}H. Thus, the resonance frequency of fluorine at 188 MHz is only slightly lower than that of the proton at 200 MHz when both are measured at 4.69 T.

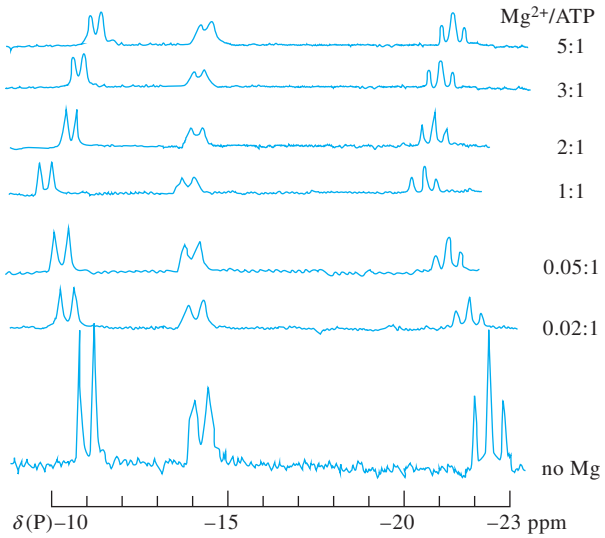

FIGURE 19-31 Fourier transform phosphorus-31 NMR spectra for ATP solution containing magnesium ions. The ratios on the right are moles of Mg^{2+} to moles of ATP. (From J. W. Akitt, *NMR and Chemistry*, 2nd ed., p. 245, London: Chapman & Hall, 1983. With permission.)

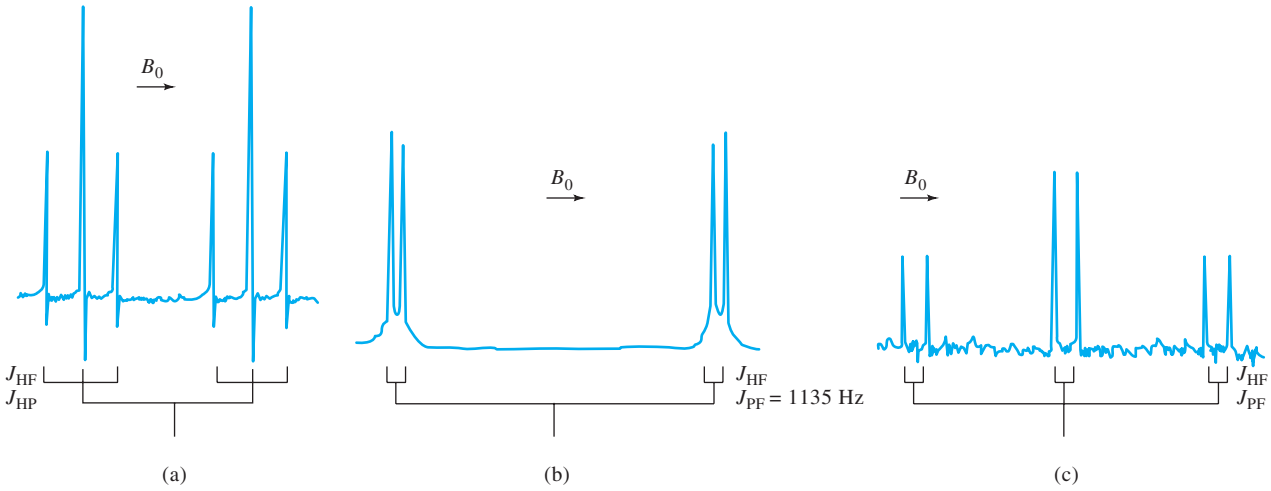

FIGURE 19-32 Spectra of liquid PHF_2 at −20°C: (a) ^1H spectrum at 60 MHz; (b) ^{19}F spectrum at 94.1 MHz; (c) ^{31}P spectrum at 40.4 MHz. (From R. J. Myers, *Molecular Magnetism and Molecular Resonance Spectroscopy*, Englewood Cliffs, NJ: Prentice-Hall, 1973. With permission.)

Fluorine absorption is also sensitive to the environment, and the resulting chemical shifts extend over a range of about 300 ppm. In addition, the solvent plays a much more important role in determining fluorine peak positions than in determining those of protons.

Empirical correlations of the fluorine shift with structure are relatively sparse when compared with information concerning proton behavior. It seems probable, however, that the future will see further developments in this field, particularly for structural investigation of organic fluorine compounds.

Proton, ^{19}F, and ^{31}P spectra for the inorganic species PHF_2 are shown in Figure 19-32. In each spectrum, spin-spin splitting assignments can easily be made based on the discussion in Section 19B-3. Using a modern multinuclear instrument, three of these spectra could be obtained at a single magnetic field strength.

19G MULTIPLE PULSE AND MULTIDIMENSIONAL NMR

Multiple pulse and multidimensional NMR have brought about entirely new experiments that allow us to obtain new levels of information about organic and biological molecules.

19G-1 Multiple-Pulse NMR

In the late 1960s NMR spectroscopists discovered that a vast amount of chemical information could be obtained from experiments based on multiple-pulse sequences. Here, techniques such as *inversion-recovery* and *spin-echo NMR* enabled the measurement of spin-lattice T_1 and spin-spin T_2 relaxation times. In fact, these relaxation times began to be used as additional resolution parameters. For example, in ^1H NMR, differences between the T_1 values of solute protons and water protons were used to reduce the contribution of the intense solvent resonances in aqueous solutions. In mixtures containing proteins and small biological molecules, T_2 differences were exploited to essentially eliminate the proton resonances of macromolecules and allow enhancement of the small molecule signals. Most significant, however, was the recognition that multiple pulse sequences could be used to add a second frequency dimension to NMR experiments.

19G-2 Two-Dimensional NMR

Two-dimensional NMR, or 2D NMR, comprises a set of multipulse techniques that make it possible to unravel complex spectra.[19] The two-dimensional methods can identify resonances connected by through-bond coupling, by through-space interactions, or by chemical exchange. In two-dimensional methods, data are acquired as a function of time t_2 just as in ordinary FT-NMR. Prior to obtaining this FID signal, however, the system is perturbed by a pulse for a period t_1. Fourier transformation of the FID as a function of t_2 for a fixed t_1 yields a spectrum similar to that obtained in an ordinary pulse experiment. This process is then repeated for various values of t_1, thus giving a two-dimensional spectrum in terms of two frequency variables ν_1 and ν_2 or sometimes the chemical-shift parameters δ_1 and δ_2. The nature and timing of the pulses that have been used in 2D

[19]For a brief review of 2D NMR, see D. L. Rabenstein, *Anal. Chem.*, **2001**, *73*, 214A, **DOI**: 10.1021/ac012435q. For a more detailed treatment, see H. Friebolin, *Basic One- and Two-Dimensional NMR Spectroscopy*, 5th ed., Chap. 9, Weinheim, Germany: Wiley-VCH, 2010; J. Keeler, *Understanding NMR Spectroscopy*, 2nd ed., Chap. 8, Chichester, UK: Wiley, 2010; J. B. Lambert, E. P. Mazzola, *Nuclear Magnetic Resonance Spectroscopy*, Chap. 6, Upper Saddle River, NJ: Pearson/Prentice-Hall, 2004.

NMR vary widely, and in some cases more than two repetitive pulses are used. Thus, the number of types of two-dimensional experiments that have appeared in the literature is large. Some of the most popular methods based on coherence transfer include *homonuclear correlation spectroscopy* (COSY), *total correlation spectroscopy* (TOCSY), the *incredible natural-abundance double-quantum transfer experiment* (INADEQUATE), *heteronuclear correlation* (HETCOR) *spectroscopy*, and *heteronuclear multiple quantum coherence* (HMQC) *spectroscopy*.

Figure 19-33a is a ^{13}C 2D NMR spectrum for a COSY experiment with 1,3-butanediol. Figure 19-33a is the ordinary one-dimensional spectrum for the compound. The two-dimensional spectrum is obtained as follows: with the proton broadband decoupler turned off, a 90° pulse is applied to the sample. After a time t_1, the decoupler is turned on, another pulse is applied, and the resulting FID is digitized and transformed. After equilibrium has been reestablished, this process is repeated for other values of t_1, which leads to a series of spectra that are plotted horizontally in the figure. That is, the projections along the δ_1-axis are the spectra that would be obtained without decoupling. The projection along the δ_2-axis is the same as the completely decoupled carbon-13 spectrum. It is obvious that the spectrum is made up of a quartet, two triplets, and a doublet, whose source is apparent from a consideration of the number of protons bonded to each of the four ^{13}C atoms in the molecule. This information is not obvious in the one-dimensional spectrum.

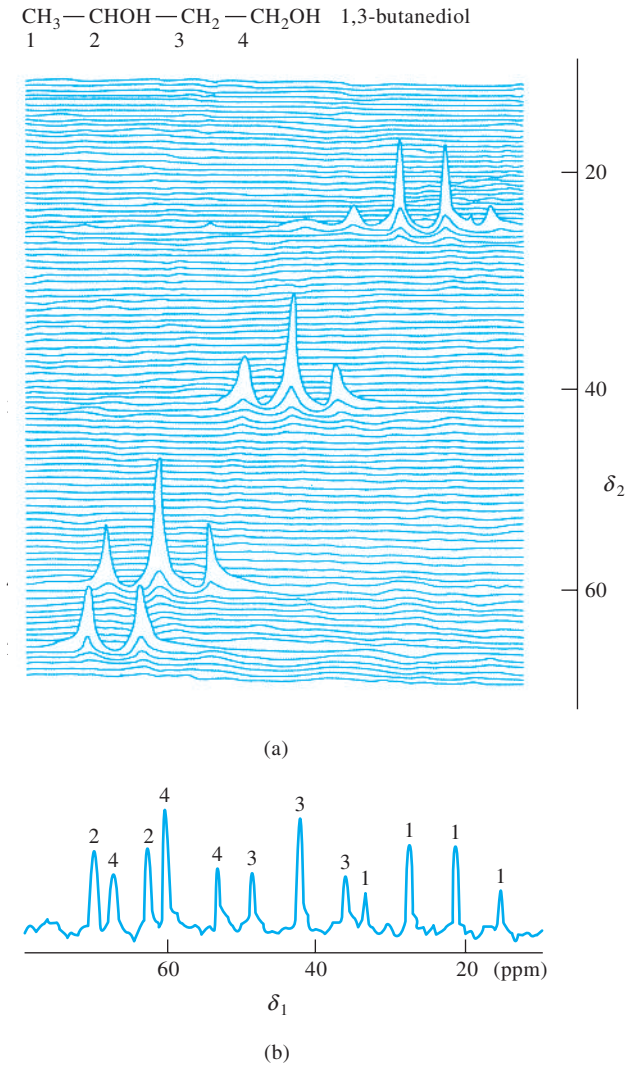

FIGURE 19-33 Illustration of the use of the two-dimensional spectrum (a) to identify the ^{13}C resonances in a one-dimensional spectrum (b). Note that the ordinary one-dimensional spectrum is obtained from the peaks along the diagonal. The presence of off-diagonal cross peaks can identify resonances linked by spin-spin coupling. (Adapted from S. Borman, *Anal. Chem.*, **1982**, *54*, 1129A, **DOI**: 10.1021/ac00248a601. Copyright 1982 American Chemical Society.)

The COSY, TOCSY, HETCOR, and HMQC experiments are great aids in interpreting proton and ^{13}C spectra. However, the INADEQUATE experiment is perhaps the definitive 2D NMR technique. This experiment is based on spin-spin coupling between directly bonded pairs of nuclei. It can trace out the carbon backbone of an organic compound one carbon at a time. The low sensitivity of INADEQUATE has, however, limited its practical utility.

Another class of two-dimensional experiments is based on the incoherent transfer of magnetization by the NOE or by chemical exchange. In *NOE spectroscopy* (NOESY), *rotating-frame Overhauser effect spectroscopy* (ROESY), and *exchange spectroscopy* (EXSY), cross peaks are observed between resonances linked by dipole-dipole interactions or chemical exchange. As an example, the one-dimensional and ROESY spectra for a nineteen-amino-acid peptide are shown in Figure 19-34. Not only could the one-dimensional proton NMR spectrum be completely assigned but the ROESY spectrum also indicated that the peptide is an α-helix in solution.

19G-3 Multidimensional NMR

Because of overlapping resonances, 2D NMR has been limited to fairly small proteins in elucidating protein structure. However, three- and four-dimensional methods have been developed that enable NMR spectroscopy to be further extended to larger and larger protein structures. A third dimension can be added, for example, to spread apart a ^{1}H-^{1}H two-dimensional spectrum on the basis of the chemical shift of another nucleus, such as ^{15}N or ^{13}C. In most three-dimensional experiments, the most effective methods for large molecules are used. Thus, COSY is not often used, but experiments like NOESY-TOCSY and TOCSY-HMQC are quite effective. In some cases, the three dimensions all represent different nuclei such as ^{1}H-^{13}C-^{15}N. These are considered variants of the HETCOR experiment. Multidimensional NMR is capable of providing complete solution-phase structures to complement crystal structures from X-ray crystallography. Hence, NMR spectroscopy is now an important technique for determining structures and orientations of complex molecules in solution.

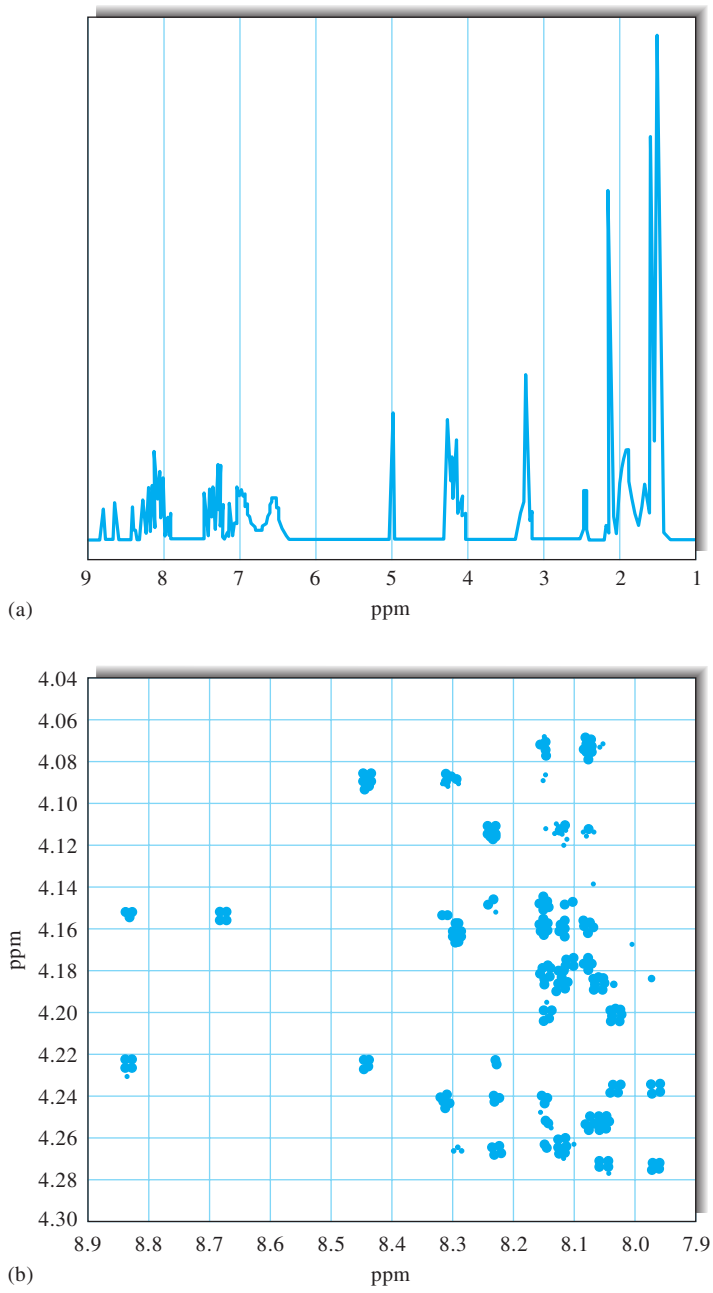

FIGURE 19-34 The 500-MHz one-dimensional ^{1}H NMR spectrum (a) and a portion of the two-dimensional ROESY spectrum (b) of a nineteen-amino-acid protein. The pulse sequence used collapses multiplets due to ^{1}H-^{1}H spin-spin coupling into singlets. The cross peaks of the dipolar interactions make it possible to completely assign the proton NMR spectrum. (Adapted from A. Kaerner and D. L. Rabenstein, *Magn. Reson. Chem.*, **1998**, *36*, 601, **DOI**: 10.1002/(SICI)1097-458X(199808)36:8<601::AID-OMR342>3.0.CO;2-C. Copyright 1998 Interscience/Wiley.)

19H MAGNETIC RESONANCE IMAGING

Since the 1970s, NMR technology has been applied increasingly to fields other than chemistry, such as biology, engineering, industrial quality control, and medicine. One of the most prominent NMR applications is that of magnetic resonance imaging, or MRI. In MRI, data from pulsed RF excitation of solid or semisolid objects are subjected to Fourier transformation and converted to three-dimensional images of the interior of the objects. The primary advantage of MRI is that images of

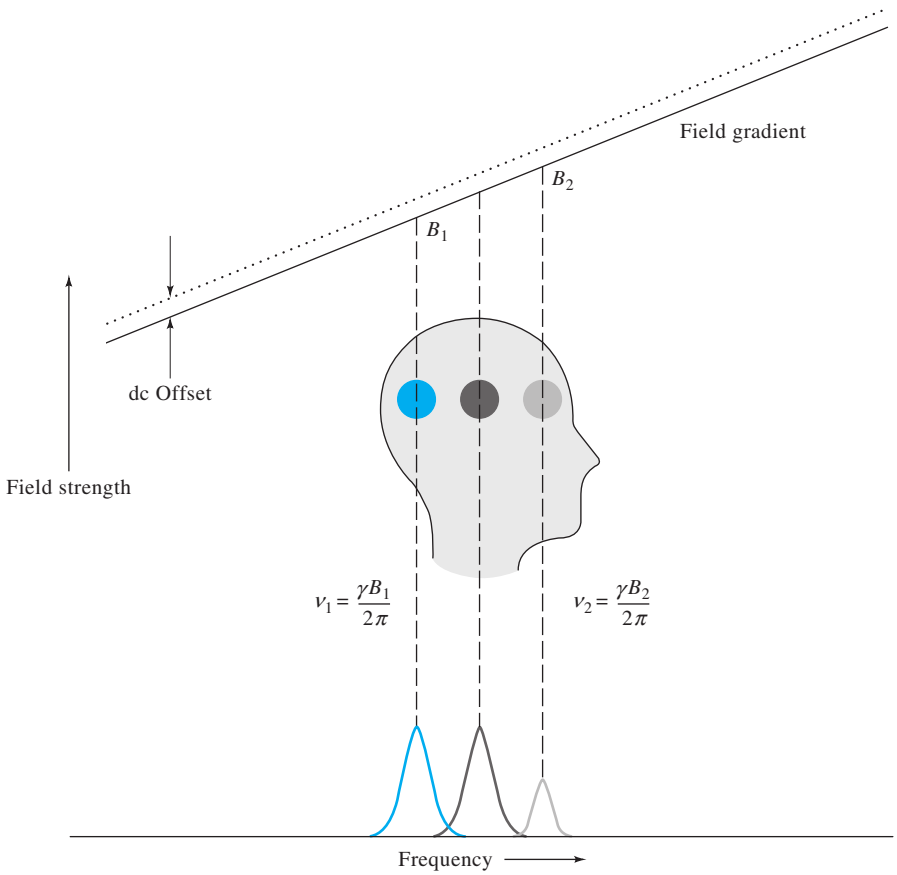

FIGURE 19-35 Fundamental concept of MRI.

objects are formed noninvasively. This means that there is little or no potential of radiation injury or other damage to human or animal subjects as might be encountered with X-ray computerized axial tomography (CAT) or other similar methods.[20] In 2003 Dr. Paul Lauterbur of the University of Illinois and Sir Peter Mansfield of the University of Nottingham in the United Kingdom shared the Nobel Prize in Physiology or Medicine for their discoveries concerning MRI.

The fundamental concept of MRI is depicted in Figure 19-35. In MRI, the magnetic field strength is deliberately varied throughout the subject under study to give a profile such as that shown at the top of the figure. This linear variation, or field gradient, in B is created by auxiliary coils in the magnet bore that are under the control of the computer of the magnetic resonance instrument. Protons in different locations in the subject experience different magnetic field strengths B_1 and B_2 for two of the regions shown in the figure. Equation 19-10, the Larmor equation, suggests that these nuclei exhibit different resonance frequencies, ν_1 and ν_2 in this instance. For example, if a magnetic field gradient of 1×10^{-5} T/cm is applied along the bore, or the z-axis, of an MRI magnet, a resonance frequency range of $(2.68 \times 10^8 \text{ radians s}^{-1}\text{ T}^{-1})(1 \times 10^{-5}\text{ T/cm})/(2\pi \text{ radians}) = 425$ Hz results. In other words, protons 1 cm apart along the field gradient in the subject have resonance frequencies that differ by 425 Hz. Thus, by changing the center frequency of the NMR probe pulse in increments of 425 Hz, it is possible to probe successive 1-cm positions in the direction of the magnetic field gradient. Each consecutive RF pulse produces an FID signal that encodes the concentration of protons at each 1-cm position along the direction of the field gradient. When the FIDs are subjected to Fourier transformation, concentration information is produced as indicated by the heights of the peaks at the bottom of Figure 19-35. In practice, the position of the slice along the z-axis may be changed by adding a dc offset to the auxiliary coils as shown by the dashed field gradient in Figure 19-35. Each slice is probed by changing the pulse width of

[20]For detailed discussions of MRI theory and applications, consult J. P. Hornak, *The Basics of MRI* (http://www.cis.rit.edu/htbooks/mri/); H. Witjes, A. W. Simonetti, L. Buydens, *Anal. Chem.*, **2001**, *73*, 548A, **DOI**: 10.1021/ac0125187; S. A. Huettel, A. W. Song, and G. McCarthy, *Functional Magnetic Resonance Imaging*, Sunderland, MA: Sinauer Associates, 2004; R. B. Buxton, *Introduction to Functional Magnetic Resonance Imaging*, Cambridge, UK: Cambridge University Press, 2002.

the RF pulse to tune its frequency to the precession frequency of the protons in the slice. The middle peak in Figure 19-35 corresponds to the center circle representing the signal from protons in the center position of the subject's head. If the applied field gradient is made larger, the thickness of the examined slice is made smaller.

The position-selection process described in the previous paragraph provides spatial information in one dimension along the *z*-axis by flipping the spins of the protons within the selected slice. Information within each of the slices along the *z*-axis is acquired in a slightly different way, as shown schematically in Figure 19-36. The chosen slice is represented in the figure as a two-dimensional grid lying in the *x*-*y* slice with rows 1, 2, and 3 and columns a, b, and c. For simplicity, the grid is shown as a 3 × 3 array of elements, but in practice the slice might have 128 × 128, 256 × 256, or 512 × 512 elements, with each element, or pixel, having an area of 1 mm × 1 mm in the sample. In such three-dimensional imaging experiments, the *z*-axis field gradient is selected to give a slice thickness of 1 mm, then it is turned off. At this point in the measurement sequence, all protons in the slice have their spins flipped. A second gradient is applied to the subject perpendicular to the *z*-axis by using a second set of *y*-axis coils oriented at a right angle to the axis of the magnet bore. Nuclei at different positions along the *y*-axis precess at different frequencies depending on their position in the field gradient. When this second *y*-axis field gradient is turned off, all nuclei at a distance corresponding to row 1 on the *y*-axis of Figure 19-36 have precessed through a fixed phase angle whose magnitude is proportional to the size of the gray, pie-shape angular sections of the circles in row 1. Thus, the distance along the *y*-axis *is encoded in the phase angle* of the precessing protons represented by the gray pie slices.

As soon as the *y*-axis gradient is terminated, a third set of magnet coils perpendicular to both the *z*-axis and the *y*-axis coils are then activated. This action produces a field gradient in the third dimension along the *x*-axis. Because the nuclei in column b have experienced a stronger magnetic field than those in column a, they precess at a higher frequency whose magnitude is represented by the blue pie slices. Similarly, the nuclei in column c have the largest frequency in the 3 × 3 pixel array of Figure 19-36. The result is that the positions of the nuclei in the *x* dimension *are encoded by their precession frequencies*. The total precession angle, which is indicated by the circular arrows in the figure, is unique for each element of the grid, and thus the position of each is encoded in the total angle. The receiver coils are turned on during the application of this last frequency-encoding phase, and an FID is recorded. The complete cycle of (1) slice

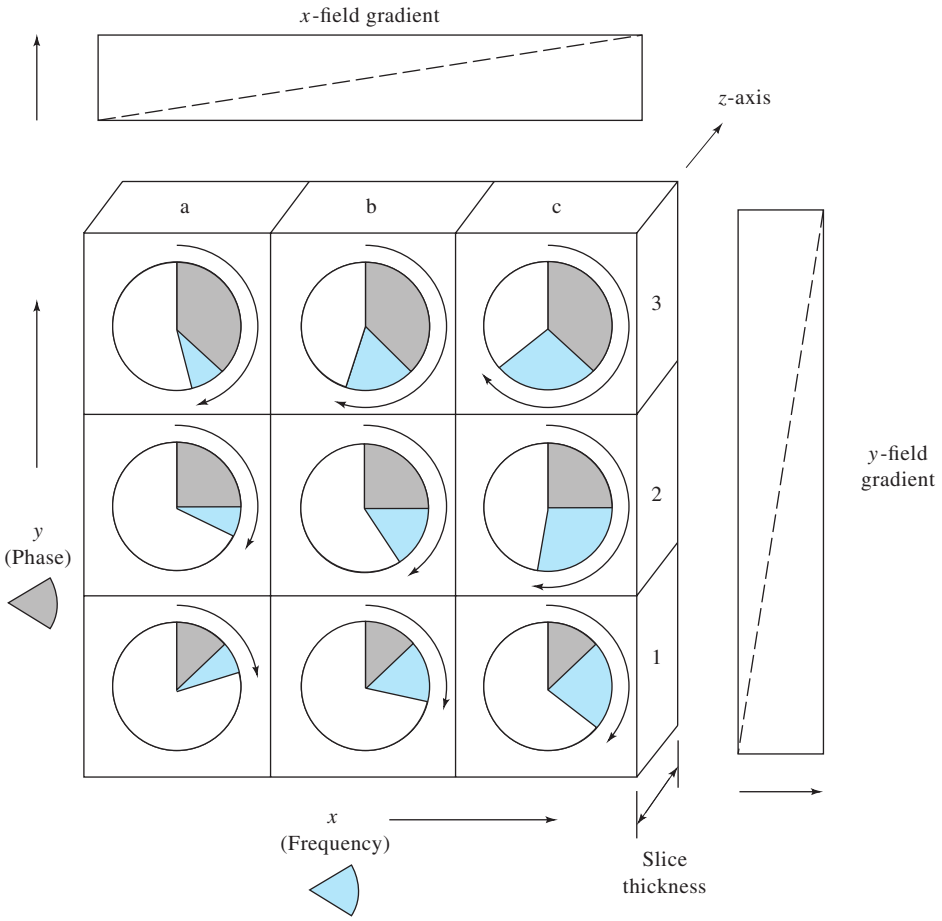

FIGURE 19-36 Acquisition of information within slices along the *z*-axis.

selection, (2) phase encoding in the y dimension, (3) frequency encoding in the x dimension, and (4) recording the FID requires only a few hundred milliseconds at most. The next step in collecting the data is to turn on the z-axis coils to once again flip the spins of the nuclei in the slice and repeat the sequence with a somewhat larger y-axis gradient to phase-encode row 2. This step is followed by the application of the x-axis gradient to frequency-encode columns a, b, and c and the acquisition of the FID for row 2. Finally, the entire measurement sequence is repeated for row 3, and a corresponding FID is acquired. The result of the process for the entire 3×3 slice is a set of three FIDs representing the time-domain resonance signal S, each of which is a function of the x and y field gradients G_x and G_y, respectively. The time-domain signal $S(G_x, G_y)$, which contains information related to the total precession angle, is subjected to a two-dimensional Fourier transformation. The result is a frequency-domain signal $S(\omega_x, \omega_y)$ whose frequencies in the x and y dimensions are directly proportional to the distances d_x and d_y. That is,

$$S(G_x, G_y) \rightarrow S(\omega_x, \omega_y) \rightarrow S(d_x, d_y)$$

The two-dimensional distance information in $S(d_x, d_y)$ is at last combined for all of the slices in the z dimension to provide a three-dimensional array of data. Each element of the array contains an intensity that is proportional to the concentration of protons in a volume element, or *voxel*, corresponding to each set of coordinates x, y, and z. Note that with the exception of the magnet, which must have a rather large bore and a large static field strength of 0.5 to 4.7 T, instruments for MRI and high-resolution NMR are identical in function. Precisely the same pulse-sequencing techniques and data-enhancement procedures are used in both types of instruments. Although the foregoing discussion is considerably simplified, the basic sequencing and encoding schemes are realistic. Clever and timely application of various RF pulse sequences and magnetic field gradients, appropriate Fourier transformations, and data analysis and reconstruction software routines produce three-dimensional images. Structures inside subjects may be reconstructed from the three-dimensional data arrays as illustrated in the group of four MRI images of Figure 19-37. The images are true

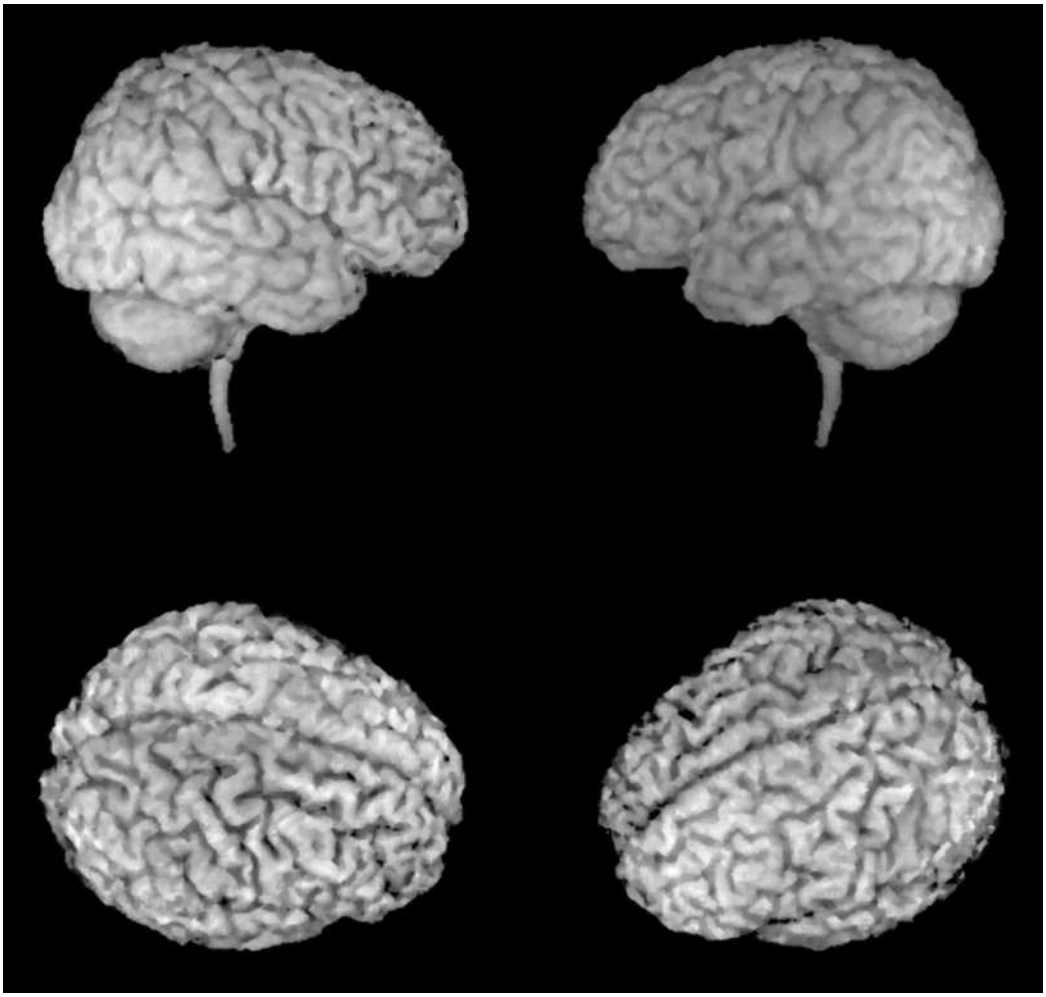

FIGURE 19-37 Structures inside subjects may be reconstructed from the three-dimensional data arrays. (Image courtesy of C. D. Smith, Memory Disorders Clinic, Sanders-Brown Research Center on Aging, University of Kentucky Medical Center. With permission.)

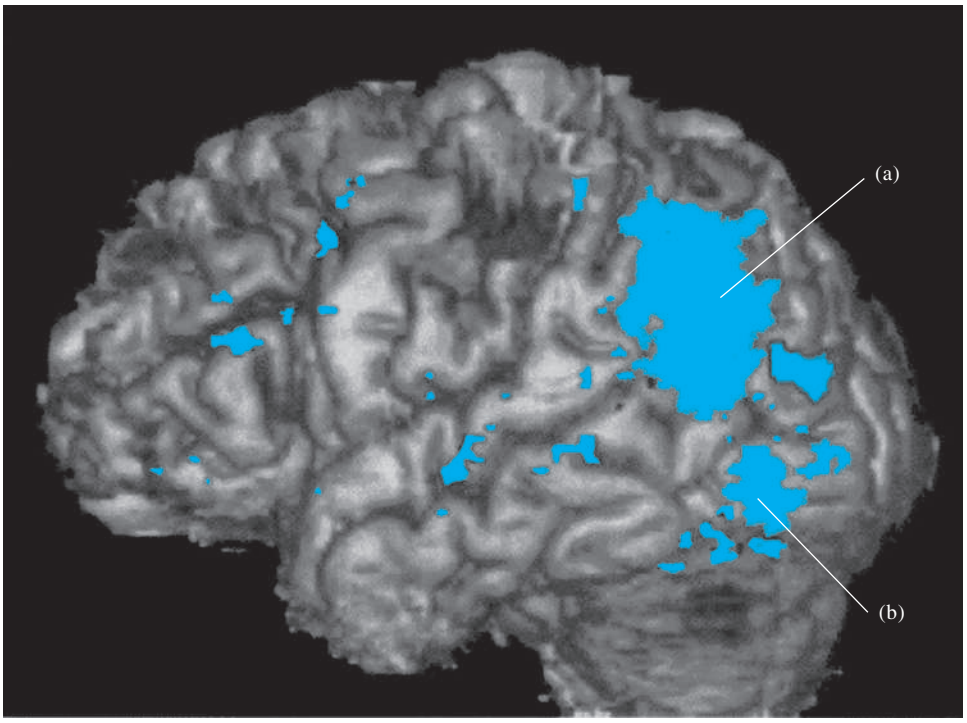

FIGURE 19-38 Brain activity in the left hemisphere resulting from naming tasks revealed by fMRI. (From C. D. Smith, A. H. Andersen, Q. Chen, L. X. Blonder, J. E. Kirsch, and M. J. Avison, *NeuroReport*, **1996**, *7*, 781. With permission.)

three-dimensional brain reconstructions calculated by using a single set of MRI data from a young female patient with Rasmussen's encephalitis. These images show the dramatic shrinkage in the front right portion of the brain characteristic of this rare illness. The ability to generate high-resolution (millimeter-scale) images from true three-dimensional data is a unique strength of the MRI technique.

A second magnetic resonance image presented in Figure 19-38 demonstrates functional MRI (fMRI) mapping of visual-confrontation naming in the left hemisphere of the brain. The dark portion of the map demonstrates statistical differences in signal intensity due to changes in cerebral blood oxygenation from activation of brain regions engaged in a naming task compared to a control task. The task undertaken by the subject in this case was the naming of standardized line drawings of a series of seven subjects. The map shows activation of the *angular gyrus*, the large dark patch in the upper-right region of the brain, and the so-called *area 37*, the smaller light gray region in the lower-back region. Both regions of the brain are known to be involved in language processing. Mapping of brain regions involved in specific types of human brain processing and execution is a current intensive area of research. Advantages of fMRI compared with other techniques are the noninvasive nature of the technique, reproducibility, speed of data acquisition, and high intrinsic spatial resolution.

MRI has become a mainstay in the arsenal of medical diagnostic tools. The application of MRI in the food industry and in other areas of science and commerce has been hampered by the high cost of MRI installations. However, as the sophistication and ease of application of data-enhancement procedures, exotic pulse sequences, and data-acquisition protocols continue to evolve, especially for nuclei other than ^{1}H, MRI will doubtless become an indispensable tool for the noninvasive investigation of materials.

» QUESTIONS AND PROBLEMS

*Answers are provided at the end of the book for problems marked with an asterisk.

Problems with this icon are best solved using spreadsheets.

19-1 Explain the difference in the way a CW and an FT-NMR experiment is performed.

19-2 What are the advantages of an FT-NMR measurement over a CW measurement? What are the disadvantages?

19-3 In NMR spectroscopy, what are the advantages of using a magnet with as great a field strength as possible?

19-4 How can spin-spin splitting lines be differentiated from chemical-shift lines?

19-5 Define

(a) magnetic anisotropy

(b) the shielding constant

(c) the chemical-shift parameter

(d) CW-NMR measurements

(e) Larmor frequency

(f) coupling constants

(g) first-order NMR spectra

19-6 A nucleus has a spin quantum number of 7/2. How many magnetic energy states does this nucleus have? What is the magnetic quantum number of each?

* **19-7** What is the absorption frequency in a 11.7-T magnetic field of (a) ^{1}H, (b) ^{13}C, (c) ^{19}F, and (d) ^{31}P?

* **19-8** What is the Larmor frequency for ^{13}C in magnetic fields of (a) 1.41 T, (b) 4.69 T, (c) 7.05 T, (d) 11.7 T, (e) 18.8 T, and (f) 21.2 T?

* **19-9** A resonance is displaced 90 Hz from TMS at a magnetic field strength of 1.41 T. What will be the frequency difference at (a) 4.69 T, (b) 7.05 T, (c) and 18.8 T? What will be the chemical shifts δ at these same magnetic field strengths?

19-10 Why is ^{13}C-^{13}C spin-spin splitting not observed in ordinary organic compounds?

* **19-11** Calculate the relative number of ^{19}F nuclei in the higher and lower magnetic states at 25°C in magnetic fields of (a) 2.4 T, (b) 4.69 T, and (c) 7.05 T.

19-12 What is the difference between longitudinal and transverse relaxation?

19-13 Explain the source of an FID signal in FT-NMR.

19-14 What is a rotating frame of reference?

19-15 How will ΔE for an isolated ^{13}C nucleus compare with that of a ^{1}H nucleus?

19-16 Calculate the resonance frequency of each of the following nuclei in a 11.7-T magnetic field: (a) ^{19}F and (b) ^{31}P.

* **19-17** What is the ratio of the number of nuclei in the upper magnetic energy state to the number in the lower energy state of ^{13}C in a 500-MHz instrument if the temperature is 300 K?

19-18 Briefly compare the ^{1}H and ^{31}P NMR spectra of methyl phosphorous acid $P(OCH_3)_3$ at 7.05 T. There is a weak spin-spin coupling between phosphorus and hydrogen nuclei in the compound.

19-19 In the room-temperature ^{1}H spectrum of methanol, no spin-spin coupling is observed, but when a methanol sample is cooled to −40°C, the exchange rate of the hydroxyl proton slows sufficiently so that splitting is observed. Sketch spectra for methanol at the two temperatures.

» QUESTIONS AND PROBLEMS (continued)

19-20 Use the following coupling constant data to predict the ^{1}H and the ^{19}F spectra of the following:

Species	*J*, Hz
(a) F—C≡C—H	21
(b) CF_3—CH_3	12.8
(c) $(CH_3)_3$—CF	20.4

19-21 Predict the appearance of the high-resolution ^{13}C spectrum of (proton decoupled)

(a) methyl formate.

(b) acetaldehyde.

(c) acetone.

19-22 Repeat Question 19-21 for the case when the protons are not decoupled. Note that ^{13}C—^{1}H coupling constants are generally in the range of 100 to 200 Hz.

19-23 What is a frequency lock system in an NMR spectrometer? Describe the two types of lock systems.

* **19-24** What are shims in an NMR spectrometer, and what are their purpose?

* **19-25** Why are liquid samples spun while being examined in an NMR spectrometer?

19-26 Predict the appearance of the high-resolution proton NMR spectrum of propionic acid.

19-27 Predict the appearance of the high-resolution proton NMR spectrum of

(a) acetone.

(b) acetaldehyde.

(c) methyl ethyl ketone.

19-28 Predict the appearance of the high-resolution proton NMR spectrum of

(a) ethyl nitrite.

(b) acetic acid.

(c) methyl-*i*-propyl ketone.

* **19-29** Predict the appearance of the high-resolution proton NMR spectrum of

(a) cyclohexane.

(b) diethyl ether.

(c) 1,2-dimethoxyethane, $CH_3OCH_2CH_2OCH_3$.

19-30 Predict the appearance of the high-resolution proton NMR spectrum of

(a) toluene.

(b) ethyl benzene.

(c) *i*-butane.

*19-31 The proton NMR spectrum in Figure 19-39 is for an organic compound containing a single atom of bromine. Identify the compound.

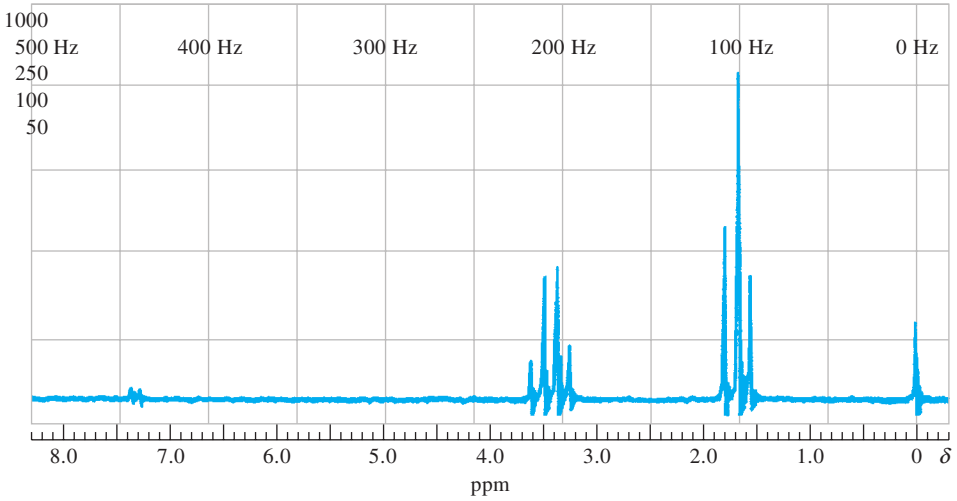

FIGURE 19-39 Proton NMR spectrum. (Courtesy of Agilent Technologies, Santa Clara, CA.)

19-32 The proton NMR spectrum in Figure 19-40 is for a compound having an empirical formula $C_4H_7BrO_2$. Identify the compound.

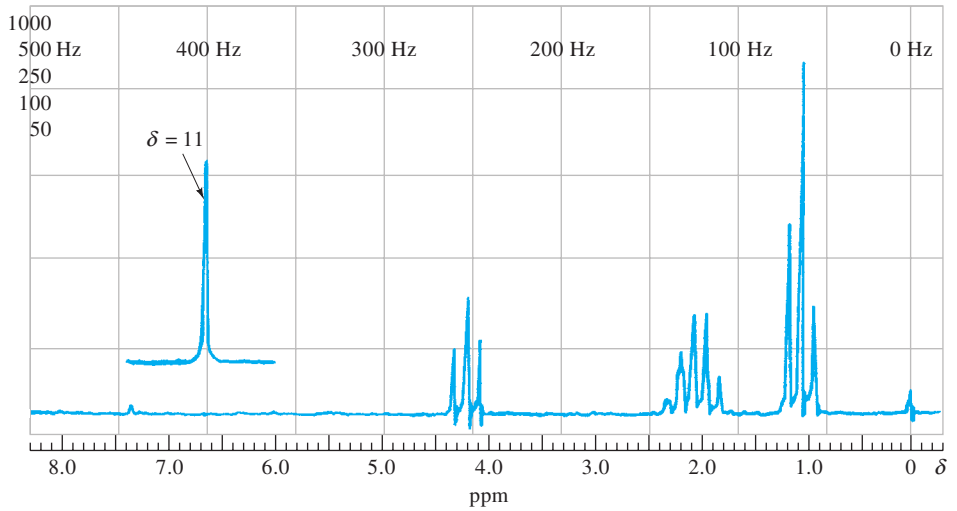

FIGURE 19-40 Proton NMR spectrum. (Courtesy of Agilent Technologies, Santa Clara, CA.)

QUESTIONS AND PROBLEMS (continued)

*19-33 The proton NMR spectrum in Figure 19-41 is for a compound of empirical formula C_4H_8O. Identify the compound.

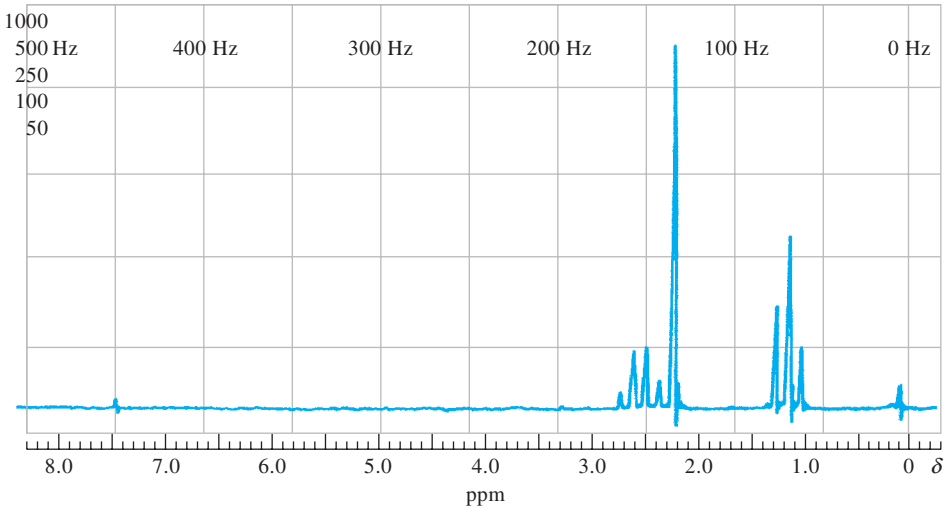

FIGURE 19-41 Proton NMR spectrum. (Courtesy of Agilent Technologies, Santa Clara, CA.)

19-34 The proton NMR spectrum in Figure 19-42 is for a compound having an empirical formula $C_4H_8O_2$. Identify the compound.

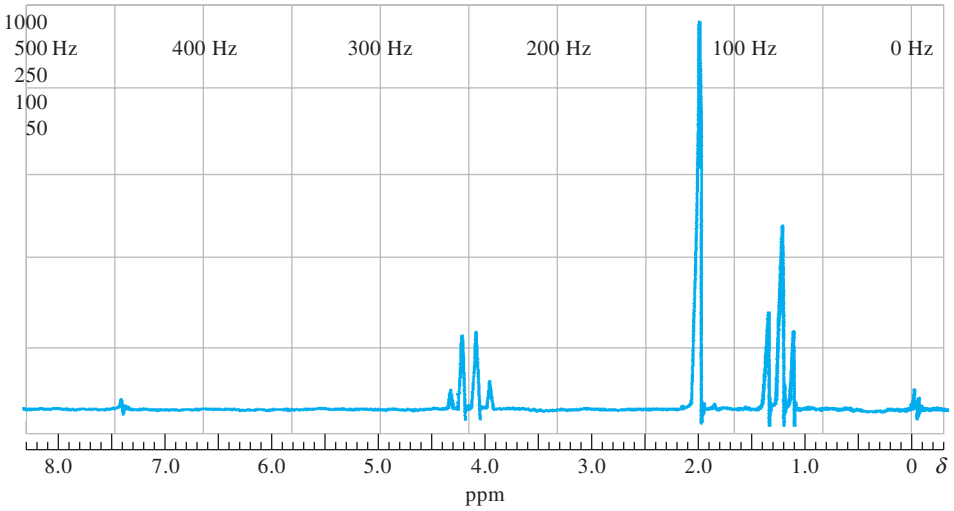

FIGURE 19-42 Proton NMR spectrum. (Courtesy of Agilent Technologies, Santa Clara, CA.)

19-35 The proton spectra in Figure 19-43a and b are for compounds with empirical formula C_8H_{10}. Identify the compounds.

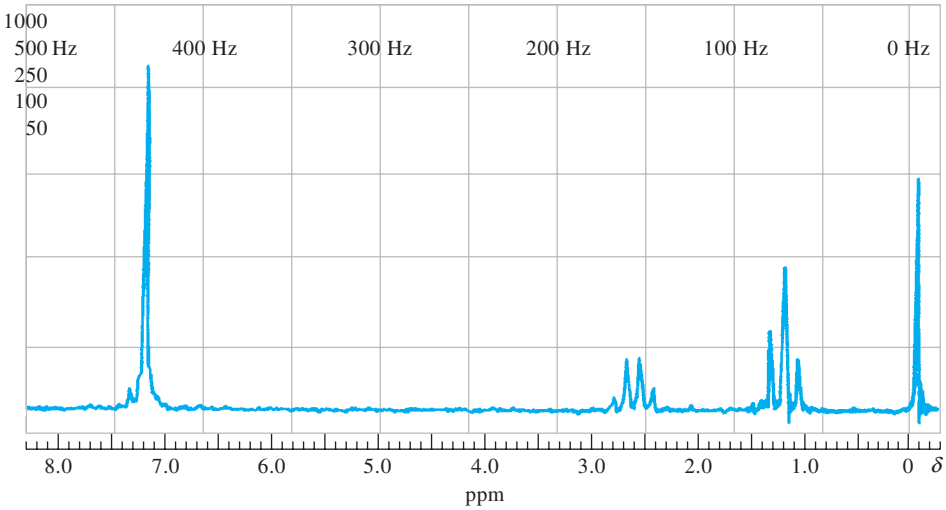

(a)

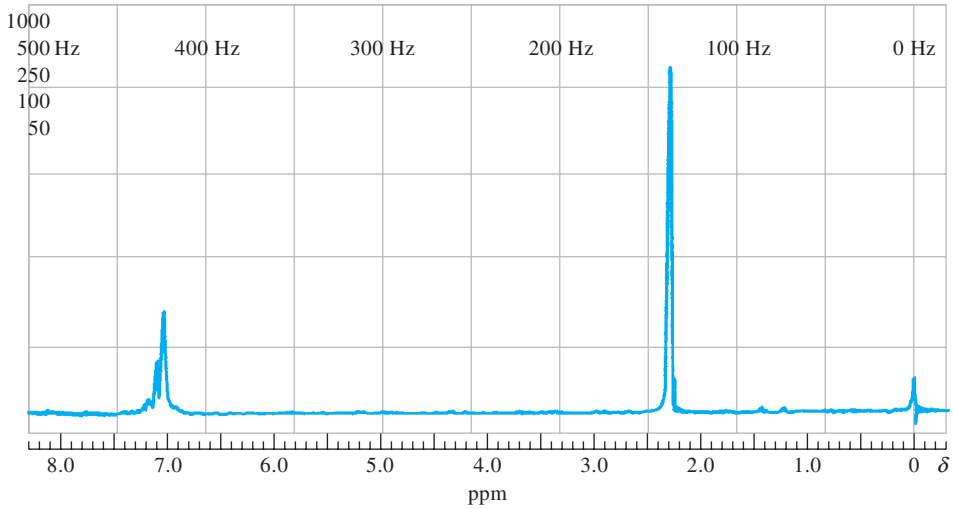

(b)

FIGURE 19-43 Proton NMR spectra. (Courtesy of Agilent Technologies, Santa Clara, CA.)

» QUESTIONS AND PROBLEMS (continued)

19-36 From the proton NMR spectrum in Figure 19-44, deduce the structure of this hydrocarbon.

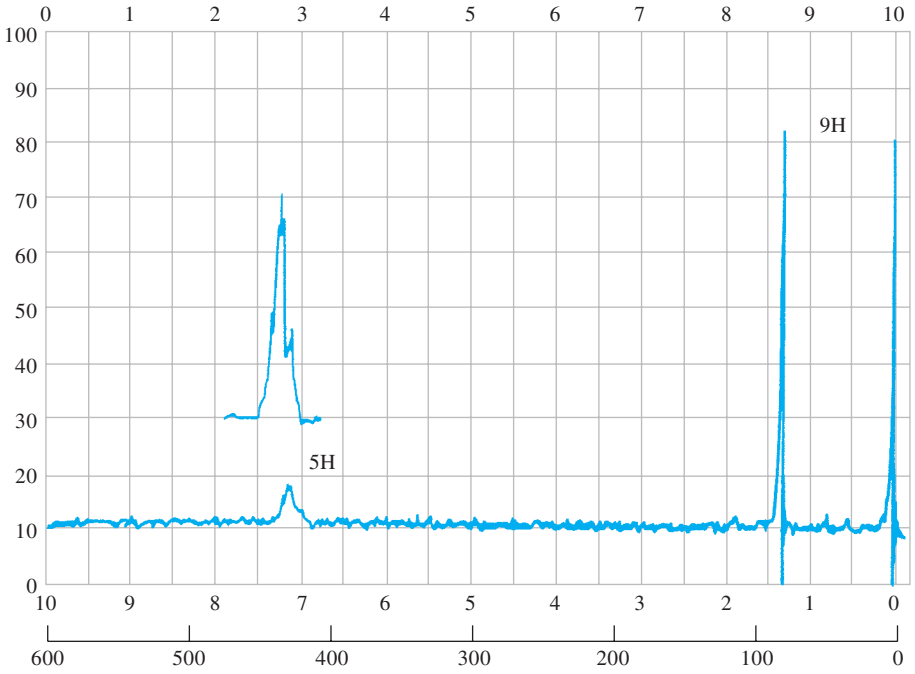

FIGURE 19-44 Proton NMR spectrum. (From C. J. Pouchert, *The Aldrich Library of NMR Spectra*, 2nd ed., Milwaukee, WI: The Aldrich Chemical Company. With permission.)

* **19-37** From the proton spectrum given in Figure 19-45, determine the structure of this compound, a commonly used painkiller; its empirical formula is $C_{10}H_{13}NO_2$.

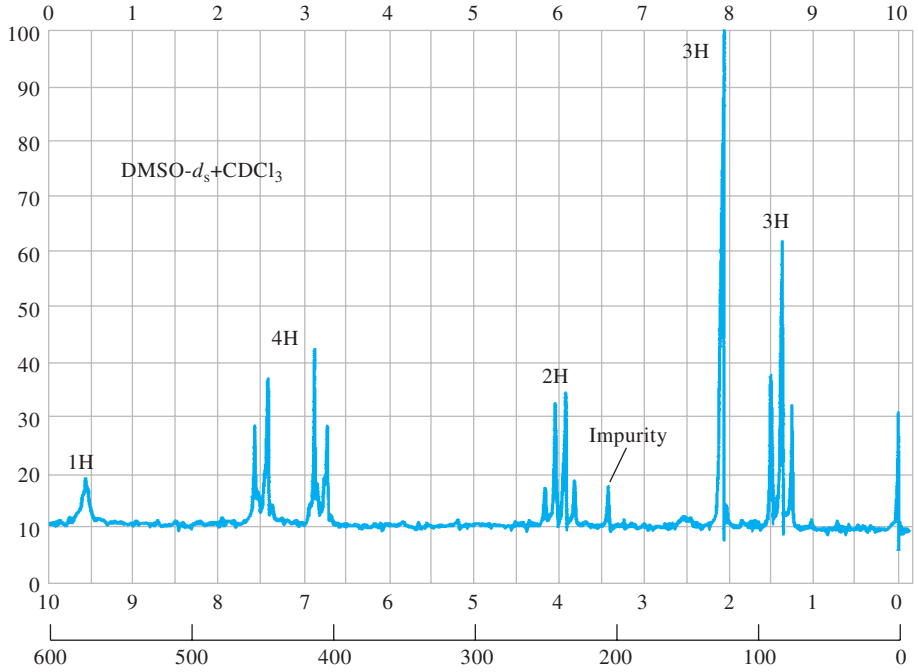

FIGURE 19-45 Proton NMR spectrum. (From C. J. Pouchert, *The Aldrich Library of NMR Spectra*, 2nd ed., Milwaukee, WI: The Aldrich Chemical Company. With permission.)

19-38 Explain how a band of frequencies is obtained from an oscillator, which is essentially a monochromatic source of RF radiation. How could a band broad enough to cover the entire ^{13}C spectrum (200 ppm) be obtained?

19-39 Describe sources of folded spectral lines.

19-40 What is the nuclear Overhauser effect and its source?

19-41 What are the sources of band broadening in ^{13}C spectra of solids? How are lines narrowed so that high-resolution spectra can be obtained?

Challenge Problem

19-42 (a) What are the major advantages and disadvantages of two-dimensional NMR methods over conventional one-dimensional techniques?

(b) Describe in detail the pulse sequences that are used in the COSY and HETCOR experiments. For both, describe the behavior of the magnetization vector *M* as a result of the applied pulses. Consult note 19 for assistance in learning more about the details of two-dimensional NMR methods.

(c) From the 300-MHz ^1H NMR spectrum of phenanthro[3,4-b]thiophene reproduced in Figure 19-46, identify the resonances of H_1 and H_{11} as a pair. Can you assign any of the other resonances?

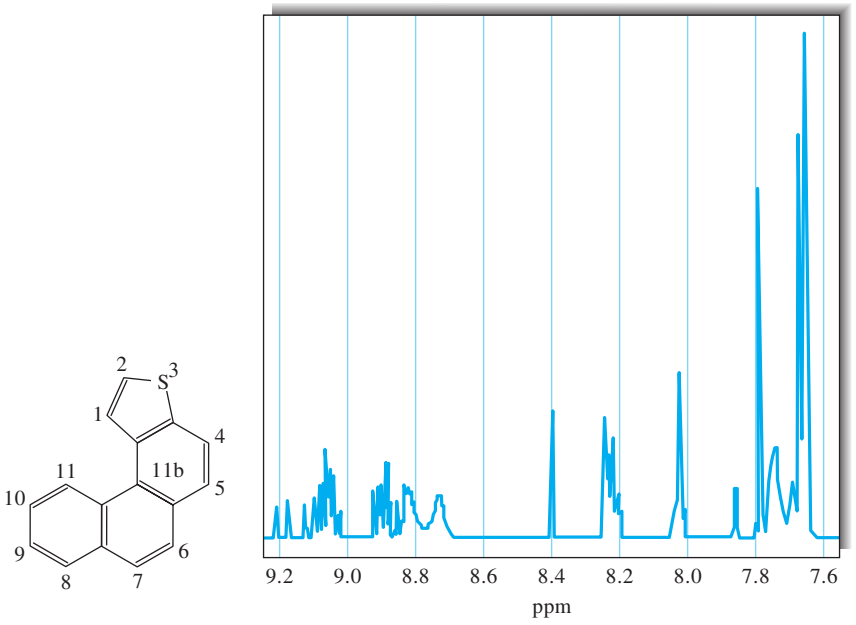

FIGURE 19-46 Proton NMR spectrum of phenanthro[3,4-b]thiophene at 300 MHz. (From G. E. Martin and A. S. Zektzer, *Two-Dimensional NMR Methods for Establishing Connectivity*, New York: Wiley-VCH, 1988. With permission.)

» QUESTIONS AND PROBLEMS (continued)

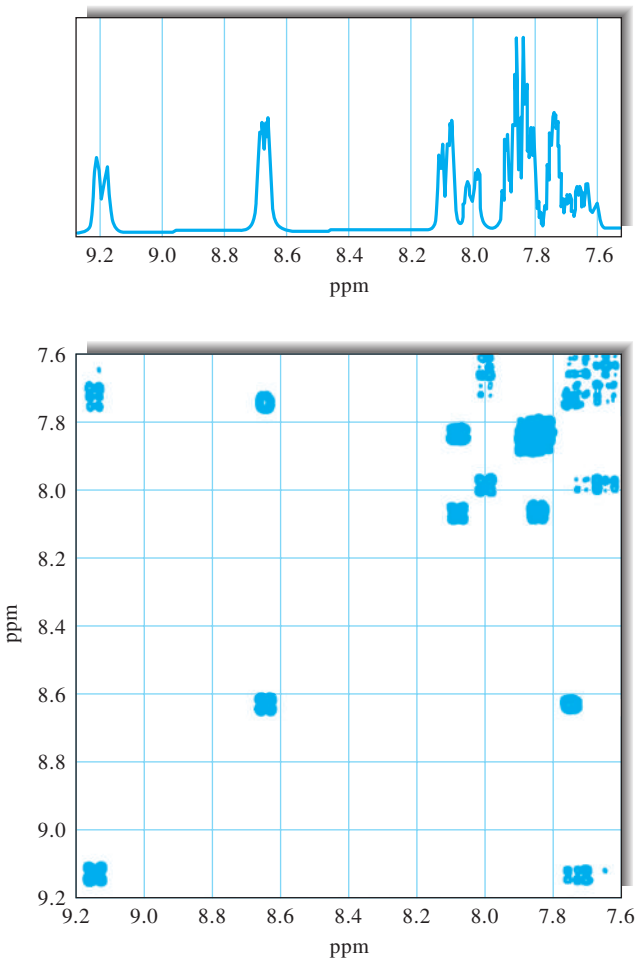

FIGURE 19-47 The 300-MHz COSY spectrum of phenanthro[3,4-b] thiophene. (From J. B. Lambert and E. P. Mazzola, *Nuclear Magnetic Resonance Spectroscopy*, Upper Saddle River, NJ: Pearson/Prentice-Hall, 2004. With permission.)

(d) From the 300-MHz COSY spectrum in Figure 19-47, describe how you would distinguish the resonances of H_1 and H_{11}.

(e) In the COSY spectrum of Figure 19-47, assign resonances to H_2, H_8, H_9, and H_{10}. Give the rationale for your assignments.